

UCLA

UCLA Electronic Theses and Dissertations

Title

[18F]FDDNP PET in Tauopathies: Correlation to post mortem Pathology in a Case of Progressive Supranuclear Palsy (PSP)

Permalink

<https://escholarship.org/uc/item/1q7561c3>

Author

Villegas, Brendon Josef

Publication Date

2017

Peer reviewed|Thesis/dissertation

UNIVERSITY OF CALIFORNIA

Los Angeles

[¹⁸F]FDDNP PET in Tauopathies: Correlation
to *post mortem* Pathology in a Case of
Progressive Supranuclear Palsy (PSP)

A dissertation submitted in partial satisfaction
of the requirements for the degree of
Doctor of Philosophy in Biomedical Physics

by

Brendon Josef Villegas

2017

© Copyright by
Brendon Josef Villegas

2017

ABSTRACT OF THE DISSERTATION

[¹⁸F]FDDNP PET in Tauopathies: Correlation
to *post mortem* Pathology in a Case of
Progressive Supranuclear Palsy (PSP)

by

Brendon Josef Villegas

Doctor of Philosophy in Biomedical Physics

University of California, Los Angeles 2017

Professor Jorge R. Barrio, Chair

This investigation of [¹⁸F]FDDNP was conducted in an effort to confirm the presence of disease in a patient with Progressive Supranuclear Palsy (PSP) and to correlate the *ante mortem* PET scan results to the *post mortem* pathology. The immunohistochemical and immunofluorescent staining of Paired Helical Filamentous (PHF) tau (AT8) and Amyloid Beta (6F/3D) misfolded proteins demonstrated a widespread deposition in the cortical and subcortical nuclei, the white matter, cerebellar white matter and the medulla oblongata. The *in vitro* autoradiography demonstrated a neocortical signal comprised of well-delineated amyloid beta in the nucleated layers I/II and hyperphosphorylated tau in the deeper layers III through VI. The autoradiography was well correlated with the immunohistochemical staining in adjacent tissue slides. The binding of the parametric [¹⁸F]FDDNP distribution volume ratio

(DVR) correlated well (Spearman's $\rho = 0.962$, $p = .004$) with the deposition of tau but not with the presence of amyloid beta (Spearman's $\rho = -0.829$, $p = .041$). The [^{18}F]FDDNP DVR signal appears to be primarily due to the large amount of bound hyperphosphorylated tau (p-tau) and the amyloid beta negligibly contributes to the total signal. Unlabeled FDDNP was shown to bind to tau in the form of globose tangles in the rostral ventromedial medulla as confirmed with both Thioflavin S and PHF-tau Immunofluorescence.

The binding of [^{18}F]FDDNP to the human neuroanatomy was investigated in two cohorts of distinct tauopathies and compared to the binding in two tau-negative cohorts against control patients. A cohort of PSP patients ($n=12$) with a mean age of 63.8 years and a cohort of Chronic Traumatic Encephalopathy (CTE) patients ($n=14$) with a mean age of 58.1 years are both characterized by the presence of various degrees of tau pathology in their brains. The cohort of Parkinson's Disease (PD) patients ($n=16$) with a mean age of 63.2 years is initially characterized by clinical symptoms similar to PSP [^{18}F]FDDNP is able to differentiate between PD and PSP with statistical significance ($p < .05$) in the striatum; particularly within the caudate nucleus. The Huntington's Disease (HD) patients ($n=15$) with a mean age of 36.8 years display motor degeneration from a loss of striatal medium spiny neurons with no presence of amyloid beta or p-tau. It has further been demonstrated with statistical certainty that CTE is discernible from control patients in the, the amygdala, the midbrain, the caudate nucleus and the anterior cingulate gyrus ($p < .05$). On the other hand, the HD and PD cohort were both found to have decreased binding of [^{18}F]FDDNP binding in caudate nucleus when compared to all the control patients ($p < .05$). In the tauopathy cases studied, [^{18}F]FDDNP has successfully demonstrated its differential capability to discriminate between PSP, CTE and PD. The [^{18}F]FDDNP DVR signal in the cases of PSP and CTE closely correlated with hyperphosphorylated tau deposition, as confirmed by *post mortem* autopsy with a case of PSP.

The dissertation of Brendon Josef Villegas is approved.

Nagichettiar Sataymurthy

Gary W. Small

Henry Huang

Jorge R. Barrio, Committee Chair

University of California, Los Angeles

2017

I dedicate this dissertation to my family, for whom without, I would not be here.

Table of Contents

ABSTRACT OF THE DISSERTATION	II
LIST OF FIGURES.....	VIII
LIST OF TABLES.....	IX
LIST OF EQUATIONS	X
ACKNOWLEDGEMENTS.....	XI
PREFACE	XV
VITA	XVII
PRESENTATIONS & PUBLICATIONS.....	XVIII
CHAPTER ONE: PURPOSE AND ORGANIZATION	1
1.1 SPECIFIC RESEARCH AIM 1: CORRELATION OF <i>ANTE MORTEM</i> [¹⁸ F]FDDNP PET AND <i>POST MORTEM</i> BRAIN TAU PATHOLOGY DISTRIBUTION IN A CASE OF PROGRESSIVE SUPRANUCLEAR PALSY (PSP).	4
1.1.1 Methodology for [¹⁸ F]FDDNP PET signal co-registration with immunohistochemical staining.	5
1.2 SPECIFIC RESEARCH AIM 2: MAPPING BRAIN [¹⁸ F]FDDNP PET PARAMETRIC DISTRIBUTION VOLUME RATIO (DVR) TO COMPARE NEURODEGENERATIVE TAUOPATHIES WITH CONTROLS.	6
1.2.1 Methodology for [¹⁸ F]FDDNP binding comparison amongst a variety of neurodegenerative disease cohorts.	7
CHAPTER TWO: BACKGROUND AND RELATED INFORMATION	9
2.1 ALZHEIMER’S DISEASE (AD).....	10
2.2 AMYLOID-β PROTEIN	13
2.3 HYPERPHOSPHORYLATED TAU PROTEIN.....	15
2.4 PROGRESSIVE SUPRANUCLEAR PALSY (PSP)	17
2.5 HUNTINGTON’S DISEASE.....	18
2.6 PARKINSON’S DISEASE.....	19
2.7 CHRONIC TRAUMATIC ENCEPHALOPATHY (CTE)	20
2.8 MOLECULAR IMAGING: POSITRON EMISSION TOMOGRAPHY (PET).....	21
2.9 [¹⁸ F]FDDNP	22
2.10 COMPARATIVE FLUORESCENCE	23
2.11 ALTERNATIVE TRACERS	23
2.12 SYNTHESIS OF [¹⁸ F]FDDNP AND IN VIVO HUMAN IMAGING	24
2.13 DISTRIBUTION VOLUME RATIO (DVR) TOMOGRAPHIC MAPS USING LOGAN ANALYSIS AND COMPARTMENTAL MODELING	25
CHAPTER THREE: CORRELATION OF <i>ANTE MORTEM</i> [¹⁸ F]FDDNP TO <i>POST MORTEM</i> [¹⁸ F]FDDNP SIGNAL IN THE BRAIN OF A PROGRESSIVE SUPRANUCLEAR PALSY PATIENT	27
3.1 INTRODUCTION.....	27
3.2 MATERIAL & METHODS	30

3.2.1 [¹⁸ F]FDDNP Synthesis (Product provided by Dr. Jie Liu).....	30
3.2.2 [¹⁸ F]FDDNP PET in PSP.....	33
3.2.3 Patient History	33
3.2.4 [¹⁸ F]FDDNP PET Distribution Volume Ratio (DVR) Image Analysis	34
3.2.5 <i>Post mortem</i> PSP Brain Tissue Preparation	35
3.2.6 Slide preparation.....	38
3.2.7 Cryomicrotomy.....	38
3.2.8 Cryomacrotomy	39
3.2.9 Hyperphosphorylated Tau (AT8) Immunohistochemistry	40
3.2.10 Amyloid-beta (6F/3D) Immunohistochemistry	41
3.2.11 Immunofluorescence	42
3.2.12 Fluorescent Histochemistry	43
3.2.13 <i>In vitro</i> Macro-autoradiography	44
3.2.14 <i>In vitro</i> Microautoradiography	45
3.2.15 Immunohistochemical Pathology Scoring.....	47
3.2.16 Data Analysis.....	49
3.3. RESULTS	50
3.4 STATISTICS	62
3.5 DISCUSSION	64
CHAPTER FOUR: COMPARISON OF THE <i>IN VIVO</i> [¹⁸F]FDDNP PET IMAGING AMONG COHORTS OF PROGRESSIVE SUPRANUCLEAR PALSY (PSP), PARKINSON’S DISEASE (PD), HUNTINGTON’S DISEASE (HD), CHRONIC TRAUMATIC ENCEPHALOPATHY (CTE) AND HEALTHY CONTROL PATIENTS.	70
4.1 INTRODUCTION.....	70
4.2 MATERIALS & METHODS	73
4.2.1 [¹⁸ F]FDDNP patient imaging protocol	73
4.2.2 PET Image Reconstruction and Motion Correction	74
4.2.3 [¹⁸ F]FDDNP parametric DVR Image Co-registration and format conversion.....	74
4.2.4 Progressive Supranuclear Palsy (PSP) cohort Imaging.....	75
4.2.5 Parkinson’s Disease (PD) cohort Imaging	75
4.2.6 Huntington’s Disease (HD) cohort Imaging.....	76
4.2.7 Chronic Traumatic Encephalopathy (CTE) cohort Imaging	76
4.2.8 Younger Control (<60 yrs) cohort Imaging.....	77
4.2.9 Older Control (>60 yrs) cohort Imaging	77
4.2.10 Distribution Volume Ratio (DVR) Logan Analysis	77
4.2.11 [¹⁸ F]FDDNP Parametric DVR Image Analysis.....	78
4.2.12 Statistical Analysis	78
4.3 RESULTS	80
4.4 DISCUSSION	91
BIBLIOGRAPHY.....	95

List of Figures

Figure 2.1. The Braak staging of Neurofibrillary changes in the Alzheimer’s Disease (AD) brain (Braak and Braak 1995).....	12
Figure 2.2 Progressive Supranuclear palsy disease progression of tau.....	18
Figure 3.2 The semi-automated synthesis module for the preparation of [¹⁸ F]FDDNP.....	30
Figure 3.1 The radiosynthetic reaction scheme for the preparation of [¹⁸ F]FDDNP.....	30
Figure 3.3 Typical analytical HPLC QC test results for [¹⁸ F]FDDNP biomarker.....	32
Figure 3.4 The gross neuroanatomical descriptions of the PSP brain tissue.....	37
Figure 3.5 The pathological scoring rubric of PHF-tau and A β ₁₋₄₂ immunohistochemistry.....	48
Figure 3.6 Co-registered T1-weighted MRI and [¹⁸ F]FDDNP DVR image.....	50
Figure 3.7 PSP Midbrain Atrophy in the T1-weighted MPRAGE MRI and [¹⁸ F]FDDNP DVR.....	51
Figure 3.8 Paired Helical Filamentous (PHF) Tau immunofluorescence and immunohistochemistry in the PSP brain.....	53
Figure 3.9 Amyloid beta (6F/3D, Dako) immunohistochemistry.....	54
Figure 3.10 Medulla oblongata PHF-tau immunohistochemistry.....	56
Figure 3.11 The <i>post mortem</i> pathology stained for tau and amyloid beta and co-registered to the [¹⁸ F]FDDNP signal.....	57
Figure 3.12 The autoradiography and fluorescent histology.....	60
Figure 3.13 The scatterplots of the correlated [¹⁸ F]FDDNP and immunohistochemical data.....	62
Figure 3.14 [¹⁸ F]FDDNP DVR vs. IHC 2-D Box plots in the 28 neuroratomical regions.....	63
Figure 3.15 The microcircuitry of the inferior olive and the olivocerebellar cortical pathway (De Zeeuw et al. 1998).....	66

List of Tables

Table 3.1. PHF-tau and Amyloid Beta Immunohistochemistry (IHC) grading values alongside their respective [¹⁸ F]FDDNP DVR values.	61
Table 3.2 Means and standard deviations of the binding of [¹⁸ F]FDDNP in 5 subclassifications of the neuroanatomy.	63
Table 3.3 The correlation coefficients between the PHF-tau and Amyloid Beta IHC compares to the [¹⁸ F]FDDNP DVR values.	64
Table 4.1 The [¹⁸ F]FDDNP DVR binding values (mean ± SD) for the select neuroanatomy across the various cohorts.	80
Table 4.2 The significant [¹⁸ F]FDDNP mean values across all cohorts.	81
Table 4.3 The significant [¹⁸ F]FDDNP mean binding values across all cohorts with the control group reclassified.	83
Table 4.4 The [¹⁸ F]FDDNP DVR patient binding values in the younger control group. (19 ROIs)	84
Table 4.5 The [¹⁸ F]FDDNP DVR patient binding values in the Older Control group (>60 yrs).	85
Table 4.6 The [¹⁸ F]FDDNP DVR patient binding values in the PSP group.	87
Table 4.7 The [¹⁸ F]FDDNP DVR patient binding values in the PD group.	88
Table 4.8 The [¹⁸ F]FDDNP DVR patient binding values in the HD group.	89
Table 4.9 The [¹⁸ F]FDDNP DVR patient binding values in the CTE group.	90

List of Equations

Equation 2.1 Logan graphical Analysis Distribution Volume Ratio (DVR).....	25
Equation 3.1 [¹⁸ F]FDDNP Total DVR signal in a select case of PSP.....	68

Acknowledgements

Thank you to my Dissertation committee for being with me on this long journey. I regard each and every one of you as an expert in the field I have researched and regard each opinion with the utmost respect. The bar you have set has always driven me to push myself as hard as I possibly can to always be a better scientist and researcher. Not many students can be so lucky to have such a well-rounded dissertation committee with opinions that are so highly respected in his field. I have often felt like I only know how to take the difficult paths, but I also realize that it is here where I seem to learn the most.

Above all others I must thank my beautiful wife whom has stuck beside me throughout the duration of my Ph.D. The many nights I would come home late from lab or be up late writing or analyzing data, you have been more understanding and supportive than anyone should ever be asked. Thank you for being a best friend in actions and not just words. I discovered many years ago, while racing around the world together, that I am always best when I am with you and my strongest when we are working together. What you have given me I will never be able to put into words, but I can always start with “I love you.”

My parents have been the greatest influence on my character and my life. My father showed me at a very young age not only what it meant to work hard, but also how important it is to show compassion to others and do what is right. My mother has always provided the logical guidance in my life and shown me how to use reason in solving problems; in science or life. She has not only given me wisdom in my life, but will always be the voice in my head guiding me through my decisions. The compassion and reasoning are what led me to working in real world applications that possess the capability to help others and to help to improve the medical healthcare of people everywhere.

I am thankful every day for the opportunity to work in Dr. Jorge Barrio’s lab and it has been a great honor to work with some of the most advanced imaging techniques on the planet. Many professors will watch over their candidates to dictate how every aspect of the research

should be performed, but I was fortunate to have a mentor who allowed me to figure out much of it through my own investigations. There have been many times where the struggle had left me feeling dejected and worn out. After speaking with Dr. Barrio my spirits were often lifted and I would leave his office with the same enthusiasm with which I began this research.

I am thankful for the support I received while I was in my Masters in Applied Physics at CSULB; Dr. Gu, Dr. Bill and Dr. Kwon. Without a strong foundation a house will not stand and it was in Long Beach I began to build the confidence required of a Ph.D. candidate.

Thank you to everyone in the lab. Jie thank you for the many batches of $[F^{18}]FDDNP$ you made for my research. Without you, I quite literally would not have been able to perform my research. Your hard work has always been an inspiration and thank you for always answering any silly chemistry question I had for you. You were always straightforward and truthful, a trait lacking in many modern scientists. You are and will always be our lab mother, so thank you for seeing your “sons” through their PhD’s.

KP thank you for the many hours spent helping solve computer issues and helping me with any issues running software. Your patience is only surpassed by your intellect. The kindness you have shown me in my times of academic need will always be appreciated.

Dr. Saty, thank you for the many conversations we have shared during my time at UCLA during my pursuits. The world has become a different place since I first began UCLA, but your words have always brightened my outlook and given me hope that many people in the World share our compassion and hope. Thank you for always offering advice and help whenever it has been needed.

Dr. Huang thank you for allowing me the opportunity to work alongside your lab and use all the many fruits of your hard labor over these years. Your dedication to the field of molecular imaging, mathematics and computer science is an inspiration to know that it is possible for a scientist to know a multitude of topics and be good at all of them.

Dr. Small, thank you for being a part of my dissertation committee and donating your time when I have asked you to listen to my thoughts and research on these topics. Your clinical expertise in these fields has been a guiding force for me to not only learn this material I present before you, but to understand the importance of practicality in the face of innovation.

Vlado, thank you for the guidance during the time we shared at UCLA. I always appreciated the help and the candid conversations in between our work. Thank you for having so much information than I seemed to never find in textbooks. I enjoyed the laughs we shared and if I listen carefully enough I can almost hear it in the halls of the B-level in CHS.

Andrew, it has been a privilege to get to know you and I have been thankful for our many entertaining conversations, both academic and others. Thank you for disagreeing with me on a regular basis. You showed me how important it is to be able to have discussions with people who have opinions that are different from your own. I have full faith that you will find your place in this World and you will contribute great things. Thank you for all the support and help you provided me while stumbling through my early beginnings in lab.

Claudio, thank you for all the help you provided while you worked in Dr. Barrio's lab. Especially for all the help you would lend whenever I had a question for you, most notably the immunohistochemistry. Thank you for giving a physicist a shot at working in biology and for being a mentor both in lab and life. Your friendship has been worth its weight in exotic antibodies.

Dr. Yazeed Alhiyari, you have been a friend and a brother during my time at UCLA. You were one of the first people to help me learn molecular biology techniques and coming from my "Physics only" background, we both had our work cut out for us. Thank you for all the knowledge and help you have given me over the years. You are one of the most talented researchers I have ever come to personally know and I have faith you will find your way back to the lab one day because it would be a travesty for science, should you not. The laughs and running we have shared during our time were what helped get me through my PhD.

Mike McNitt-Gray, I cannot thank you enough for accepting me in this program and taking a chance on a student from Riverside. My time at UCLA was filled with laughter, joy and tears; I am thankful you were a part of most of it. Thank you for letting me sit in on one of your lectures almost 9 years ago, as it was the beginning of my attendance at UCLA and membership to the exclusive BMP program. Thank you for being a support for all of us students during our time here.

Reth, thank you for your help and support throughout my time at UCLA. I have enjoyed sharing many memories with you and being able to call you a friend. I am sure our families will be friends for a long time to come.

Terry Moore, I know you cannot read this but I know that you are smiling down from heaven. You were the reason I joined Dr. Barrio's lab and you were also the one who helped me so many times while I was bouncing between the BMP program and reality television. For such a small woman you had so much life and a huge heart. The world lost a bright shining star on this Earth the day you passed, but inevitably stars are meant to shine in the heavens to be shared with all. I will never forget you and every time I hear the beat of a drum, I will think of you. You were my BMP mother and I can't help but know that you would be proud of what I have done here and that I have finished.

Adora Borealis, I hope one day to make you proud. I will do my best to make this world a better place for you. You are more than simply inspiration to your father; you are hope. I love you with all my heart.

There have been many people along the way who helped me in some shape or form and I have appreciated each and every one of you. It is said that it takes a village to raise a child. I know now that it takes a department to raise a Ph.D. and sometimes several departments. I am a Bruin and I will always "Fight, fight fight!"

Preface

[¹⁸F]FDDNP has been established in previous work as an excellent *in vivo* imaging tool for neurodegenerative disease. It has previously demonstrated an ability to differentiate between the binding of [¹⁸F]FDDNP in a healthy control patient against: Alzheimer's Disease, mild cognitive impairment, Gerstmann–Sträussler–Scheinker Disease, Parkinson's Disease, Progressive Supranuclear Palsy and most recently, Chronic Traumatic Encephalopathy. The ability of [¹⁸F]FDDNP to bind to both amyloid and tau proteins *in vivo* has widespread potential applications to distinguish with these neurodegenerative diseases.

During the course of my study it has become clear how important it is for us to understand the fundamental differences in neurodegenerative diseases. In the next few decades, the human population is on course to triple the number of dementia patients found worldwide. If we have done nothing to prevent or treat these massively growing disease populations, we will be faced with a devastating economic and emotional burden.

In this scientific investigation, I received a portion of brain tissue from a former patient who donated their most precious organ to help my research. Throughout the course of work with this brain tissue, I have not forgot how important it is for all of us to donate our organs after our deaths. I am thankful that someone was selfless enough to donate their brain in the hopes that one day they might help a stranger afflicted with the same debilitating disease.

In correlating the presence of tau to the binding of [¹⁸F]FDDNP, it was astounding at the density of hyperphosphorylated tau (p-tau) in the brain of the PSP patient. Particularly in the white matter of the cerebellum, the tau fibrils appeared in highest density at the white matter-granular layer interface. Understanding the point of origins for hyperphosphorylated tau might one day provide insight into the molecular underpinnings. Studying neurodegenerative disease needs to be done in populations at the earliest stages of the disease to have any chance at identifying the key molecular machinery responsible for such eventual large-scale neurological destruction. [¹⁸F]FDDNP demonstrated binding in regions with heavy amounts of tau and it

should be considered a strong radiotracer to image tauopathies. Since the concept of amyloid and tau neurodegeneration has slowly begun to shift away from the “Amyloid Cascade Hypothesis.” It is more important now more than ever that we begin to turn our attention to tau and the mechanisms that induce its aberrant aggregation.

Vita

1998-2000	Riverside Community College Riverside Scholar
2000-2004	University of California, Riverside Riverside Scholar
2004	University of California, Riverside Bachelors of Science (BS) in General Physics
2006-2009	California State University of Long Beach Graduate Student Researcher/Lab Instructor
2009	California State University of Long Beach (CSULB) Masters of Science (MS) in Applied Physics
2010-2014	Cota-Robles Fellow Dept. of Molecular & Medical Pharmacology (UCLA)
2010-2017	Graduate Student Researcher Dept. of Molecular & Medical Pharmacology David Geffen School of Medicine Los Angeles, CA
2013	Pharmacology Student Representative Dept. of Molecular & Medical Pharmacology (UCLA)
2015	Biological Sciences Council Member (UCLA)
2015	Masters of Science in Biomedical Physics Dept. of Molecular & Medical Pharmacology University of California, Los Angeles (UCLA)
2017	Doctorate of Philosophy in Biomedical Physics (<i>expected</i>) Dept. of Molecular & Medical Pharmacology The Barrio Lab University of California, Los Angeles (UCLA)
2017	Postdoctoral Research The Scafoglio Lab David Geffen School of Medicine University of California, Los Angeles (UCLA)

Presentations & Publications

April O'Brien, Brendon Villegas, J.Y. Gu, Sputtered magnesium diboride thin films: Growth conditions and surface morphology, *Physica C: Superconductivity*, Volume 469, Issue 1, 2009, Pages 39-43, ISSN 0921-4534, <http://dx.doi.org/10.1016/j.physc.2008.10.006>.

Spring 2015 Research Colloquium Dept. of Physics & Biology in Medicine
University of California, Los Angeles (UCLA) Los Angeles, CA

Villegas, B. The *ante mortem* [^{18}F]FDDNP correlation to the *post mortem* [^{18}F]FDDNP signal and neuropathology in a select case of Progressive Supranuclear Palsy (PSP). 2017 (Unpublished)

CHAPTER ONE: PURPOSE AND ORGANIZATION

Neurodegenerative diseases are chronic conditions affecting a large portion of the human population; inevitably resulting in the death of the afflicted patient. The stark conditions facing neurodegenerative diseases stem from a lack of effective therapeutics. In the rare occasions where specific genetic mutations have been identified associated with the disease, as in the case of Huntington's disease no successful adjuvant therapies have yet demonstrated efficacy to contain the progression of disease (Kipps et al. 2005). It has been reasonably extrapolated that due to an increasing life span in conjunction with an increasing population, the worldwide population of dementia patients will triple in magnitude over the next 33 years (Gaugler 2016). The burden of a disease will not only take a massive emotional toll on the human population, but it will also be economically devastating if proper measures have not been taken to prepare or prevent dementia based on current projections (Wimo et al. 2017). In the age where the distended family has replaced the nuclear family, many elderly will not have family members in close proximity to them. If research has not made advances in understanding the earliest molecular underpinnings of neurodegenerative disease in an effort to prevent disease, the toll may be untenable. Molecular Imaging may be one of the few imaging modalities capable of providing *in vivo* insight into these neurodegenerative pathologies before they progress through the human brain. Positron Emission Tomography (PET) allows a non-invasive look into the affected neuroanatomy to provide some qualitative and quantitative information about the progression of a patient's disease in the presence of small but detectable amounts of the binding target. As an example, the use of the pioneering Positron Emission Tomography (PET) radiotracer 2-deoxy-2-(¹⁸F)fluoro-D-glucose (FDG) established that PET imaging is capable of detecting metabolic changes in tumor growth prior to morphological changes seen in a Magnetic Resonance Images (MRI) (Gallamini, Zwarthoed, and Borra 2014).

In the early twenty-first century, PET imaging began to turn its focus towards neurodegenerative disease, in an effort to better characterize and explore the underlying

pathology that had previously been discernible only at patient autopsy. In 1996, the compound DDNP was identified as a fluorescent dye capable of binding to molecular targets with a fluorescent Stokes shift to allow the differentiation between bound and unbound targets *in vitro* (Jacobson et al. 1996). In 2001, the hydrophobic compound was radiofluorinated and 2-(1-(6-fluoroethyl)(methyl)amino)-2-naphthyl}ethylidene)malononitrile ($[^{18}\text{F}]\text{FDDNP}$) demonstrated an ability to bind to amyloid beta plaques and neurofibrillary tangles in the brains of Alzheimer's Disease (AD) patients (Shoghi-Jadid et al. 2002). $[^{18}\text{F}]\text{FDDNP}$ has also been shown to bind to the *post mortem* brain tissue of Alzheimer's Disease and Dementia with Lewy Bodies (DLB) pathology *in vitro* (Smid et al. 2006; Smid et al. 2013). A previous study of PSP patients revealed several regions of the brain that were capable of differentiating between PSP and Parkinson's Disease; most notably the binding of $[^{18}\text{F}]\text{FDDNP}$ to the midbrain (Kepe et al. 2013). The binding of $[^{18}\text{F}]\text{FDDNP}$ to hyperphosphorylated tau pathology in a neurodegenerative tauopathy is evidence of the strength of the radiotracer as a possible diagnostic tool. This dissertation is the first-time evidence that the *in vivo* binding of $[^{18}\text{F}]\text{FDDNP}$ in the brain of a patient with PSP is correlated to the *in vitro* binding of in the *post mortem* brain tissue $[^{18}\text{F}]\text{FDDNP}$ binds to the cross- β pleated sheet formation present in both amyloid and hyperphosphorylated tau fibrils (Miller, Ma, and Nussinov 2011). The $[^{18}\text{F}]\text{FDDNP}$ binding affinity to $\text{A}\beta_{1-42}$ was calculated *in vitro* using synthesized amyloid fibrils revealing both a low and high affinity binding site (Agdeppa et al. 2001). The synthetic process used to produce stable hyperphosphorylated tau can produce a variety of tau fibrils; making it more difficult to accurately characterize the *in vitro* binding affinity of $[^{18}\text{F}]\text{FDDNP}$ to the native hyperphosphorylated tau found in the diseased brain (Xu et al. 2010).

In the last 26 years, clinicians and neuroscientists have postulated that the amyloid beta proteins have been the driving force behind dementias such as Alzheimer's Disease; termed the "amyloid cascade hypothesis" (Hardy 2017). However, the evidence seems to suggest that hyperphosphorylated tau is the driving pathology behind the neurodegenerative process in

Alzheimer's Disease (Sevigny et al. 2016). The misfolded hyperphosphorylated tau protein appears to correlate better to cognitive dysfunction in diseased patients (Brier et al. 2016). The lack of efficacy of anti-amyloid therapies has raised additional questions about the association between cognition and amyloid deposition (Lockhart et al. 2007).

The ability to track neurodegenerative disease in its earliest stages of deposition or what is referred to as “preclinical,” may ultimately be the first major step in identifying a therapeutic window capable of curbing the massive cell loss in the diseased patient brain. The examination of an *in vivo* [¹⁸F]FDDNP scan of a PSP patient and comparison to the *in vitro* [¹⁸F]FDDNP binding and immunohistochemical staining in the *post mortem* pathology demonstrates our ability to track the p-tau pathology; which ultimately might be a more accurate indicator of neurodegenerative disease progression. This study is important, as it enlightens our understanding of the binding of [¹⁸F]FDDNP to hyperphosphorylated tau (p-tau) in the native PSP brain. We are also provided with a better understanding of the *in vivo* binding of [¹⁸F]FDDNP to the tau signal in the Distribution Volume Ratio (DVR) images of neurodegenerative disease patients.

Distinguishing the binding of [¹⁸F]FDDNP to amyloid beta or p-tau in patients with full or partial tauopathies can make it difficult to discriminate between neurodegenerative diseases where comorbidity may exist. Progressive Supranuclear Palsy can be misdiagnosed as Parkinson's Disease in the early course of the disease as a progressive loss of dopaminergic neurons may result in an overlap of symptoms between the two diseases (Liscic et al. 2013). CTE and PSP are both tauopathies and while clinically they may differ symptomatically, they share several regions of brain anatomy that are heavily burdened by hyperphosphorylated tau. Huntington's disease (HD) is a motor disease with destructive mutant Huntingtin inclusions caused by abnormal CAG repeats that does not typically contain any tau or amyloid beta (Ross and Tabrizi 2011). The cohort of HD patients act as a sort of neurodegenerative disease negative control as the HD patients experience motor dysfunction but do not possess either tau or

amyloid pathology. The healthy control patients provide a baseline [¹⁸F]FDDNP signal for what could be considered healthy human brains with normal pathological aging. Appropriately diagnosing a patient may tremendously impact the treatment a patient receives and [¹⁸F]FDDNP can potentially diagnose and track therapeutic efficacy in the patient brain.

A portion of time spent on this research was devoted to determining the appropriate experimental methods to study the *post mortem* brain tissue of a patient who had previously been imaged *in vivo* with [¹⁸F]FDDNP. This dissertation also reflects the massive time spent developing a sectioning technique for the brain tissue, collecting data from the brain specimen and analyzing it through several different experimental methods. The other major portion of this work consisted of the production and analysis of 98 individual [¹⁸F]FDDNP DVR 3-dimensional maps of every patient brain from 6 distinct cohorts; each with 19 different Regions of Interest (ROI's) analyzed with several statistical methods to determine if any significance exists between the regional group means.

1.1 Specific Research Aim 1: Correlation of *ante mortem* [¹⁸F]FDDNP PET and *post mortem* Brain Tau Pathology Distribution in a Case of Progressive Supranuclear Palsy (PSP).

This work seeks to investigate the *in vivo* [¹⁸F]FDDNP binding seen in the brain of a patient with PSP to the *in vitro* autoradiography and immunohistochemical staining found in the *post mortem* brain tissue. The aim is to investigate the binding of [¹⁸F]FDDNP in the neuroanatomy in an effort to determine if it is either amyloid beta, hyperphosphorylated tau (p-tau), a composite of the two proteins or neither. The unique feature of Progressive Supranuclear Palsy is that the disease is a tauopathy and the absence of amyloid beta is typical of the disease. [¹⁸F]FDDNP has a binding affinity for both amyloid and tau, which allows the unique opportunity to study the radiotracer binding to p-tau in the neurodegenerative disease brain without the presence of amyloid. The hypothesis posits that the elevated binding of [¹⁸F]FDDNP

in the PSP patient brain should reflect the hyperphosphorylated tau (p-tau) pathology we find in the corresponding neuroanatomy.

1.1.1 Methodology for [¹⁸F]FDDNP PET signal co-registration with immunohistochemical staining.

The tissue sections are sliced on either a cryomicrotome or a cryomacrotome and subsequently mounted on glass slides for further investigation. The presence of p-tau in the brain regions labeled by [¹⁸F]FDDNP can be demonstrated through both immunohistochemical (IHC) staining and immunofluorescence (IF). The monoclonal mouse antibodies recognizing the Paired Helical Filamentous tau (PHF-tau) and Amyloid beta (6F/3D) reveal the deposition pattern in the PSP brain through immunohistochemical staining (IHC). Optical IHC staining is resolved with Diaminobenzidine (DAB) and can be used for direct comparison to [¹⁸F]FDDNP macroautoradiography on adjacent tissue slides.

Comparative fluorescence allows us to visualize the comparison between the binding of FDDNP and known binding agents for tau and amyloid at the microscopic level. Histofluorescence with “cold,” unlabeled FDDNP demonstrates the specific types of pathological isoforms the radiotracer [¹⁸F]FDDNP is labeling in the PSP patient brain. In the PSP brain, we expect to encounter a variety of pathological hallmarks all formed from the underlying p-tau; each isoform presenting a unique geometry, size and morphology. The immunofluorescence uses the same PHF-tau antibody as the immunohistochemical staining in conjunction with a fluorescent secondary antibody (Alexafluor 488, Thermofisher) to visualize under a fluorescent microscope. Thioflavin S is a fluorescent dye that fluoresces when bound to neurofibrillary tangles or amyloid beta *in vitro* and can be viewed with minimal background signal using the standard FITC filter set (ex 470±20 nm, em 515± 20 nm) (Sun, Nguyen, and Bing 2002).

The [¹⁸F]FDDNP Distribution Volume Ratio (DVR) image is co-registered to a structural Magnetic Resonance Image (MRI) of the patient brain to properly extract the corresponding binding values measured through IHC and autoradiography. The stained *post mortem* tissue

was manually aligned to the MRI using notable structures in the brain anatomy and guidance with a 7.0 T MRI brain atlas with coregistered cryomacrotome sections (Salles and Gorgulho 2010). The 28 different regions of the brain sampled for comparison were selected to provide an adequate representation of the gross anatomy with the tissue available for this study.

The cutting of the brain tissue to a maximum thickness of 40 μm is necessary for proper optical visualization of the stains under the light microscope with minimal background. The difficulty of slide preparation cannot be underestimated, since proper microscopic visualization is a factor of tissue thickness, tissue integrity, consistent sectioning and quality mounting to the glass slide. The large hemisphere sections of brain tissue cut on the cryomacrotome have the advantage of displaying immunohistochemical staining in a single plane. The large coronal tissue section (**Figure 3.4-II**) was cut into smaller pieces on the cryomicrotome for high magnification of the immunohistochemistry and immunofluorescence. The large and medium sized slides were photographed using a Canon T4i Rebel digital camera mounted on a vertical arm attached to a wooden base where the slides could be photographed. Most conventional optical and fluorescent microscopes have a stage limitation so that glass slides physically larger than 50 mm x 75 mm will not fit on the viewable area and tissue sections greater than a 20 μm thickness will have increased background under high magnification.

1.2 Specific Research Aim 2: Mapping Brain [^{18}F]FDDNP PET Parametric Distribution Volume Ratio (DVR) to Compare Neurodegenerative Tauopathies with Controls.

In this portion of my research the focus was investigating whether [^{18}F]FDDNP PET is capable of differentiating between Alzheimer's Disease (AD), Mild Cognitively Impaired (MCI) and healthy age-matched control patients (Small et al. 2006). [^{18}F]FDDNP PET demonstrates a statistically significant brain binding difference between subjects with Progressive Supranuclear Palsy and Parkinson's Disease (Kepe et al. 2013). A group of CTE patients showed a heavy binding of [^{18}F]FDDNP in the amygdala and midbrain as compared to age-matched control

patients [^{18}F]FDDNP (Kepe et al. 2013; Barrio et al. 2015). This is the first large (N=98) retrospective study comparing the binding of [^{18}F]FDDNP amongst multiple neurodegenerative diseases and healthy control patients. The ability to diagnostically distinguish between certain neurodegenerative diseases using [^{18}F]FDDNP is expected to provide a huge advantage for clinicians; especially in the early stages of disease progression.

Chronic Traumatic Encephalopathy and Progressive Supranuclear Palsy share the common pathological burden of widespread hyperphosphorylated tau (p-tau) throughout the brain. PSP and Parkinson's Disease often share clinical profiles and may have overlapping symptoms, which can make proper treatment difficult for the healthcare provider. The cohort of HD patients does not share any particular symptom or pathology with the other diseases. In a few rare cases of HD, the clinical symptoms or pathology that contained the mutant HTT gene do have p-tau co-localized with the HTT inclusions, but this appears to be atypical (Vuono et al. 2015). The healthy control patients serve to establish a baseline of the mean binding of [^{18}F]FDDNP in pathologically unremarkable patients.

1.2.1 Methodology for [^{18}F]FDDNP binding comparison amongst a variety of neurodegenerative disease cohorts.

Each patient in this study was infused with a bolus injection of 10 mCi of [^{18}F]FDDNP radioactivity and dynamically scanned for approximately 60 minutes post injection in the PET scanner. The cohorts consisted of patients classified as: Progressive Supranuclear palsy (n=12), Parkinson's Disease (n=16), Huntington's disease (n=15), Chronic Traumatic Encephalopathy (n=14), a Healthy Control Group above 60 years (n=24) and a Healthy Control Group below 60 years (n=17). The diseased patients were statistically tested against both younger and older control groups as well as a larger control group consisting of both control groups (n=41). The control group was reclassified in a larger cohort to more adequately compare the baseline binding of [^{18}F]FDDNP in a group that would be a better representation of binding in the neuroanatomy of healthy individuals across a spectrum of pathologically normal individuals.

Each dynamic [^{18}F]FDDNP PET scan is registered using either the summed images as a perfusion PET image (ECAT HR+, Siemens) or a CT scan (Biograph PET/CT, Siemens). The radioactivity in the cerebellar cortex is an optimal region to generate a Time Activity Curve (TAC) since it is typically free of disease. The linear portion of the TAC is used to estimate the concentration of radiotracer using the Logan graphical analysis in which every voxel of the PET signal is a representation of a Distribution Volume Ratio (DVR) of the concentration in the target tissue (C_T) to the reference tissue (C_R) (Wong et al. 2007). The first 6 minutes of the dynamic scan act as a perfusion image to highlight the neuroanatomy in order to delineate the Regions of Interest (ROI's) in each patient brain. Each image was co-registered using Statistical Parametric Mapping software (SPM12) and 19 individual ROI's were drawn on the 3-Dimensional [^{18}F]FDDNP DVR image using the software Amide (Loening and Gambhir 2003; Friston et al. 1994). Some patients had T1-weighted Magnetic Resonance Images (MRI) that were used to draw ROI's on the caudate nucleus and putamen; for all others the striatum was drawn on the summed images in the same manner as the other ROI's. The extracted DVR values will be evaluated with the software program SPSS to determine if any statistically significant differences exist between the cohort means in each Region of Interest (ROI).

CHAPTER TWO: BACKGROUND AND RELATED INFORMATION

Neurodegenerative diseases have been successfully impacted field by medical imaging in the last 50 years; shedding light on clinical diagnoses that were previously only discernible at patient autopsy. In particular, molecular imaging has helped elucidate the underlying molecular pathology that dominates many diseases such as Alzheimer's Disease (AD), Parkinson's Disease (PD) and cancer. The positron is a charged particle with the same mass of an electron but with a positive charge; the inevitable collision of the two particles is an annihilation event. Positron Emission Tomography (PET) imaging utilizes the positron-electron annihilation event resulting in two coincident 511 keV gamma rays emitted 180° apart; recorded by a surrounding detector ring. The detections are processed using filtered back projection to trace the detections along a Line of Response (LOR) to reconstruct a 3-dimensional image (Phelps et al. 1975). The LOR will have different regions of attenuation as it passes through bone and soft tissue; the gamma rays will be corrected appropriately. The functional imaging allows the *in vivo* detection of biomarkers or dynamic biological pathways that might otherwise be impossible to detect non-invasively. Detection of the earliest stages of neurodegeneration are key to understanding the etiology of such diseases and will be crucial in determining the underlying mechanisms necessary to develop effective therapeutics.

In 1935, Austrian physicist Erwin Schrodinger devised a thought experiment entitled "Schrodinger's Cat" to illustrate the complexity of Quantum Mechanics in a simplistic fashion (Schrödinger 1935). "Schrodinger's Cat" describes a cat inside a box with a vial of poisonous gas that becomes unleashed at some point, but the observer is unsure about the condition of the cat until they are able to look inside the box. It is being said that the very act of opening the box affects whether the cat is alive or dead; or until the observation is made, Schrodinger's cat exists in a duality where it can be both alive and dead. The analogy extends well to the investigation of biological systems in which it is necessary to perturb a system in order to study the characteristics of that system. When any biological system is studied, the tool being used to

investigate becomes part of the system and it can no longer be regarded as being static. PET radiotracers are not exempt from this concept, but it can be said that the trace amounts of probe used in human studies helps to essentially eliminate the impact they might have on the human biology.

2.1 Alzheimer's Disease (AD)

Alzheimer's Disease (AD) was first reported in 1906 by Dr. Alois Alzheimer as "a peculiar severe disease of the cerebral cortex" (Alzheimer 1906). Using a combination of histopathological stains, Dr. Alzheimer would discover "neurofibrillary tangles" and "amyloid beta plaques" in patients exhibiting this particular debilitating neurological disease (Alzheimer 1906). Along with the hallmark pathology, Dr. Alzheimer would note that these patients exhibited brain atrophy and he even studied a brain that contained "plaque only" pathology; believing that this patient was in an earlier stage of the disease (Alzheimer 1906). The brain disease associated with the plaques and tangles would later be coined "Alzheimer's Disease" by Dr. Alzheimer's mentor, Dr. Kraepelin (Graeber et al. 1997). The discovery of AD would mark the beginning of an investigative era of neuropathology where the two hallmark proteins, amyloid beta and hyperphosphorylated tau, would become the focus in studying the cause of neurodegenerative disease.

In 2010, it was estimated there were approximately 4.7 million individuals, 65 or older, living in the United States with Alzheimer's Disease (AD) and that total is projected to triple by the year 2050 to 13.8 million (Hebert et al. 2013). In 2015 it was estimated that approximately 46.8 million people were living with AD worldwide and by the year 2050, it is projected to rise to 131.5 million people (Prince 2016). Aside from the emotional toll on the family and patients afflicted with Alzheimer's Disease, there is a substantial economic cost inevitably incurred from treatment, hospitalization and some form of long-term care. It was reported that AD patients who received Medicaid assistance in the United States cost an average 19 times more than those patients without AD who also received Medicaid assistance (Gaugler 2016). As we face a tripling

population of patients who will require a substantive emotional and economic cost, it is imperative that we begin to understand the driving molecular mechanisms behind the amyloid beta and hyperphosphorylated tau misfolded protein pathologies. The large number of clinical manifestations of Alzheimer's Disease have allowed researchers to develop clinical guides in order to properly evaluate AD symptoms that describe a more accurate staging of the underlying pathology and underlying disease pathology. The CERAD rating system is designed to characterize the anatomical locations tau and amyloid deposition in the *post mortem* brain tissue and an appropriate intensity score for the IHC staining (Mirra et al. 1991). Proper *ante mortem* staging of AD symptoms can provide better treatment and easing of clinical symptoms, but sadly does very little to slow the progression of the disease and prevent the inevitable death of the patient. There have been statistically significant risk factors that have been found to be associated with Alzheimer's Disease; such as Apolipoproteins E3 and E4 or genetic heritage (Raber et al. 2000; Gaugler 2016). A pathological guide was created to stage the pathological progression of AD at autopsy (**Figure 3.5**), but of course this is only useful at autopsy to confirm the disease and properly stage it (Braak and Braak 1995). The Braak staging is based on the both the density and region of neurofibrillary tangles in the brain and the predictable pattern in idiopathic Alzheimer's Disease; comprising the majority of Dementia patients everywhere.

Alzheimer's Disease was discovered 116 years ago and since its discovery there have been no major advances in understanding how the disease originates in the human brain. For many years, scientists and researchers have held steadfast to a belief that amyloid beta fragments are the driving force behind the pathology and neurodysfunction. It is hypothesized that the mis-spliced amyloid beta results in a cytotoxic microenvironment and spreads like a prion disease, infecting other cells, resulting in heavy neuronal loss and causing the downstream production of hyperphosphorylated tau (Karran, Mercken, and De Strooper 2011). The debate over the origins

of Alzheimer's Disease will undoubtedly continue until there is more insight into the earliest stages of neurodegeneration.

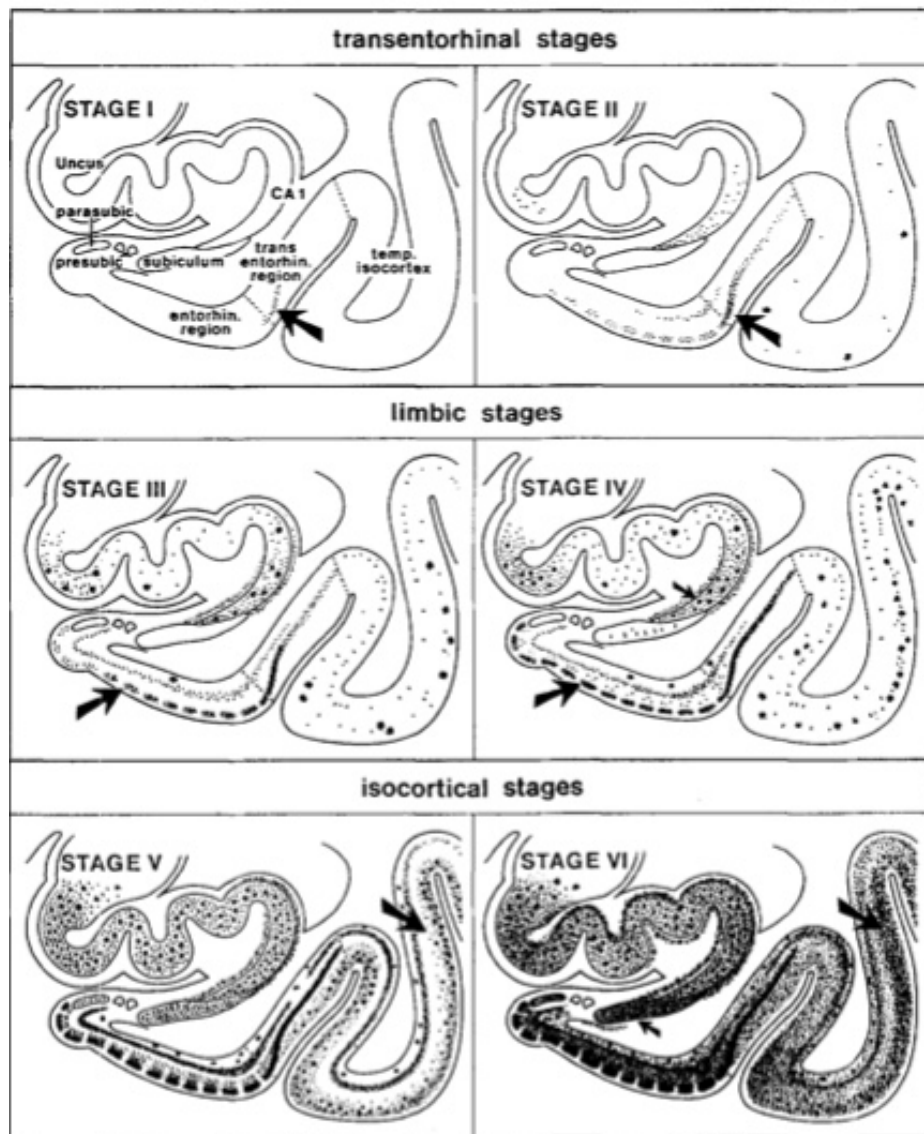


Figure 2.1. The Braak staging of Neurofibrillary changes in the Alzheimer's Disease (AD) brain (Braak and Braak 1995).

The staging of the progression of Alzheimer's Disease based on the pathological progression of neurofibrillary changes throughout the diseased brain. The staging of the Alzheimer brain is based on the tau pathology as Neurofibrillary Tangles (NFT) formation seen in the hippocampal formation, entorhinal region, transentorhinal region and the temporal cortex. The early stages I and II show deposition in the transentorhinal region of tau in sparse deposits. Stages III and IV show deposition in the limbic region of the brain, specifically in the hippocampal formation. At this stage of progression in the disease, there is no detectable atrophy or heavy change in the neocortex of the AD brain. At stages V- VI there is massive cell loss in the neocortex and the tau burden is dense in the limbic circuitry. At the final stages of the disease it is suggested that the disruption between the limbic circuitry and the neocortex most likely results in many of the clinical dysfunctions seen in the late stages of the disease.

2.2 Amyloid- β Protein

The insoluble amyloid- β protein is formed by the mis-splicing of the Amyloid Precursor Protein (APP) at a variety of residues; which results in the production of amyloid beta peptides of varying amino acid lengths (Kang et al. 1987). The β -secretase enzyme cleaves the extracellular domain of the APP transmembrane protein and it is the final cleavage of the remaining protein fragment by the γ -secretase enzyme in the transmembrane domain that produces the insoluble amyloid beta fragments (Tabaton and Tamagno 2007). Some of the Amyloid beta peptides that have been measured ranged from 30 to 55 amino acids with the two most abundant of those peptides associated with the plaque pathologies: A β 40 and A β 42 (Olsson et al. 2014). The Amyloid Precursor Protein is thought to be involved in synaptic formation, cell signaling and both structural and functional plasticity among the roles it may play (Turner et al. 2003; Priller et al. 2006). The normal splicing of the Amyloid Precursor Protein under healthy circumstances probably results in amyloid beta proteins that perform some normal signaling function and solubilize in the extracellular space afterwards. The abnormal splicing of APP results in varying lengths of the insoluble amyloid beta peptides which have been found deposited in regions exhibiting neurodegeneration (Koo, Lansbury, and Kelly 1999). The insoluble proteins that remain in the extracellular space will eventually begin to aggregate and form senile plaques. This co-localization of plaques and neuronal death has aided in fueling the amyloid cascade hypothesis; which attributes the clinical advancement of Alzheimer's Disease to the pathological increase in amyloid- β (Karran, Mercken, and De Strooper 2011). The amyloid cascade hypothesis posits that the appearance of the insoluble amyloid beta protein initiates a "cascade" of cellular dysfunction resulting in neurodegeneration and cell loss. It has even been suggested that the appearance of neurofibrillary tangles is a secondary pathological result of the cytotoxicity exhibited by the amyloid beta misfolded proteins (Hardy 2017).

Recent innovations in clinical therapies have resulted in the development of a variety of treatments to clear amyloid- β from the parenchyma of the diseased brain as measured by the CSF (Blennow et al. 2010). Several of these immunotherapies have demonstrated an ability to successfully clear amyloid- β from the brains of transgenic mice and humans (Sevigny et al. 2016). One major concern in consideration of neurocognitive improvement is the assessment of the amyloid burden in relation to the patient performance on the Mini Mental State Examination (MMSE) administered by the clinicians. The MMSE itself is a 30-point examination to measure cognitive impairment in a patient who may already have begun to exhibit cognitive decline (Tombaugh and McIntyre 1992). The sensitivity of the MMSE may not be completely indicative of the patient neuropathology and by itself may not be a reliable measure of cognitive improvement (Lacy, Kaemmerer, and Czipri 2015). The FDA approved the [^{18}F]-labeled PET radiotracer, Florbetapir in 2012 to be used to confirm the presence of the Alzheimer's Disease pathology, amyloid beta (Beach et al. 2014). Florbetapir has demonstrated a binding affinity for the beta-amyloid protein *in vitro* and it appears to also demonstrate an affinity for amyloid *in vivo*. One major concern in using Florbetapir is its low specificity and the low retention in the hippocampus; one of the first neuroanatomical regions to display amyloid- β in Alzheimer's Disease (Tauber et al. 2013). Florbetapir is capable of positively identifying 69.1% of the population classified between Braak stages III and V, but fails to classify 31.9% of AD patients in the same Braak Staging window as having a negative scan and being non-AD (Beach et al. 2014). This inadequate diagnosis of AD using Florbetapir may make it difficult to correlate cognitive improvement with the MMSE score after administration of a clinical therapy. Since Florbetapir is the standard PET imaging diagnostic aid at the moment, its failure to discriminate a portion of the AD population ultimately diminishes the reliability of the radiotracer as a pathological assessment. Assumptions are made that a positive Florbetapir signal indicates some Braak stage of AD and the presence of amyloid is the cause of a patient's cognitive decline. Statistical changes measured after a clinical therapy using a Florbetapir scan,

may be misleading to the researcher if the *in vivo* binding is not measuring all the pathology present in the diseased brain.

It has recently been demonstrated that the presence of A β ₁₋₄₂ in elevated levels of cognitively healthy seniors appears to be a part of the normal aging process and has resulted in a new classification entitled “pathological aging” (Maarouf et al. 2011). It has also been suggested through *in vitro* studies with amyloid- β 1-40 and 1-42, that the peptides are able to maintain their monomeric structure up to a length of approximately 3 μ m, at which a conversion process occurs and aggregation increases the formation of amyloid beta oligomers (Nag et al. 2011). It is this oligomeric form of amyloid beta many believe creates the cytotoxic environment inhibiting neuronal functions such as long-term and short-term potentiation (Walsh et al. 2002; Wang et al. 2002). The A β oligomers are shown to exist in a wide array of sizes from less than 10 kDa to greater than 100 kDa in size, increasing the difficulty of investigating structure and function behind the mechanisms that might induce cytotoxicity in the microenvironment (Ahmed et al. 2010).

2.3 Hyperphosphorylated Tau Protein

When Dr. Alzheimer first observed the hallmark pathology that would later bear his namesake, he not only observed Amyloid beta plaques, but also neurofibrillary tangles (Alzheimer et al. 1995). Neurofibrillary tangles arise from the microtubule associate protein tau (MAPT), which is essential for *in vitro* microtubule assembly along with α and β tubulin (Weingarten et al. 1975; Wang and Mandelkow 2016). These tau isoforms form intracellularly and can be found aggregated in the form of paired helical filamentous (PHF) tau consisting of two 10 nm neuropil threads wound with a half periodicity of 80 nm (Morishima-Kawashima et al. 1995). The tau isoforms that are measured in the PHF-tau are found to have undergone hyperphosphorylation and it is critical in the formation of the coiled fibrils. The hyperphosphorylated tau pathologically presents in neurons and in some cases glial processes, but overall tends to correlate better with the clinical progression of Alzheimer’s Disease and

better parallels neurological dysfunction than the presence of amyloid beta plaques (Murray et al. 2015).

The tau (τ) protein is an abundant protein found in the Central Nervous System (CNS) and is a member of a class of proteins known as Microtubule Associated Proteins (MAP). The tau protein has six isoforms found in the human brain and are encoded by the q-arm of Chromosome 17 located at 17q21. The alternative splicing at exons 2, 3 or 10 in the mRNA transcript result in either 3 or 4 repeat sections in the carboxy terminus (Tawana and Ramsden 2001). The six tau isoforms found in the human brain range in length between 352 to 441 amino acids. In the healthy human brain the 3R forms of tau are slightly more abundant than the 4R tau proteins. The tau proteins are found in different distributions at early stages of human development; which supports the idea that the ratio and distribution of tau proteins might change into adulthood (Buee et al. 2000). The extracellular hyperphosphorylated tau (p-tau) is often seen as fibrils or ghost tangles in the presence of destroyed neurons. It is thought that the tau oligomers can disrupt cellular processes such as autophagy, axosomal transport and normal healthy cellular processes (Gendreau and Hall 2013).

The tau protein is typically expressed intracellularly, but recently emerging evidence has suggested that neuronal stimulation might induce tau release to the extracellular space where its exact function is not fully understood. The propagation of hyperphosphorylated tau pathology throughout different brain regions is thought to possibly transmit via a leaky membrane once the axonal degeneration begins to occur or through exocytosis into the synaptic cleft where it can be uptaken at the post synapse (Wang and Mandelkow 2016). Certain diseases such as Alzheimer's Disease are limited in their expression of p-tau to the grey matter regions in the brain, but some brain diseases such as Progressive Supranuclear Palsy or Chronic Traumatic Encephalopathy see an upregulation of the protein in both the grey and white matter of the brain. The prevailing question associated with the presence of p-tau appears to be the role

associated with neuroinflammation in glial cells and the role they play in the downstream neurodegeneration (Leyns and Holtzman 2017).

2.4 Progressive Supranuclear Palsy (PSP)

Progressive Supranuclear Palsy was originally referred to as Steele-Richardson-Olszewski syndrome after the research team of doctors who first described the disease (Tawana and Ramsden 2001). The multisystem disease was first described in their paper as a “supranuclear ophthalmoplegia affecting chiefly vertical gaze, pseudobulbar palsy, dysarthria, dystonic rigidity of the neck and upper trunk, and other less constant cerebellar and pyramidal symptoms.” It was initially noted as a neurodegenerative disease, the symptoms were distinct from other motor diseases. It was also postulated that PSP could have been present in the population for some time, but due to the rigidity feature of the disease might in fact have been mistaken for Parkinson’s Disease (Steele 1964). PSP is classified as a “4-Repeat tauopathy” due to the overly abundant 4R-tau proteins found throughout the patient brain.

A previous [¹⁸F]FDDNP study on striatum, thalamus, subthalamic area, midbrain and the cerebellar white matter (Kepe et al. 2013). Using the cerebellar gray matter of the brain as a well perfused, relatively disease free area as the reference region from which to create a DVR image works well since it is has been demonstrated through immunohistochemistry that the cerebellar cortex remains relatively unaffected by the misfolded tau protein (Piao et al. 2002). The mean DVR values in the striatum, thalamus, subthalamic area, midbrain and the cerebellar white matter were respectively (1.443, 1.478, 1.434, 1.367 and 1.209) in the PSP patients while in the control patients the means measured (1.250, 1.250, 1.233, 1.167 and 1.076) (Kepe et al. 2013). The significant binding increase in the PSP patient brain can be attributed to the presence of hyperphosphorylated tau, assuming that the tauopathy was the primary affliction causing neurological dysfunction at the time of scanning. The presence of hyperphosphorylated tau in the cerebellar white matter is a hallmark of PSP and helps to distinguish it from other tauopathies (Liscic et al. 2013).

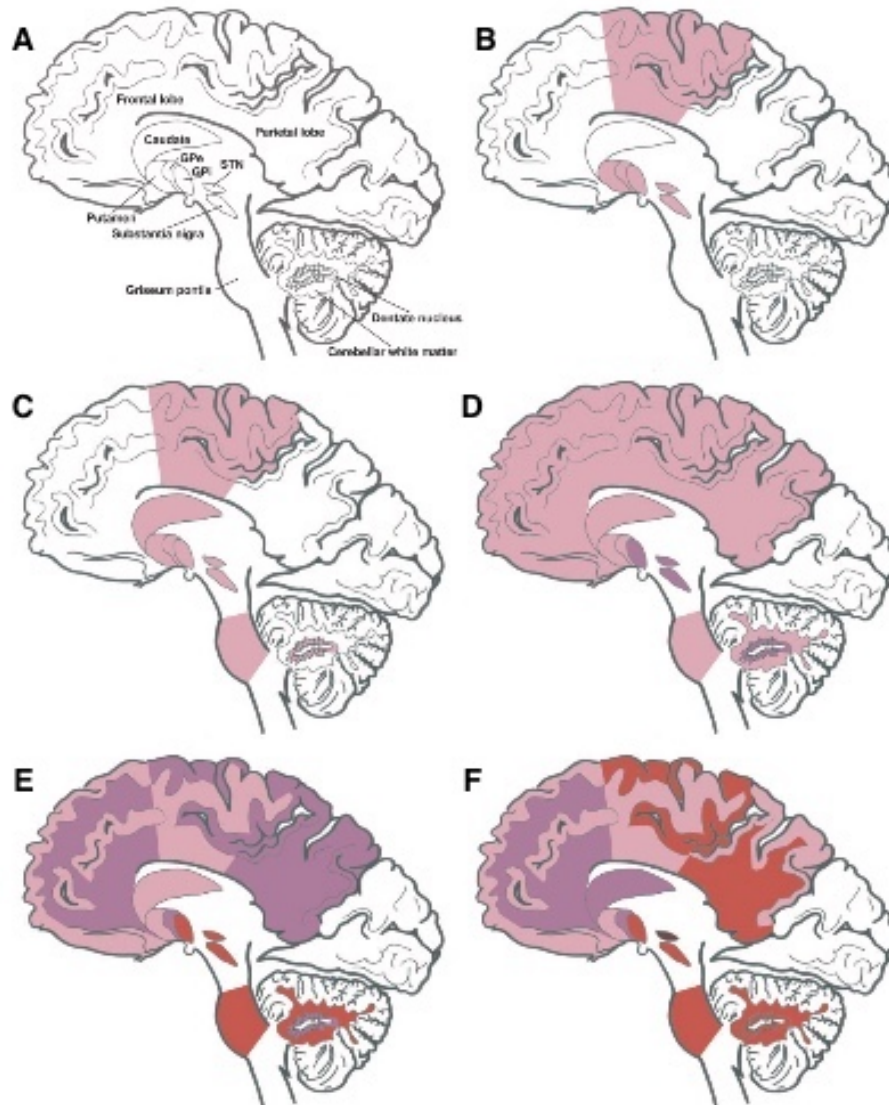


Figure 2.2 Progressive Supranuclear palsy disease progression of tau.

A model of the distribution of median coiled body and tau fibril pathology in the progression of PSP disease in the human brain. **A.** Shows the anatomy of the figure and **B – F** show the progression of the disease. A previous scale had been developed to differentiate PSP-Richardson’s (PSP-RS) from PSP-Parkinsonism (PSP-P). It was reported that despite the clinical spectrum between patients and the heterogeneity of tau deposition, the progression tends to appear similarly across patients. Color scheme represented by white/grade 0; purple/grade 2; red/grade 3; brown/grade 4. **B.** PSP-tau score 0-1 **C.** PSP-tau score 2-3 **D.** PSP-tau score 4-5 **E.** PSP-tau score 6-7 **F.** PSP-tau score >7. This progression model helps provide some insight into how tau progresses in the patient and the severity of the disease (Williams et al. 2007).

2.5 Huntington’s Disease

Huntington’s disease is a neurodegenerative disease that is autosomal dominant and results in an expansion of the polyglutamine (polyQ) segment in the first exon (EX1) in the

Huntingtin protein (Htt) (Kim 2013). The disease results in a significant amount of these large mutant Htt proteins (>35 kDa) within the cytoplasm of the cell. The exact molecular mechanism that induces cell apoptosis is not completely understood, but is widely accepted that cytotoxicity results in a substantial loss of GABA producing medium spiny neurons in the basal ganglia of the Huntington's patient (Ehrlich 2012). The cell loss causes substantial atrophy and a loss of projection fibers extending from the striatum to the substantia nigra pars reticulata (SNr) and globus pallidus externus (GPe) (Kipps et al. 2005). The Huntington's disease onset occurs at a reasonably young age for neurodegeneration; typically in the patient's late 30's or early 40's. In 2013 a research group crystallized mutant Huntington's (mHtt) protein fragments with inserted histidine residues and it appeared that the polyglutamine fragments formed a β sheet conformation; which may offer a motif for [^{18}F]FDDNP binding (Kim 2013). It is this β sheet structure found in amyloid beta plaques and hyperphosphorylated tau protein aggregation that has led some researchers to suggest it as a key component in developing local cytotoxicity (Teplow 1998). The typical HD patient will not exhibit amyloid- β or hyperphosphorylated tau in their brain anatomy unless there is comorbidity present at the time of death.

2.6 Parkinson's Disease

Parkinson's Disease is another disease of the basal ganglia system, but unlike Huntington's Disease where a loss of the medium spiny neurons is the cause of the motor dysfunction, it is the loss of dopaminergic neurons in the substantia nigra pars compacta (SNc) and denervation of the striatum that create a dopamine deficit (Dickson 2017). The pathological hallmarks of idiopathic PD are not only the loss of neurons, but the accumulation of Lewy bodies and Lewy neurites as a result of alpha-synuclein aggregation. The typical Parkinson's patient appears to respond positively to Levodopa (synthetically produced Dopamine) in the early stages of clinical PD. When the cell loss reaches a tipping point, the treatment becomes ineffective and no medical intervention will prevent the terminal endpoint for the patient. It has also recently been suggested that α -synuclein aggregates to amyloid fibrils and the secondary

structure of these fibrils is the same β -structure seen in the misfolded amyloid beta and hyperphosphorylated tau quaternary structure (Vilar et al. 2008). Pure PD patients do not exhibit plaques or tangles, but they may appear in Dementia with Lewy Bodies (DLB) or Parkinson's Disease with Dementia (PDD) (Tsuboi, Uchikado, and Dickson 2007). The Parkinsonism symptoms can be experienced by a variety of neurodegenerative diseases that are not PD.

2.7 Chronic Traumatic Encephalopathy (CTE)

Chronic Traumatic Encephalopathy is a neurodegenerative disease recently confirmed in concussive sports; observed throughout history under a variety of pseudonyms. In the 21st century patients afflicted by CTE had been coined "punch drunk" a sub classification clinically referred to as *dementia pugilistica* (Martland 1928). In the beginning of the 22nd century we would adopt the clinical term "Chronic Traumatic Encephalopathy," adequately named by the examining physician Dr. Bennet Omalu as a "progressive neurodegenerative disease... [which] presents clinically a composite syndrome of mood disorders and behavioral and cognitive impairment, with or without sensorimotor impairment" (Omalu 2014). The degenerative brain pathology has been connected to concussive head trauma where the brain is exposed to a rapid acceleration-deceleration event or series of events (McKee et al. 2009). The minimal amount of brain trauma necessary to induce CTE is still not well understood. An experimental study involving monkeys was used to study brain injury where it was determined that shear strain resulted in stretching and tearing of axons inducing cerebral injury (Gennarelli, Adams, and Graham 1981). Chronic Traumatic Encephalopathy has become a greater concern for the U.S. National Football League as a recent study revealed 87% of the study's 202 former football players were found to have pathologically confirmed CTE at autopsy (Mez et al. 2017).

CTE diagnoses may involve a spectrum of disease, but the widespread pathological hallmarks are hyperphosphorylated tau (p-tau) presenting as neurofibrillary tangles (NFT's) and astrocytic tangles. In many cases co-morbidity reveals additional pathology such as amyloid-

beta, TDP-43 and α -inclusions (McKee et al. 2013). The pathology of CTE is pathologically rated in 4 distinct stages I through IV, spreading through cerebral foci to the limbic area until completely covering the cerebral cortices of the brain with tau pathology (McKee et al. 2013). The clinical diagnosis of CTE can present as either of two distinct profiles: behavioral and mood disorders or cognitive dysfunction (Stern et al. 2013).

2.8 Molecular Imaging: Positron Emission Tomography (PET)

Positron Emission Tomography (PET) imaging has been a constantly evolving modality since the introduction of radionuclides to medicine in the first part of the 21st century (Shukla and Kumar 2006). The positron was first predicted by Paul Dirac in 1931 by his relativistic electron equation (Dirac 1928). At the time, it was difficult for many physicists to comprehend the existence of an antiparticle to the electron (Pashby 2012). The positron itself is a very short-lived particle since it is not able to travel very far before interacting with an electron in an electron-positron annihilation event. When the positron-electron annihilation was discovered, the possibility of collimating coincident gamma rays appeared advantageous when compared to static imaging from single source gamma ray emitters (Nutt 2002). The first radionuclides with short half-lives and few available cyclotrons, made it difficult for physicians or researchers to envision any sort of tomographic reconstruction that would be useful for widespread diagnosis or treatment (Ter-Pogossian 1992). The improvement of PET imaging has occurred over many decades as a result of technological innovation and computer processing capability. The adaptation of Single Photon Emission Computed Tomography (SPECT) to a detector ring and the invention of Computed Tomography (CT) using gamma rays laid the foundation for modern-day PET imaging (Rich 1997)

Since evolving from its rudimentary forms in the 1950's, PET imaging has shed considerable light on a multitude of physiological processes that were previously impossible to study *in vivo* (Shukla and Kumar 2006). The radiotracer, 2-deoxy-2-[¹⁸F]fluoroglucose (2-FDG), a glucose analog, has long since been considered to be the gold standard in displaying

regions of hypo- and hypermetabolism in human physiology (Nutt 2002). An improvement in the sensitivity of the detector elements, the reconstructive speed of computer algorithms and a variety of targeted radiotracers are allowing wider applications for imaging biological processes (Shukla and Kumar 2006). The radioisotope fluorine-18 was initially used as a bone scanning tracer, but its 110-minute radioactive half-life offered a huge advantage in experimental scan time over other isotopes and became a popular isotope for PET imaging (Blau, Nagler, and Bender 1962). The human brain has been one of the most heavily studied regions with PET imaging and has begun to reveal key components in diseases that have plagued mankind throughout human history. PET imaging is capable of revealing the underlying molecular biomarkers that are often impossible to detect through any other *in vivo* methods.

2.9 [¹⁸F]FDDNP

In 2001, the Barrio Lab at the University of California, Los Angeles (UCLA) designed a radiofluorinated compound 2-(1-{6-[(2-[¹⁸F]fluoroethyl)(methyl)amino]-2-naphthyl}ethylidene) malononitrile or [¹⁸F]FDDNP, in an effort to track the levels of amyloid- β plaques and hyperphosphorylated tau proteins in the brains of diseased patients. [¹⁸F]FDDNP was created from its parent compound, DDNP; a compound that was shown to demonstrate specificity for amyloid- β senile plaques (SP) and Neurofibrillary Tangles (NFT). Fluorescent titrations with the experimental “gold standard” synthetic fibrils A β_{1-40} demonstrated that [¹⁸F]FDDNP retains a high affinity binding site ($K_d=0.12$ nM) and a lower affinity binding site ($K_d=1.86$ nM) (Shoghi-Jadid et al. 2002). The tau binding affinities have not been calculated due to the difficulty of raising synthetic tau fibrils *in vitro* and inducing the proper aggregation and fibrilization to reflect the hyperphosphorylated tau protein found in the native tau pathology. In utilizing synthetic tau fibrils, there are still many of the intermediate steps of the oligimerization process of tau that are not well understood and it appears that the incubation medium is a prerequisite for successful tau fibril growth (Xu et al. 2010). It has been theorized through computational binding models that the binding mechanisms of [¹⁸F]FDDNP occur as a result of the strong

hydrophobic and π -stacking interactions at two distinct sites on the amyloid fibrils (Parikh and Klimov 2015).

2.10 Comparative Fluorescence

Thioflavin T and Thioflavin S are two histological dyes long desired for their ability to bind to amyloid plaques and tangles with a high affinity, but they also served as the foundation from which many of the amyloid PET tracers would be developed. These neutral benzothiazoles not only recognize binding sites in the senile plaques (SPs) and neurofibrillary tangles (NFTs), but also provide a characteristic fluorescent emission shift once the compound is bound (Biancalana and Koide 2010). Thioflavin S binds to plaques and tangles and shows an increase over the background fluorescence using the fluorescent microscope FITC filter set (EX:460 - 490 nm, DM:505 nm, EM:515 – 550 nm) (Kelenyi 1967). When it was realized that PET radiotracers might be capable of detecting brain disease *in vivo* a search began for new imaging agents capable of penetrating the blood brain barrier (BBB).

2.11 Alternative Tracers

The benzothiazole salt backbone of the Thioflavins became the focus of a hunt for radiotracer analogues that would bind to plaques and tangles with an equally high affinity in spite of a radioactive substitution. At the onset of Amyloid imaging development, [^{18}F]FDDNP was valued for its characteristic ability to bind both plaques and tangles with high affinity. Another compound called N-methyl-[^{11}C]2-(4'-methylaminophenyl)-6-hydroxybenzothiazole (Pittsburgh Compound B or PiB) was synthesized shortly after and it was noted for its high affinity for amyloid beta *in vitro* (Klunk et al. 2004). The initial development of PiB proved promising, but the ^{11}C isotope (20 minute half-life) substitution for the longer-lived ^{18}F isotope (110 minute half-life) provides more clinical application time. Florbetapir, Florbetaben and Flutemetamol were the first PET amyloid imaging agents to receive FDA approval but not as a diagnostic agent for Alzheimer's disease (Landau et al. 2013; Sabri et al. 2015; Snellman et al. 2014). The *in vivo* binding seen in demented patients reflects the amyloid pathology in regions

known to have certain amyloid deposition and correlates well with some of the cognitive impairment seen in patients (Klunk et al. 2005). PiB was found to also display elevated binding in the white matter of diseased patients as well as in control patients; resulting in a discussion about the possibilities of non-specific binding occurring with PiB (Lockhart et al. 2007). As the medial temporal region of the brain is known to be one of the first regions to display plaques and tangles in the diseased brain, it does not display high binding of PiB in any of the stages of AD; which calls into question the nonspecific binding (Tolboom et al. 2009). It has also been demonstrated *in vitro* that PiB has an affinity for Estrogen Sulfotransferase 1E1 (SULT1E1) and may be binding the enzyme *in vivo* rather than the amyloid (Cole et al. 2010). The obsession with tracking amyloid beta throughout the duration of disease progression might be misleading as it has recently been demonstrated that removing the amyloid protein or solubilizing the protein in the AD brain did not halt the progression of cognitive dysfunction in patients clinically defined as those with mild cognitive impairment. There is also concern about studies reporting 10% - 30% of patients who are scanned and identified as being PiB PET positive, but displaying no cognitive impairment at the time of scan or follow up (Cohen et al. 2012).

The amyloid cascade hypothesis has been the central theme in the investigative treatment field for neurodegenerative disease, perhaps it is time to rethink certain central hypotheses and examine both tau and amyloid critically to evaluate their roles in pathogenesis (Okamura and Yanai 2010).

2.12 Synthesis of [¹⁸F]FDDNP and *in vivo* human imaging

[¹⁸F]FDDNP is prepared by Dr. Jie Liu using a tosyloxy precursor radiolabelled after bombarding ¹⁸O-enriched water using an 11 MeV proton beam produced in the UCLA cyclotron (Liu et al. 2007). The radiosynthesis process produces high yielding chemical and radiochemical purities (>99%) at specific activities in the range of 4 to 8 Ci/μmol (Liu et al. 2007). The patients are given an attenuation followed by a bolus injection between 5 and 10

mCi containing 5% Ethanol, 45% saline and 50% human serum albumin (HSA) to reduce the non-specific binding.

The radiofluorination process in the preparation acts to replace a hydroxyl group with the radioactive fluorine-18 ion as a result of a similar steric profile and electroaffinity (Liu et al. 2007). Recent radiofluorination innovations have made it possible to label proteins and antibodies; undoubtedly opening a new era of molecular (Rodriguez et al. 2016).

2.13 Distribution Volume Ratio (DVR) tomographic maps using Logan analysis and compartmental modeling

The Logan graphical analysis (**eq. 2.1**) was developed by Jean Logan as a method to estimate the ratio of concentration of a reversible radiotracer in a brain reference region $C_R(t)$ in relation to the target tissue $C_T(t)$ without having to sample the patient's arterial blood supply to quantify the tracer concentration in the blood to formulate the input function $C_P(t)$.

$$\frac{\int_0^t C_T(\tau) d\tau}{C_T(t)} = \text{DVR} \frac{\int_0^t C_R(\tau) d\tau}{C_T(t)} + b$$

Equation 2.1 Logan graphical Analysis Distribution Volume Ratio (DVR)

The equation used to solve for the DVR values in the image are calculated using the $[^{18}\text{F}]\text{FDDNP}$ concentration in the cerebellar grey matter ($C_R(t)$) in relation to the target tissue ($C_T(t)$). At some time $t > t^*$ the slope becomes constant and we are able to solve for b (y-intercept) and determine the DVR value. (Logan et al. 1996)

The Logan analysis was adapted to a Single Reference Tissue Model (SRTM) for the reversible radiotracer $[^{18}\text{F}]\text{FDDNP}$, where the cerebellum is used as the site of nonspecific binding. The modeling of $[^{18}\text{F}]\text{FDDNP}$ can be reduced to a simple two-compartmental model where the blood-plasma itself represents a compartment and the brain represents another compartment. Since the bound and unbound tracer cannot be distinguished by signal alone, the steady state of the Time Activity Curve (TAC) reveals the $[^{18}\text{F}]\text{FDDNP}$ specifically bound to either amyloid beta or p-tau. The concentration of the radiotracer in the blood can be estimated from the Time Activity Curve (TAC) if the linear portion of the curve reaches a steady state after

some time $t > t^*$ where the b-intercept is independent of t^* (Wong et al. 2007). The cerebellar grey matter is used as the reference region since it is typically unaffected by disease and retains normal influx and efflux of the radiotracer. The DVR parametric is a 3-dimensional representation produced with [^{18}F]FDDNP as a ratio between the protein containing regions and the non-protein containing region. The normalization to the cerebellum should be relatively comparable across both diseased and non-diseased patients so that comparison across cohorts should be adequate.

CHAPTER THREE: CORRELATION OF ANTE MORTEM [18F]FDDNP TO POST MORTEM [18F]FDDNP SIGNAL IN THE BRAIN OF A PROGRESSIVE SUPRANUCLEAR PALSY PATIENT

3.1 Introduction

[18F]FDDNP has been successfully used to image Alzheimer's Disease (Shin et al. 2011), Gerstmann-Sträussler-Scheinker disease (Kepe et al. 2010), Chronic Traumatic Encephalopathy (CTE) (Barrio et al. 2015) and Progressive Supranuclear Palsy (Kepe et al. 2013). In the imaging study of Alzheimer's Disease (AD), [18F]FDDNP was able to differentiate between patients with confirmed AD and those patients with Mild Cognitive Impairment (MCI) with statistical significance (Small et al. 2006). In AD patients, the binding of [18F]FDDNP has been reported as confined primarily to the cortical regions, while also displaying signal in the medial temporal region; known for its high abundance of amyloid beta plaques and neurofibrillary tangles in the earliest stages of Alzheimer's Disease (Tauber et al. 2013).

In 1964, physicians Steele, Richardson and Olszewski reported a series of patients presenting with "progressive brain disease featured by supranuclear ophthalmoplegia affecting chiefly vertical gaze, pseudobulbar palsy, dysarthria, dystonic rigidity of the neck and upper trunk, and other less constant cerebellar and pyramidal symptoms" (Steele, Richardson, and Olszewski 1964). The clinical conditions were well correlated with the presence of neurofibrillary tangles, gliosis and neuronal loss in various neuroanatomy and termed "Progressive Supranuclear Palsy" (Steele, Richardson, and Olszewski 1964).

Progressive Supranuclear Palsy as a disease is referred to as a "tauopathy," due to the abundance of the hyperphosphorylated tau protein that dominates both the grey and white matter regions with heavy neuronal loss and gliosis. The tau (τ) protein is an abundant protein found in the Central Nervous System (CNS) and is a member of a class of proteins known as Microtubule Associated Proteins (MAPs). The human tau protein has six isoforms found in the

brain and is encoded by the q-arm of Chromosome 17 located at 17q21 (Buee et al. 2000). The alternative splicing at exons 2, 3 or 10 in the mRNA transcript result in either 3 or 4 repeat sections in the carboxy terminal (Tawana and Ramsden 2001). The six tau isoforms found in the human brain range in length between 352 to 441 amino acids. In the healthy human brain the 3R forms of tau are slightly more abundant than the 4R tau proteins (Buee et al. 2000). The phosphorylated tau isoform has been found in the fetal human brain during development, which gives rise to the idea that the overexpression of phosphorylated tau in neurodegenerative disease might be a reactivation of this prenatal pathway (Brion et al. 1993). A previous [¹⁸F]FDDNP study on Progressive Supranuclear Palsy patients demonstrated elevated binding levels in the subthalamic nuclei, the midbrain and the cerebellar white matter (Kepe et al. 2013). The mean [¹⁸F]FDDNP DVR binding values as compared to the cerebellar grey matter in the striatum, thalamus, subthalamic area, midbrain and the cerebellar white matter were respectively (1.443, 1.478, 1.434, 1.367 and 1.209) of the PSP patients while in the control patients the mean DVR values measured (1.250, 1.250, 1.233, 1.167 and 1.076) (Kepe et al. 2013). Immunohistochemistry has demonstrated that the cerebellar cortex remains relatively unaffected from the misfolded tau protein in most cases of patients with PSP (Piao et al. 2002). The significant binding increase in the PSP patients can be attributed to the presence of hyperphosphorylated tau in the cases where the tauopathy was the dominant pathology and no co-pathology was present at the time of scanning. The presence of hyperphosphorylated tau (p-tau) in the cerebellar white matter is a hallmark of PSP and helps to distinguish it from other tauopathies (Wakabayashi and Takahashi 2004).

Progressive Supranuclear Palsy patients express Neurofibrillary Tangles (NFT's) similar to Alzheimer's Disease in the neocortex; however the tangles are exhibited in different pathological forms and structures (Buee et al. 2000). In the PSP patient brain, p-tau proteins can present in a variety of pathologies including: globose tangles, neuropil threads, flame-shaped NFT's, enlarged neurons (EN), coiled bodies, neuritic plaques (NP) and the pathology

critical to the diagnostic criteria for PSP; tufted astrocytes (TA's) (Armstrong, Lantos, and Cairns 2007).

The *in vivo* binding of any radiotracer inside the human brain occurs in a closed system; essentially making it extremely difficult for us to know exactly what binding sites our Positron Emission Tomography (PET) images reflect. The [¹⁸F]FDDNP binding affinity (K_D) has been quantified *in vitro* using Aβ₄₀ fragments, but the tau fibrils are more difficult to synthesize and make it tough to reproduce the native hyperphosphorylated tau proteins.(Agdeppa et al. 2001) The binding of [¹⁸F]FDDNP has been successfully demonstrated in patient brains containing either amyloid beta, hyperphosphorylated tau pathology or a combination of both (Smid et al. 2006).

An advantage of working with animals in the investigation of PET radiotracers is the ability for the experimenter to co-register the radiotracer signal to the neuroanatomy. The researcher is able to inject a bolus of radioactivity, dynamically scan the animal and using *ex vivo* autoradiography, determine the location of binding to neuroanatomy in the animal brain. [¹⁸F]FDDNP was studied in a similar fashion and this information was also used to demonstrate the competitive binding occurring between Naproxen, a NSAID (non-steroidal anti-inflammatory drug) and amyloid beta. Naproxen demonstrated the blockade and attenuation of *in vivo* [¹⁸F]FDDNP signal seen in the triple-transgenic rat model exhibiting amyloid plaques and amyloidosis (Teng et al. 2011). The animal model offers a glimpse into the binding that occurs in the animal brain, but unfortunately for the researcher, we cannot be sure what binding is taking place in the human brain without examining the gross human brain tissue.

In vitro autoradiography allows us the opportunity to co-register the *post mortem* brain tissue to the *ante mortem* [¹⁸F]FDDNP signal seen in the parametric DVR images. The positive autoradiography signal can be correlated to the underlying pathology stained through immunohistochemistry for both amyloid beta and hyperphosphorylated tau proteins. A similar evaluation of a former patient diagnosed with Dementia with Lewy Bodies (DLB) was performed

and the *post mortem* brain tissue of the patient seemed to reflect both the pathology measured through *in vitro* immunohistochemistry (IHC) and the *in vitro* [^{18}F]FDDNP autoradiography.

3.2 Material & Methods

3.2.1 [^{18}F]FDDNP Synthesis (Product provided by Dr. Jie Liu)

The biomarker 2-(1-{6-[(2- ^{18}F]Fluoroethyl)(methyl)amino]-2-naphthyl}ethylidene) malononitrile ([^{18}F]FDDNP) was prepared following USP 823 guidelines at UCLA Biomedical Cyclotron Facility (Liu et al. 2007). The radiosynthetic reaction utilized for the preparation of this biomarker is depicted in **Figure 3.1**. The preparation was carried out in a five-unit semi-automated synthesis module as shown in **Figure 3.2**. The biomarker was released for *in vivo*/*in vitro* utilization after it passed all the necessary quality control (QC) tests mandated by the USP 823 guidelines.

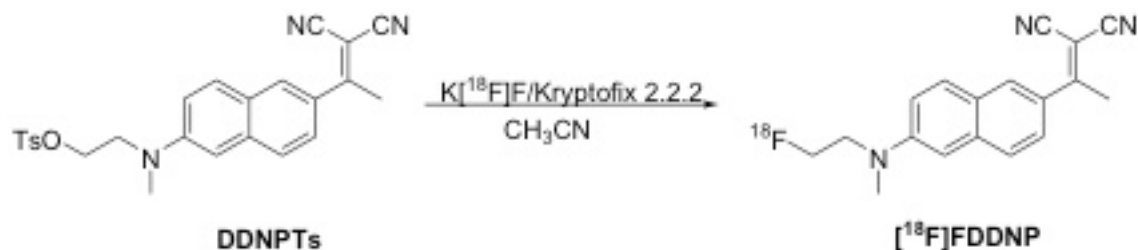


Figure 3.2 The semi-automated synthesis module for the preparation of [^{18}F]FDDNP.

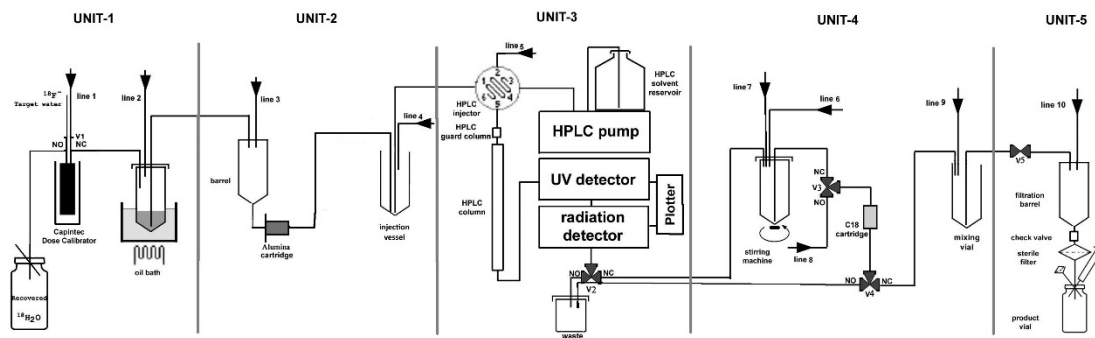


Figure 3.1 The radiosynthetic reaction scheme for the preparation of [^{18}F]FDDNP.

No-carrier-added [^{18}F]fluoride ion was produced by 11 MeV proton bombardment of 98% enriched ^{18}O water. The aqueous [^{18}F]fluoride ion was trapped on an anion exchange resin cartridge to recover the ^{18}O water. The [^{18}F]fluoride ion was subsequently released by passing

0.25% aqueous solution (0.4 mL) of potassium carbonate into a glass reaction vessel pre-loaded with Kryptofix 2.2.2. (10 mg) dissolved in 1.0 mL of acetonitrile (MeCN). The solution was evaporated at 115° C with a stream of nitrogen gas (flow rate: 20 – 22 mL/min) bubbling into it. The residue was dried by the azeotropic distillation with MeCN (3 × 0.5 mL). To the dry residue, a solution of the DDNPTs precursor (2.2 - 2.5 mg) in MeCN (0.7 mL) was added and the reaction mixture was heated at 93° C for 15 min. The solution was cooled with nitrogen stream for 1 min. The mixture was then passed through an Alumina Light Sep-Pak (Waters Associates), which was pre-rinsed with anhydrous MeCN (6 mL). More anhydrous MeCN (2 x 0.5 mL) was used to rinse the reaction vessel and the Sep-Pak. The collected MeCN eluent was diluted with ice-cold aqueous solution of 0.1 M ammonium acetate (NH₄OAc) and 0.02 M ascorbic acid (1.5 mL) and then injected into semi-preparative HPLC column (Waters Symmetry, PrepC18 7 μ , 7.8 x 300 mm). The HPLC column was eluted with a mixture of 50% MeCN and 50% 0.1 M NH₄OAc and 0.02 M ascorbic acid in sterile water at a flow rate of 5.0 mL/min. The effluent from the HPLC column was monitored with a UV detector ($\lambda = 440$ nm) followed by a gamma radioactive detector. The HPLC fraction containing chemically and radiochemically pure [¹⁸F]FDDNP product that eluted with a retention time of ~ 21 min was collected for 1.25 min. The collected HPLC fraction was diluted with water (9 mL) and then passed through a Waters tC18 Sep-Pak (50 mg). The tC18 Sep-Pak was washed with sterile water (20 mL). The [¹⁸F]FDDNP product was then eluted off the Sep-Pak with ethanol (0.5 mL) into a glass vessel and mixed with saline (5.0 mL) and 25% human serum albumin (4.0 mL). The [¹⁸F]FDDNP solution thus obtained in alcohol/saline/human serum albumin was sterilized by passing through a Millex® GV filter (0.22 μ m) into a sterile multi-dose vial. A sample of [¹⁸F]FDDNP in alcohol/saline mixture before the addition of human serum albumin was withdrawn and diluted with ethanol for chemical and radiochemical quality control tests. The sterility and pyrogenicity quality control tests were conducted with an aliquot of the [¹⁸F]FDDNP product withdrawn, under sterile conditions, from the multi-dose vial.

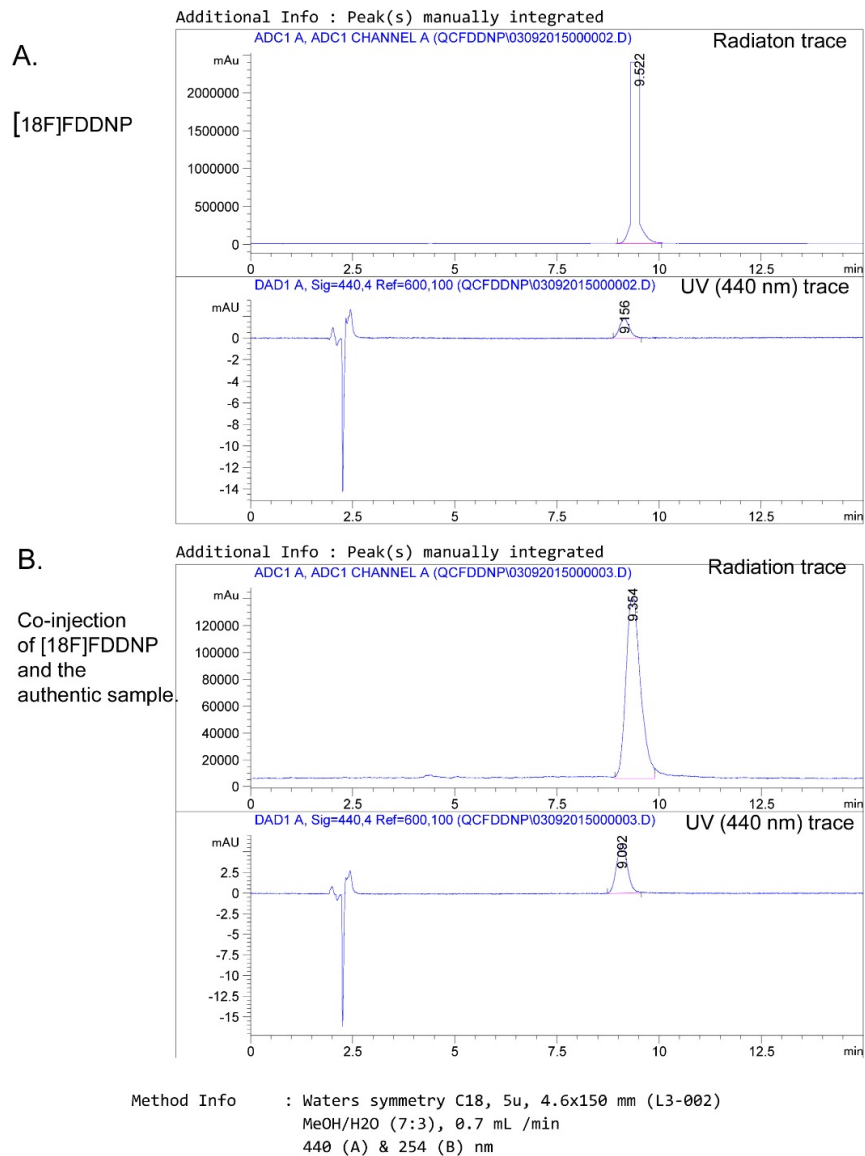


Figure 3.3 Typical analytical HPLC QC test results for [¹⁸F]FDDNP biomarker.

The top trace in figure A shows the radioactive purity (determined with a radioactivity detector) while the bottom trace indicates the chemical purity (determined with an UV detector). Both these purities are > 99 %. Figure B shows the radioactivity trace on the top and the chemical purity at the bottom for the same batch of [¹⁸F]FDDNP after the sample was spiked with an authentic non-radioactive standard FDDNP.

Each chemical and radiochemical purities as well as endotoxin and sterility tests for the possible microbial contamination as per USP 823 guidelines. **Figure 3.3** shown above represents a set

of typical analytical HPLC chromatograms demonstrating the chemical and radiochemical purities of the [¹⁸F]FDDNP biomarker.

3.2.2 [¹⁸F]FDDNP PET in PSP

The radiotracer [¹⁸F]FDDNP was synthesized at the Biomedical Cyclotron located on the UCLA campus as previously described (Liu et al. 2007). The compound was synthesized for patient study and a portion of the volume was used to quantify the chemical purity of radioactive [¹⁸F]FDDNP using High Performance Liquid Chromatography (HPLC) and Thin Layer Chromatography (TLC). [¹⁸F]FDDNP has a radioactive half-life ($\tau_{1/2}$ =109.8 minutes), which demands sufficient activity to allow 10 mCi of activity to be available at a later time for patient injection. The hydrophobic nature of [¹⁸F]FDDNP required that it was dissolved in a concentration of 10% Ethanol and diluted to 1% in saline with human serum albumin acting to reduce the nonspecific binding *in vivo* (Liu et al. 2007).

The patient was scanned on the Positron Emission Tomography (PET) ECAT HR scanner (Siemens, CTI) at the UCLA Ahmanson Medical Center. Prior to the bolus injection of [¹⁸F]FDDNP, a 10-minute attenuation scan was acquired for accurate image reconstruction. As the patient lay supine in the PET scanner, a bolus of [¹⁸F]FDDNP radioactivity between 5 mCi and 10 mCi was injected intravenously and a dynamic scan was recorded in 20 frames. The frames consisted of: 6 x 30 second frames, 4 x 180 second frames and 10 x 300 second frames for a total scan time of 65 minutes. The PET scan used in this study was corrected for decay, scatter, attenuation in the scanner and reconstructed using filtered back projection (Hann filter, 5.5 mm FWHM). The ECAT HR PET scanner reconstructs each frame with 63 contiguous planes and a 2.42 mm plane separation. Motion correction was performed on the dynamic scan prior to performing a Logan analysis as described in previous experiments (Wardak et al. 2010).

3.2.3 Patient History

A 65-year old Caucasian male, retired tennis professional who actively played tennis well into his later life was diagnosed with “likely Progressive Supranuclear Palsy.” In a 2009

evaluation with the UCLA neurologist Dr. Yvette Bordelon, the patient described a 4-year history of progressive difficulties with balance and falling in the past. During the same interview, the patient presented with vertical supranuclear gaze palsy, moderately slow saccades, square wave jerks, moderate hypomimia, slowness of getting up and mild bradykinesia in his bilateral hand movements. The patient reported an initial improvement in response to Sinemet®, a Carbidopa-Levodopa treatment, leading the clinician to note that it was a “likely PSP case”(Bordelon. unpublished Clinical Notes, 2009). In this session with the patient it was noted that he had exhibited cognitive, mood and motor symptoms during the disease progression. The patient did not experience double vision, but did suffer from sleep apnea. He benefited from the use of a Continuous Positive Airway Pressure (CPAP) mask, which improved sleeping and alleviated daytime fatigue.

In the same clinical visit, Dr. Bordelon administered a Mini Mental State Exam (MMSE) to the patient, consisting of a standard 30-question test to measure cognitive impairment. The patient scored 24 on the MMSE, which denotes no cognitive impairment, but lies on the cut off for mild cognitive impairment in the range of 18 to 23 (Tombaugh and McIntyre 1992). A Progressive Supranuclear Palsy Rating Scale (PSPRS) scale was administered with the subject scoring a 24 on the evaluation on a 100 point scale with a larger value indicating a greater severity of the PSP disease (Golbe and Ohman-Strickland 2007). The patient would succumb to symptoms related to his disease in 2011 and his brain was donated to study Progressive Supranuclear Palsy.

3.2.4 [¹⁸F]FDDNP PET Distribution Volume Ratio (DVR) Image Analysis

The first six minutes (7 frames) of each dynamic [¹⁸F]FDDNP scan were summed to provide a 3-dimensional perfusion image on which six bilateral regions of interests were drawn on the cerebellar gray matter adjacent to the edge of the brain. The cerebellar Regions of Interest (ROI's) were placed on the dynamic [¹⁸F]FDDNP scans and the raw values were extracted to produce a Time Activity Curve (TAC). Using Logan graphical analysis, the linear

portion of the TAC was used to generate a parametric Distribution Volume Ratio (DVR) image as a ratio of the binding of [^{18}F]FDDNP in the region of interest to the bound radioactivity in the cerebellar gray matter; which is typically free of pathology. Using a simplified two compartmental model of [^{18}F]FDDNP in the human brain allows the quantification of specific binding in the patient brain using the cerebellar grey matter in the dynamic scan as a reference tissue region rather than physically sampling the arterial blood to quantify the plasma concentration (Wong et al. 2007). Sampling the blood of patients exhibiting motor symptom disorders can be quite challenging, especially when considering that the procedure is performed while the patient is lying supine in the PET scanner.

Statistical Parametric Mapping (SPM12) software was used to co-register the patient's T1-weighted MPAGE Magnetic Resonance Image (MRI) to the [^{18}F]FDDNP parametric DVR image (Friston et al. 1994). The structural MRI was manually positioned to reflect the histological planes in which the brain was sectioned at patient autopsy. The co-registered MRI and DVR were imported into the software program Amide and used to draw 28 neuroanatomical Regions of Interest (ROIs) chosen to reflect regions to sample as an adequate amyloid beta and hyperphosphorylated tau through immunohistochemical staining visualized with Diaminobenzidine (DAB) (Loening and Gambhir 2003). A 3-dimensional ROI was drawn for each target region on the MRI and the DVR values were extracted for each respective ROI. The ROI's were drawn in the following brain regions: medial and lateral temporal lobes, frontal lobe, occipital lobe, cerebellar grey matter, cerebellar white matter, anterior and posterior cingulate gyri, caudate nucleus, putamen, insula and medulla oblongata.

3.2.5 *Post mortem* PSP Brain Tissue Preparation

Six pieces of *post mortem* tissue were received by Dr. Vladimir Kepe from the Brain Bank at UCLA, sectioned in the pathology department in August of 2013. The brain tissue was donated by a patient who was previously imaged as part of the Positron Emission Tomography (PET) radiotracer [^{18}F]FDDNP imaging study of patients with Progressive Supranuclear Palsy .

The tissue pieces contained a section of the medulla oblongata, the cerebellum, a left and right hemispheric coronal section cutting through the premotor cortex at the temporal poles, a sagittal section of the occipital lobe and a section of the frontal lobe sliced in the coronal plane. The tissue sections ranged in thicknesses between 2 cm – 3 cm, approximately. The large coronal sections joining the left and right hemispheres were split along the medial longitudinal fissure and separated into the left and right section. One of the sections had the temporal pole attached while the other section did not contain any part of the temporal lobe. Each of the tissue sections were preserved in a 10% formalin solution (3.7% Formaldehyde in Phosphate Buffered Saline (pH=7.4) solution and maintained at this concentration. The tissue sections were each rinsed in three changes of PBS (pH=7.4) buffer prior to the immersion in sucrose. To maintain tissue integrity, each tissue section was slowly changed in three graded concentrations of 10%, 20% and 30% sucrose in PBS buffer with 0.05% sodium azide over a period of approximately 6 weeks at 4°C. At each concentration interval, the endpoint is measured when the block of tissue sinks to the bottom of the container, as this indicates full penetration of the hypertonic solution. The large coronal section without the temporal lobe was placed in a gelatin block prior to embedding in Cryomethyl cellulose (CMC) to improve tissue integrity during slicing; but unfortunately the gelatin yielded poor IHC staining. The gelatin embedded slides maintained good tissue morphology, but the antibodies used for IHC did not appear to properly penetrate the tissue.

The large gelatin embedded section was not used as part of this study due to the unreliability of the staining. The brain tissue sections donated by the PSP patient are described by their neuroanatomy and the co-registered MRI (**Figure 3.4**) with each sampling point shared between the immunohistochemical stains and the [¹⁸F]FDDNP DVR images.

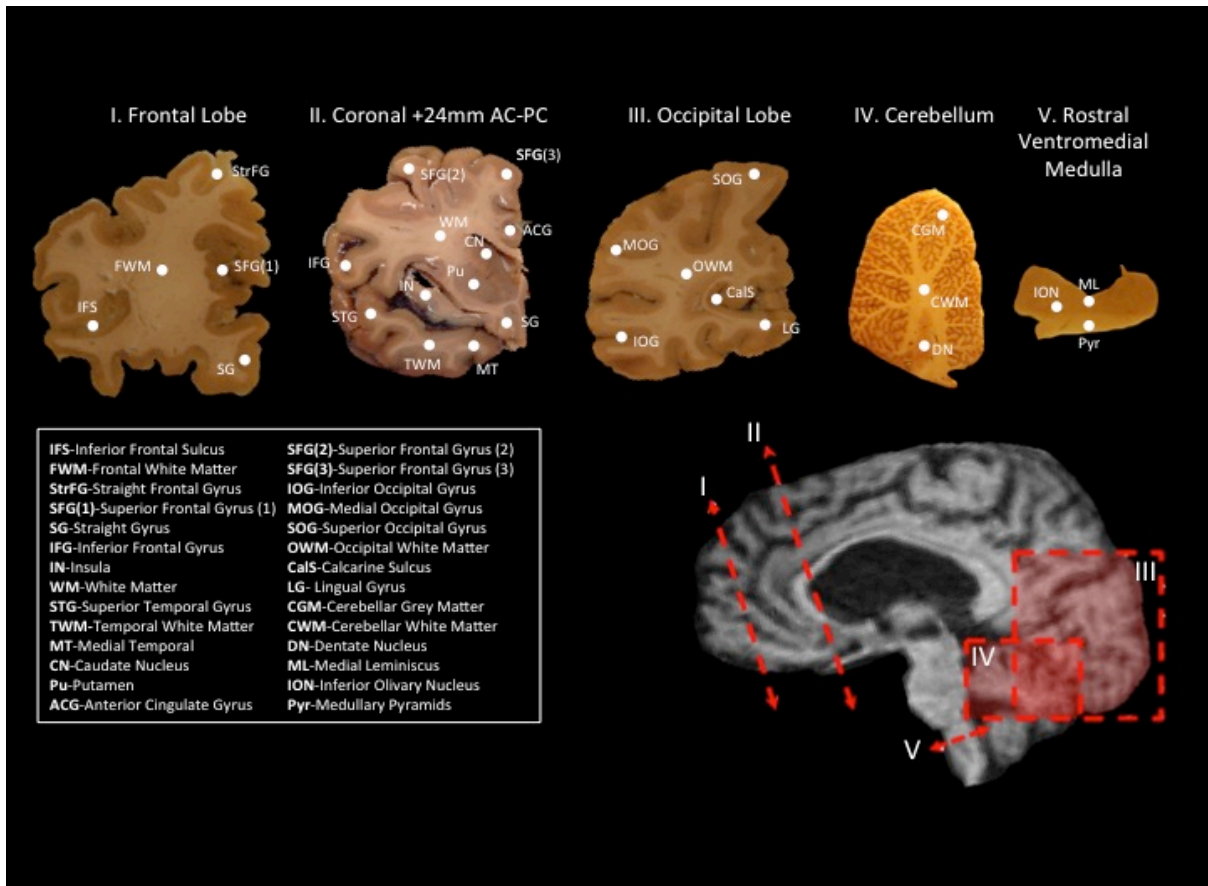


Figure 3.4 The gross neuroanatomical descriptions of the PSP brain tissue.

The tissue excised from a patient with Progressive Supranuclear Palsy. The neuroanatomical sections ranged in thickness between 5 - 15mm prior to freezing. All sections were photographed after freezing and mounting on a cryotome, with the exception of section II which was photographed prior to cutting into smaller sections. Section I was cut in the coronal plane from the left hemisphere of the frontal lobe. Section II was removed in the coronal plane slicing through the frontal lobe, striatum and temporal lobe. Section III was removed from the occipital lobe in the sagittal plane. Section IV was removed from the cerebellum in the sagittal plane including the dentate nucleus. The neuroanatomy in section V was cut in the transaxial plane through the rostral ventromedial medulla oblongata. Neuroanatomical labels denote the regions in which the density of Tau and Amyloid-beta immunohistochemical staining were scored for correlation to the intensity of the bound [^{18}F]FDDNP signal *ante mortem*.

3.2.6 Slide preparation

Large (5" x 7") glass slides were coated with a chrome alum gelatin solution, prepared by dissolving 5 g of gelatin Bloom 275 (Fisher G8-500) into 1.0 L of distilled water maintained at a temperature near, but not exceeding 45°C. Once the gelatin was dissolved, 0.5 g of Chromium potassium sulfate dodecahydrate (Fisher, C337-500) was added to positively charge the slide, in order for the slides to attract the negatively charged tissue sections. All glass slides were cleaned prior to mounting using the following steps: (1) soak slides in a 1% HCL acid bath (2) clean with a 1-2% concentration of soap in DI water (3) rinsed and boiled for 30 minutes in distilled water (4) and air dried in a covered, well ventilated, particulate-free location. After completely air-drying for 24 hours, each glass slide is dipped for 5 seconds in the gelatin solution 3 – 5 times vertically, evenly distributing the coating to minimize streaking. The slides were air dried for 24 hours in a covered, well ventilated, particulate-free location.

Smaller tissue sections were collected on Superfrost Plus® slides with both small and medium surface areas (25mm x 75mm, 50mm x 75mm). The Superfrost Plus® did not require additional coating with a chrome alum gelatin solution, but in some instances where the slide adhesion had begun to degrade an additional coating of chrom alum gelatin was added to prevent a loss of tissue sections.

3.2.7 Cryomicrotomy

The Leica 3050s cryomicrotome utilizes a sliding razor blade combined with a precision adjustment stage, which allows extremely thin sections on the order of 5 – 20 microns to be consistently cut. The tissue sections cut on the cryomicrotome were larger than those typically used on the device ($\leq 9 \text{ cm}^2$), which may require a certain amount of user familiarity and skill to maintain an even tissue coating thickness. The tissue must either be pre-frozen or frozen inside the cryostat using the chuck and heat drawing arm. Prior to sectioning, a freezing bath was prepared by filling a primary container with isopentane (2-methylbutane) and a secondary container filled with ethanol and dry ice. The primary container was placed in the secondary

container and the temperature was monitored until it reached -77°C . The tissue section was dropped in the isopentane bath until it was completely frozen in preparation for cryomicrotome sectioning. The pieces of brain tissue are frozen to the cryotome chucks using O.C.T. (Tissue Tek™, Sakura Finetek), a glycerol based resin, which remains slightly viscous at room temperature and freezes at temperatures less than 0°C . The optimal working temperature for achieving smoothly cut tissue sections is 20°C inside the cryotome chamber and 20°C at the chuck mount unit head to prevent warming tissue to adhere to the stage or excessively cold tissue sections from curling up. The tissue sections obtained were typically cut at 20 microns and were found to provide cleanly sliced sections and it is also the upper limit for fluorescent visualization. The loose sections are either collected using a warmed and properly subbed slide or placed in a 4°C chilled PBS buffer bath and the section is floated on the surface and captured with a slide while gently using a paint brush to collect the tissue section on the glass slide. Tissue sections were sliced at either 20 μm or 40 μm thicknesses, mounted on slides and placed in ice-cold acetone for 2 minutes, promptly air-dried and kept at 4°C until needed.

3.2.8 Cryomacrotomy

The tissues sectioned on the large cryomacrotome (Leica CM3600XP) were prepared with a cryomethylcellulose (CMC) solution used to freeze the tissue in a large frozen block formed with an aluminum mold. A concentration of 4% CMC w/v was prepared by stirring in 80g of CMC to 2.0 L of Distilled water. Due to the extremely hydrophobic nature of CMC, vigorous stirring is required to properly dissolve the dry powdered form. A high-powered mixer was used to decrease the mixing time and heat was applied at 60°C , but care was taken not to exceed this temperature. A freezing bath was prepared by filling a large primary container with isopentane (2-methylbutane) and a secondary container filled with ethanol and dry ice. The aluminum mold was taped at the edges so CMC would not leak into the bath during the freezing process. The CMC was pre-frozen in the aluminum mold with an opening left in the middle of the brick, large enough to place the tissue to be frozen. The temperature of the isopentane was

monitored until it reached -77°C . The tissue was placed in the center of the block and chilled CMC was placed on top and around the tissue and the aluminum tissue block was placed in the freezing bath until completely frozen solid. The surrounding aluminum mold was removed and the frozen block of CMC was left attached to the aluminum base made to fit in the cryomacrotome. The rapid freezing of the tissue is necessary to reduce small holes in the tissue that may occur from slow freezing or cracks from rapid freezing such as liquid nitrogen.

The CMC tissue block was placed in the cryomacrotome, locked in place and the unit was properly oiled prior to every use. The cryomacrotome was used to slice frozen tissue sections at 40-micron thickness and each slice was photographed with a stationary camera above the unit prior to sectioning. The tissue sections were captured with forceps collected and placed in an ice-cold PBS bath (pH=7.4, 4°C). The tissue sections were floated in the PBS bath and collected on a gelatin-coated slide using a small paintbrush to draw the tissue onto the glass slide. The tissue section was air dried for 24 hours in a place free of particulate contamination and stored with a desiccant for later use.

3.2.9 Hyperphosphorylated Tau (AT8) Immunohistochemistry

The slides stained for p-tau were either 20 μm or 40 μm mounted thicknesses. Each slide was left in Xylenes for 120 minutes and rehydrated through graded five concentrations ethanol beginning with 100% Ethanol and finishing in 100% distilled water. The slides were then placed in PBS (pH=7.4) with 0.5% Tween-20 (PBS-T) for approximately 10 minutes to reach equilibrium. A 10 mM sodium citrate solution (Sodium Citrate Dihydrate, Fisher) with 0.5% Tween-20 (pH=6.0) was prepared and maintained between 95°C – 100°C . The slides were kept in the Sodium Citrate bath for 30 minutes between 95°C - 100°C and then promptly removed to cool at ambient room temperature. The slides were then quenched for and immediately removed endogenous peroxidase by incubating with a 0.3% hydrogen peroxide in PBS-Tween 20 (PBS-T) solution for 30 minutes. Immediately following, the slides were rinsed 4 times for 5 minutes each with PBS-T on a shaker at 80 rpm. The slides were then incubated

with 1.5% horse serum (Vectastain Elite ABC Kit[®]) for 30 minutes in an effort to reduce the amount of nonspecific binding by the tau antibody. The monoclonal antibody AT8 (Thermofisher) was used to detect the hyperphosphorylated microtubule associated protein tau (MAPT) specifically recognizing the serine 202 and threonine 205 hyperphosphorylation sites (Goedert, Jakes, and Vanmechelen 1995). The serum was poured off the slide and the AT8 antibody was added at a dilution of 1:200 in the horse serum albumin PBS-T solution. The stained sections were in adjacent tissue sections whenever possible for adequate comparison between stains and [¹⁸F]FDDNP autoradiography. The immunohistochemical stains were visualized using the avidin-biotin complex to amplify the signal and diaminobenzidine (Vectastain Elite ABC Kit, Vectorlabs) to produce a discernible brown positive stain that could be photographed with the digital camera. The secondary antibody conjugated with the avidin-biotin complex (Vectastain Elite ABC Kit[®]) was incubated for 90 minutes, followed by 4 washes of PBS-T. The slides were incubated 30 minutes with the ABC solution and rinsed 4 times with PBS-T. The slides were then incubated with Diaminobenzidine (DAB) for 2 -5 minutes to achieve an optimal brown positive stain.

3.2.10 Amyloid-beta (6F/3D) Immunohistochemistry

The smaller slides used for IHC (50mm x 75mm) were 20 µm thick and 40 µm thick for the larger slides (5" x 7"). Each slide was left in Xylenes for 120 minutes and rehydrated through five graded ethanol concentrations beginning with 100% Ethanol and finishing in 100% distilled water. The slides were pretreated with 90% formic acid for 10 minutes and promptly rinsed through multiple washes with DI H₂O. Following pretreatment, the slides were then equilibrated in PBS-T (pH=7.4) for approximately 10 minutes. The slides were then quenched for endogenous peroxidase by incubating with a 0.3% hydrogen peroxide in PBS Tween-20 (PBS-T) solution for 30 minutes. Immediately following, the slides were rinsed 4 times for 5 minutes each with PBS-T on a shaker at 80 rpm. The slides were then incubated with 1.5% horse serum (Vectastain[®] Elite ABC Kit) for 30 minutes in an effort to reduce the amount of

nonspecific binding by the Amyloid Beta (6F/3D, Dako) antibody. The monoclonal antibody specifically recognizes the amino acids 660 - 669 of human amyloid A4 proteins in the diseased brain. The serum was poured off the slide and the 6F/3D antibody was added at a dilution between 1:50 and 1:100 in the horse serum albumin PBS-T solution and incubated overnight for 22 hours. The primary antibody was poured off the slides and followed by 4 washes of PBS-T on the shaker at 80 rpm. The secondary antibody conjugated with the avidin-biotin complex (Vectastain Elite ABC Kit[®]) was incubated for 90 minutes, followed by 4 washes of PBS-T. The slides were incubated 30 minutes with the ABC solution and rinsed 4 times with PBS-T. The slides were then incubated with Diaminobenzidine (DAB) for 2 -5 minutes to achieve an optimal brown positive stain.

3.2.11 Immunofluorescence

The same monoclonal mouse AT8 (Thermofisher) antibody was used to detect the hyperphosphorylated tau protein through Immunofluorescence (IF). The formalin fixed human brain tissue was pretreated prior to IF in a 30 minute bath of Sodium Citrate (pH=6.0) between 95 °C - 100°C. The tissue was defatted and rehydrated through graded ethanol concentrations. The tissue was quenched with 0.3% Hydrogen Peroxide in PBS-T for 30 minutes and immediately following, rinsed in 4 washes of PBS-T on a shaker for 5 minutes each wash. The slide sections were blocked for 30 minutes using 5% Horse serum in PBS-T. The primary anti-PHF tau antibody was incubated in the tissue at a concentration of 1:500 in PBS-T for 22 hours. The secondary mouse antibody was incubated for 90 minutes and washed 4 times with PBS-T for 5 minutes each wash. The secondary antibody used was conjugated with a fluorescent protein (Alexafluor[®] 488) for fluorescent visualization. The entire process of incubation with the secondary antibody is performed in relatively complete darkness to avoid stimulating the fluorescent antibody with background ambient light. Secondary incubation for 90 minutes and followed by 4x 5 minute washes PBS-T. The slides were incubated with a concentration of 0.1% Sudan Black B (SBB) for 20 minutes to reduce background autofluorescence. The SBB binds to

the white matter and small lipid vacuoles of lipofuscin, which fluoresce under the right conditions. The slides were subjected to another series of washing with 4x 5 minute washes PBS-T to reduce the fluorescent background from nonspecific. The concentration of lipofuscin in the human brain is increased in the diseased and aging brain, which is drastically reduced with the application of SBB as it binds to the lipophilic structures.

The same procedure was used for amyloid beta fluorescence detected with the monoclonal mouse Amyloid Beta (6F/3D, Dako) antibody. The tissue was pretreated with 90% formic acid for 10 minutes, as previously described, to remove the formaldehyde from the tissue. The amyloid beta antibody was incubated at a concentration of 1:100 to produce ideal fluorescence without increasing the background signal or nonspecific binding. The same procedure using SBB was used to reduce autofluorescence in the PSP tissue.

Fluorescence visualization was performed using the Olympus IX71 inverted fluorescent microscope with stimulated fluorescent emission with a xenon lamp and a combination of the 4',6-diamidino-2-phenylindole (DAPI) and the Fluorescein isothiocyanate (FITC) filters. The DAPI filter was used to view the DAPI emission spectrum between 420 nm and 460 nm, capturing approximately 32.2% of the fluorescent spectrum with no spillover from the Alexafluor® 488 (fluorescent profile. The FITC filter was used to view the Alexafluor® 488 fluorescence with 11.1% of the DAPI signal spilling over in the fluorescence profile. The DAPI is a nuclear stain so it is easily distinguished from Alexafluor® 488 excitation profile (Wiederschain 2011).

3.2.12 Fluorescent Histochemistry

The PSP medulla oblongata tissue slides were treated in Xylenes for 120 minutes and rehydrated through baths containing: 100% Ethanol, 95% Ethanol, 85% Ethanol, 75% Ethanol, 50% Ethanol until completely rehydrated in 100% DI H₂O. Following hydration, the tissue slides were pre-treated in sodium citrate (pH=6.0) bath for 30 minutes at 95°C - 100°C to remove the formaldehyde bonds used to preserve the tissue. After several washes in PBS Tween-

20 (pH=7.4), the slides were incubated with 10 mM FDDNP in 1% Ethanol for 10 minutes and rinsed with DIH₂O. In parallel, an adjacent slide was incubated for 30 minutes and rinsed in a DIH₂O wash for 30 seconds, 2x3 minute washes in 60% isopentane, followed by a 30 second DIH₂O rinse. Both methods were tested since the first had been detailed in previous experiments and the second method was adapted from the developed protocol used for *in vitro* [¹⁸F]FDDNP autoradiography.

The fluorescence spectra of FDDNP, Thioflavin S and the Alexafluor 488 conjugated secondary antibody were examined using the same Olympus IX71 fluorescent microscope as previously mentioned. Comparative fluorescence was performed using the neuropathological standard Thioflavin S, a compound used to stain both neurofibrillary tangles and senile plaques. Detection was achieved using 0.05% Thioflavin S in 50% Ethanol and incubated for 20 minutes followed by a 70% Ethanol differentiation. The slides were rinsed and mounted with either 90% glycerol or Vectastain Hardset Mounting Medium with DAPI (Vectashield, Vector Laboratories). The FDDNP fluorescence excitation spectra was first reported to be excitable at an excitation wavelength of 430 nm – 440 nm and an emission spectrum maximum between 470 nm – 610 nm (Jacobson et al. 1996). The glycerol mounting medium was preferred over the medium with DAPI so any fluorescence spillover from the DAPI would not be mistaken for FDDNP signal.

3.2.13 *In vitro* Macro-autoradiography

The slide sections were each defatted in Xylenes for 120 minutes and rehydrated in five changes of graded ethanol (ETOH) concentrations starting at 100% ETOH and ending in 100% Distilled (DI) H₂O. The formalin fixed tissue was pretreated in a bath of 10 mM sodium citrate (pH=6.0) with .01% PBS-Tween 20 maintained between 95°C - 100 °C to remove the formaldehyde cross-linking bonds that maintain the tissue integrity. The tissue sections were incubated in the sodium citrate for approximately 30 minutes and immediately removed from the heat and set in a metal sink to draw out the heat and reduce the temperature. Once the tissue was brought to room temperature the slides were placed in two changes of distilled H₂O

and placed on the shaker at 80 rpm for 5 minutes each wash. A hydrophobic pen was used to circumscribe the tissue section on the slide and the excess water was removed from the slide.

The [^{18}F]FDDNP radiotracer was prepared through methods previously described (Liu et al. 2007) and a small amount of radioactivity ($\sim 1\text{-}2$ mCi) was used to prepare a concentration of $10\ \mu\text{Ci}/\text{mL}$ in DI H_2O . The distilled water is added to the radioactivity slowly, so as not to disrupt the radioactive fluorination as a result of “shock.” Each tissue section was covered with an adequate volume of [^{18}F]FDDNP taking care to cover the entire tissue as the concentration is extremely hydrophobic and can aggregate on the white matter. The slide section is incubated for 30 minutes in $10\ \mu\text{Ci}/\text{mL}$ of [^{18}F]FDDNP and the solution is poured off at the end of the incubation time. The slide is immediately rinsed in DI H_2O for 30 seconds at 80 rpm on the shaker, followed by 2 x 5 minute washes of 60% tert-butanol (tert-butyl alcohol) on the shaker and followed by a final 30 seconds of washing in DI H_2O on the shaker. The slides were promptly removed from their baths and air dried until no water remains on the slide. The slides were placed in an autoradiographic cassette and covered atop with plastic wrap to protect the phosphor imaging plate. The phosphor imaging plate (BAS-2025, Fujifilm) was placed on top of the slides in close contact with the plastic wrap and the cassette was clamped tightly. The imaging plate was exposed for 30 minutes and promptly removed from the cassette in darkness and placed in the phosphor imaging plate reader (BAS-5000, Fujifilm) to be read. The resultant autoradiographs were viewed with the Fuji imaging software and analyzed using the imaging analysis software (ImageJ).

3.2.14 *In vitro* Microautoradiography

The cerebellum was chosen as the region of brain tissue to examine *in vitro* microautoradiography signal due to the lack of amyloid beta and high density of p-tau in the white matter. The dentate nucleus was chosen as the focal point for the microautoradiography as it had already demonstrated binding of [^{18}F]FDDNP through macroautoradiography. The cerebellum slides were de-fattened and rehydrated in the same manner as previously described.

The slides were incubated with [^{18}F]FDDNP for 30 minutes and immediately following were placed on a shaker at 80 rpm and rinsed for 30 seconds in Distilled Water (DI H₂O), rinsed twice with 60% tert-butanol (tert butyl alcohol) and rinsed for 30 seconds in DI H₂O. The slides were removed from the water bath and dried with a dry stream of air.

After completely drying, the slides were moved to an adjacent darkroom with a Kodak safelight and a Kodak #2 filter; which emits a red light that does not contribute a background fog to the autoradiographic process. The light was never directly shone on the slides, but kept pointing in the opposite direction against a wall to use a minimal amount of light as possible. The emulsion (LM-1 Hypercoat Emulsion, Amersham) was pre-heated in a water bath and maintained between 40 °C - 45 °C, taking care not to exceed 45 °C, which can induce background fog in the autoradiograph signal. A small thin metal wire was used to fashion a tiny loop at the end of a 4-inch wire. The wire was used to stir the liquid emulsion, test the viscosity of the emulsion and apply a thin coat of emulsion on the slide. The emulsion was dripped over the dentate nucleus region of the slides (50mm x 75mm) and coated as evenly as possible. The slides were left in a light tight slide box with homemade desiccant packets of silica gel wrapped in Kimwipes™ for 30 minutes to absorb the emitted 511 keV gamma rays. After 30 minutes the slides were placed in a stopping solution of 5% acetic acid in ethanol for a total of 1 minute for each slide. The solution was rinsed off in 2 changes of DI H₂O on a shaker at 80 rpm for 2 minutes. The slides were then left in the D-19 Kodak developer in DI H₂O (160mg/mL) solution for 4 minutes. The final step is to remove the slides from the developer and place them in a Kodak Fixer solution (185 mg/mL) in DI H₂O on a shaker (80 rpm) for 8 minutes. The slides were removed from the fixer and placed in a water bath with running tap water for 30 minutes under darkroom conditions. The microautoradiography was evaluated under the microscope to determine [^{18}F]FDDNP binding and silver grain analysis (Kubota et al. 1992; Jenkins 1972).

3.2.15 Immunohistochemical Pathology Scoring

The pathological scoring for amyloid beta and p-tau in brain sections has a range of methods depending on the particular neurodegenerative disease. The CERAD scoring method is primarily focused on the pathological scoring of Alzheimer's Disease pathology and involves quantifying pathology by abundance and location (Mirra et al. 1991). The method of rating Dementia with Lewy Bodies (DLB) scores both alpha-synuclein and amyloid beta by both abundance and location (McKeith et al. 2005). The neuropathology data set is a pathology guide for pathologists conducting autopsies in an effort to determine disease, so there is not a need to quantify the pathology as much as confirm the disease. A scoring guide (Figure 3.5) was made to grade the pathology in the 28 different brain regions sampled in this study. The grading scale was similar to one that was developed in a pathological study to differentiate between Progressive Supranuclear Palsy-Parkinsonism (PSP-P) and Progressive Supranuclear Palsy-Richardson's Syndrome (PSP-RS) (Williams et al. 2007). Initially, a smaller scale was used to score the pathology, but it was determined that a scale with 5 discrete values provided a broader distribution of values. Each neuroanatomical region was analyzed under the fluorescent microscope (IX71, Olympus) viewed under a 40x magnification Field of View (FOV).


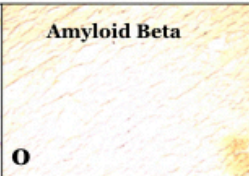
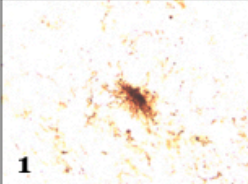


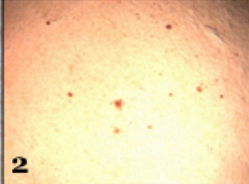
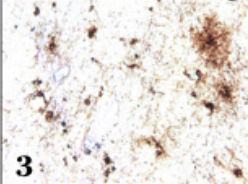
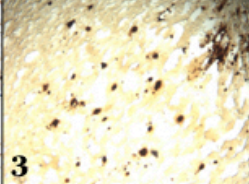
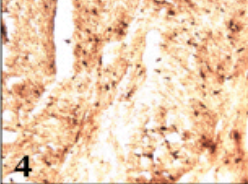
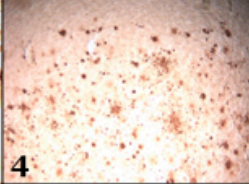
Scale	PHF-Tau	Amyloid Beta	PHF-Tau	Amyloid Beta
0	Sparse deposits/staining	No Staining Present		
1	PHF-Tau present, inclusions frequent but not in high density. Fibrils present or stained neurons, relatively few in magnified Field of View (FOV)	Sparse deposits/ staining		
2	PHF-Tau present, inclusions frequent but not in high density. Fibrils present or stained neurons, relatively few in magnified Field of View (FOV)	Amyloid-beta present and inclusions can be easily counted but do not exceed relatively few plaques per magnified FOV.		
3	PHF-Tau presence is strong, fibrils present, tangles present, neurons stained in gray matter with some adjacent unstained neurons.	A-beta plaques are present in high numbers. Counting plaques may be possible, but difficult under magnified FOV. Regions may be inconsistent in density.		
4	Heavy staining, neuronal tau inclusions present, tangles, tau fibrils, a variety of tau pathology present, neuronal inclusions are almost uniformly stained in FOV	Heavy staining, amyloid beta pathology highly dense in region. Plaque pathology too numerous to count under magnified FOV. Density of stain is consistent in the particular region.		

Figure 3.5 The pathological scoring rubric of PHF-tau and A β ₁₋₄₂ immunohistochemistry

Developed to correlate the abundance of both Amyloid- β and Paired Helical Filamentous (PHF) Tau immunohistochemical staining to the [¹⁸F]FDDNP DVR signal. Each PHF-tau image above (left) was stained using the same protocol for the anti-PHF tau antibody (AT8). Each Amyloid beta image above (right) was stained using the anti-amyloid beta (6F/3D) antibody. The immunohistochemical stains were enhanced using the Avidin-Biotin Complex (Vectastain Elite ABC Kit) and resolved with Diaminobenzidine (DAB). The scoring guide was developed in part due to a need for pathological scoring unrelated to the neurodegenerative diagnosis. The grading scale is set from 0 to 4 and each grade is described in the table to the left of the images. A score of “0” indicates no presence of the misfolded protein and a score of “4” indicated heavy staining or an abundance of the particular protein. Scores 1, 2 and 3 indicate a graduated scale with increasing pathology. The scales were also designed to be ubiquitous in both the grey and white matter, particularly due to the fact that both amyloid beta and p-tau pathologies and densities can be unique in both regions.

3.2.16 Data Analysis

Each of the 28 neuroanatomical regions was analyzed and assigned an IHC score for the both amyloid beta and hyperphosphorylated tau staining. The corresponding [¹⁸F]FDDNP DVR values were recorded for each of the sampled regions. The values for both p-tau and amyloid beta were placed in a table adjacent to each corresponding [¹⁸F]FDDNP Distribution Volume Ratio (DVR). The data was analyzed in the Statistical Package for the Social Sciences (IBM, SPSS v24). The values were plotted in a 3-dimensional graph using the software program Matlab (Matlab R2011a) with each sampling of the neuroanatomy represented by 3 variables: DVR values, hyperphosphorylated tau IHC score and Amyloid Beta IHC score. The data was represented as a 3-D scatter plot and a second plot was made with an overlaid triangular mesh to describe the macroscopic relationship between the IHC and the [¹⁸F]FDDNP signal. A heat map with a corresponding scale was overlaid on the mesh coinciding with the DVR values in the z-axis.

The 28 data points were classified into 5 subclassifications: grey matter, white matter, subcortical, cerebellar white matter and brainstem. These subclassifications were based on morphology, building a well-rounded picture of the pathology and binding of [¹⁸F]FDDNP in the PSP patient brain. The mean is a better representative of the respective regions as each individual sampling is a very small portion of the overall neuroanatomy. The means and standard deviations were calculated for each individual point and they were also calculated for the subclassifications. A multivariate linear regression analysis was conducted using the [¹⁸F]FDDNP DVR values as the dependent variable and both the tau and amyloid beta acting as the independent variables. The variances were also calculated for the sub classifications to determine if the variances were similar enough to be used in the linear regression analysis. Both data sets of tau and amyloid beta immunohistochemistry staining in relation to their [¹⁸F]FDDNP DVR signal were plotted on box plots since the IHC variables were discrete and not

continuous. Pearson and Spearman correlation coefficients were calculated for the data sets that were further divided into the subclassifications.

3.3. Results

After motion correction and attenuation correction, the DVR image was reconstructed and the resultant 3-dimensional DVR image was co-registered to the structural MRI (**Figure 3.6**). The MRI was aligned to the *post mortem* brain tissue sections using the cryosectioned MRI atlas (Salles and Gorgulho 2010). The MRI revealed the clinical diagnostic hallmarks of PSP associated with the midbrain. The PSP midbrain atrophy reveals the shrinking nuclei in the posterior brain stem region (Figure).

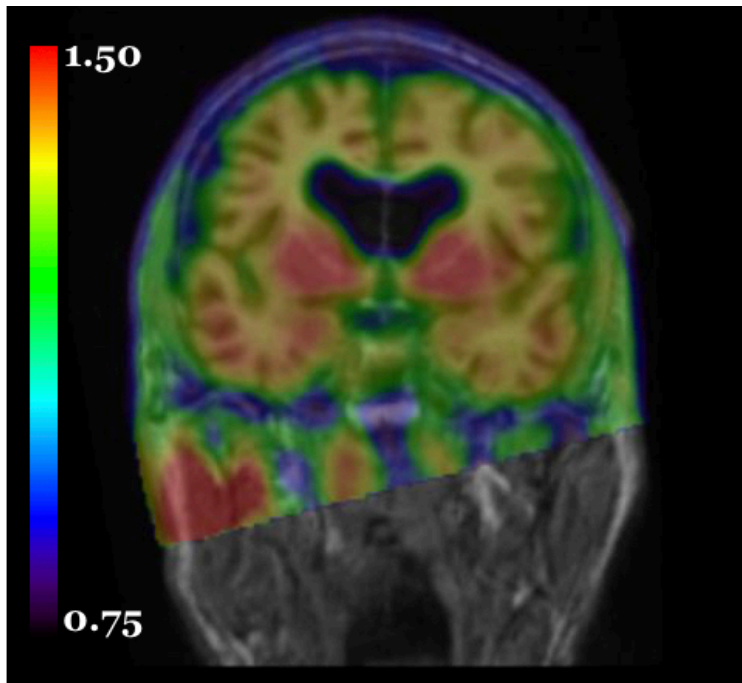


Figure 3.6 Co-registered T1-weighted MRI and [¹⁸F]FDDNP DVR image.

Shown in the coronal plane (left). The DVR image was aligned to the structural MRI using Statistical Parametric Mapping Software (SPM12) The DVR summed image was produced using the imaging software (Vinci v4.24) from frames 1 through 7 of the dynamic PET scan. The summed image and the DVR image were previously aligned in the process of producing the DVR image. The summed image is jiggled to match the structural T1-weighted MRI using a “nearest neighbors” approach. The [¹⁸F]FDDNP image is aligned using fiducial marks and structures in both images. Post-alignment the images are manually inspected to ensure alignment is correct.

The recession of the lateral margins of the tegmentum (**Figure 3.7A**) show the degeneration affecting midbrain; this particular feature of PSP is referred to as the “morning glory”(Adachi et al. 2004). The loss of dopaminergic neurons also gives the appearance of a “mickey mouse” shape in the midbrain (**Figure 3.7B**) (Itolikar, Salagre, and Kalal 2012). The “hummingbird” feature of the PSP patient brain is the final signature pathological feature of the

disease(**Figure 3.7C**). It must be noted in **Figures 3.7(D-F)**, all 3 regions show an elevated level of binding in the profiles of the midbrain, which coincides with the neuronal loss and possible white matter atrophy.

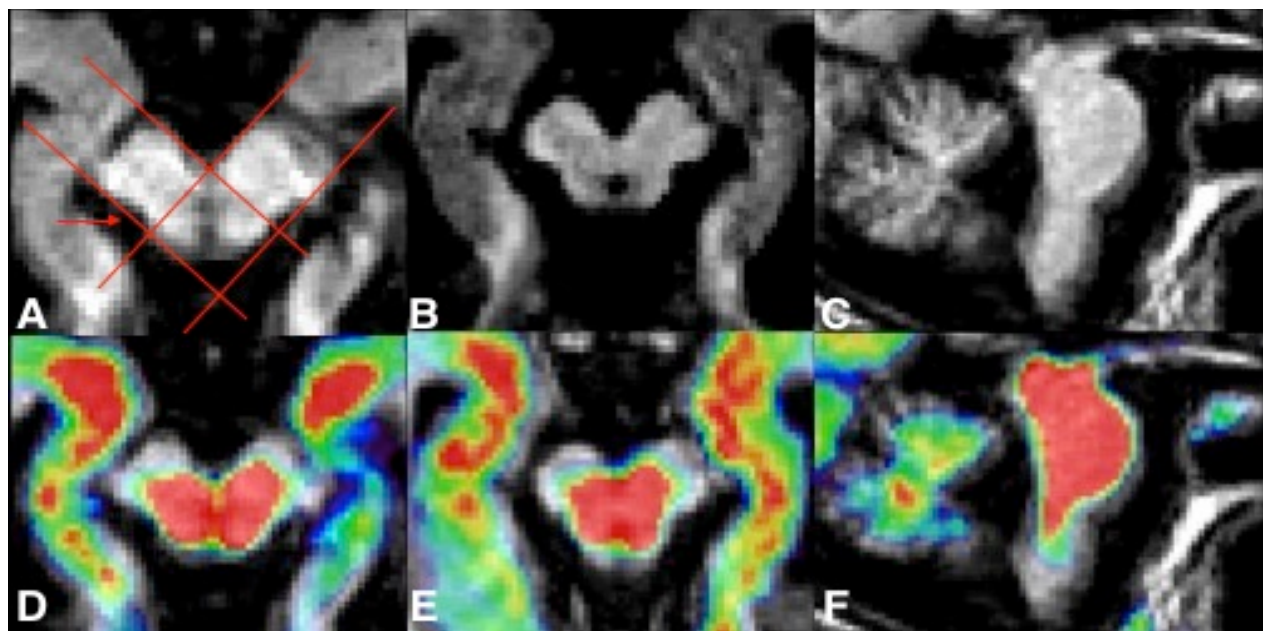


Figure 3.7 PSP Midbrain Atrophy in the T1-weighted MPRAGE MRI and $[^{18}\text{F}]$ FDDNP DVR.

As seen in (A) as what is referred to as the “morning glory” sign; which displays a reduction in the tegmentum on the lateral margin (arrow). In (B) the “Mickey Mouse” appearance of the midbrain is also a key hallmark of PSP that indicates a reduction in the dopaminergic neurons. (C) is a sagittal image of the brain stem with the midbrain displaying minimal signs of another hallmark radiologic sign known as “the hummingbird” sign; which indicates atrophy of the midbrain tegmentum. The co-registered $[^{18}\text{F}]$ FDDNP DVR image in D, E and F display elevated binding, indicating plaque and tangle pathology.

Hyperphosphorylated tau was found in every single piece of brain tissue stained for the misfolded protein at varying levels of intensity. The white matter in the cerebellum contained p-tau all throughout the white matter and in dense levels at the interface between the granular layer and the white matter (Error! Reference source not found.**Figure 3.8E**). The white matter itself contained both Tufted Astrocytes (TA) and Coiled Bodies (CB); the two signature hallmark pathologies of PSP (Error! Reference source not found.**J**). The neuronal inclusions of neuropil threads and neurofibrillary tangles appeared to be primarily confined to the deepest layers III-VI of the neocortex; where there is a large abundance of pyramidal neurons (Error! Reference

source not found. **Figure 3.8B,C**). Tufted Astrocytes (TA) appear in the brain tissue throughout the white matter and in especially large abundance in the cerebellar white matter. Using both immunohistochemistry and immunofluorescence we are able to see a considerable amount of the unique morphology throughout the samples (Error! Reference source not found. **Figure 3.8G,H**). The dentate nucleus neurons contained numerous amount of intraneuronal tau depicting the soma of the neurons and the dendrites as well (Error! Reference source not found. **Figure 3.8**). The astrocytic inclusions also provide some insight into how these supporting structures in the white matter begin to degrade (Error! Reference source not found. **Figure 3.8 I,J**). A bipolar neuron in the frontal lobe and neurons in the occipital lobe were not spared by the hyperphosphorylated tau. The p-tau morphology can vary from different regions in the brain, but in this patient case the PSP disease was so advanced the tau deposition was widespread throughout the brain. The fluorescent stains with AT8 displayed tufted astrocytes (TA's), coiled bodies (CB's) and globose tangles with a high degree of resolution (Error! Reference source not found. **Figure 3.8 F,H,J**) The detailed view of the dendritic arbors of the astrocytes demonstrate the high levels of intracellular p-tau (**Figure 3.8** Error! Reference source not found. **I,J**) as compared to the TA's (**Figure 3.8** Error! Reference source not found. **G,H**) or the CB's (**Figure 3.8** Error! Reference source not found. **E,J**)

The pathology report described the patient as having begun to experience what is known as “Alzheimerization of the brain” at the time of death. The result is A β ₁₋₄₂ proteins distributed throughout the superficial layers of neocortex in layers I and II (**Figure 3.9**). The amyloid beta plaques were found in all cortical regions of brain tissue and detected in both the putamen and the straight gyrus. The putamen and straight gyrus were the only subcortical nuclei that were found to have amyloid beta; all other regions were heavily stained with p-tau and were devoid of amyloid.

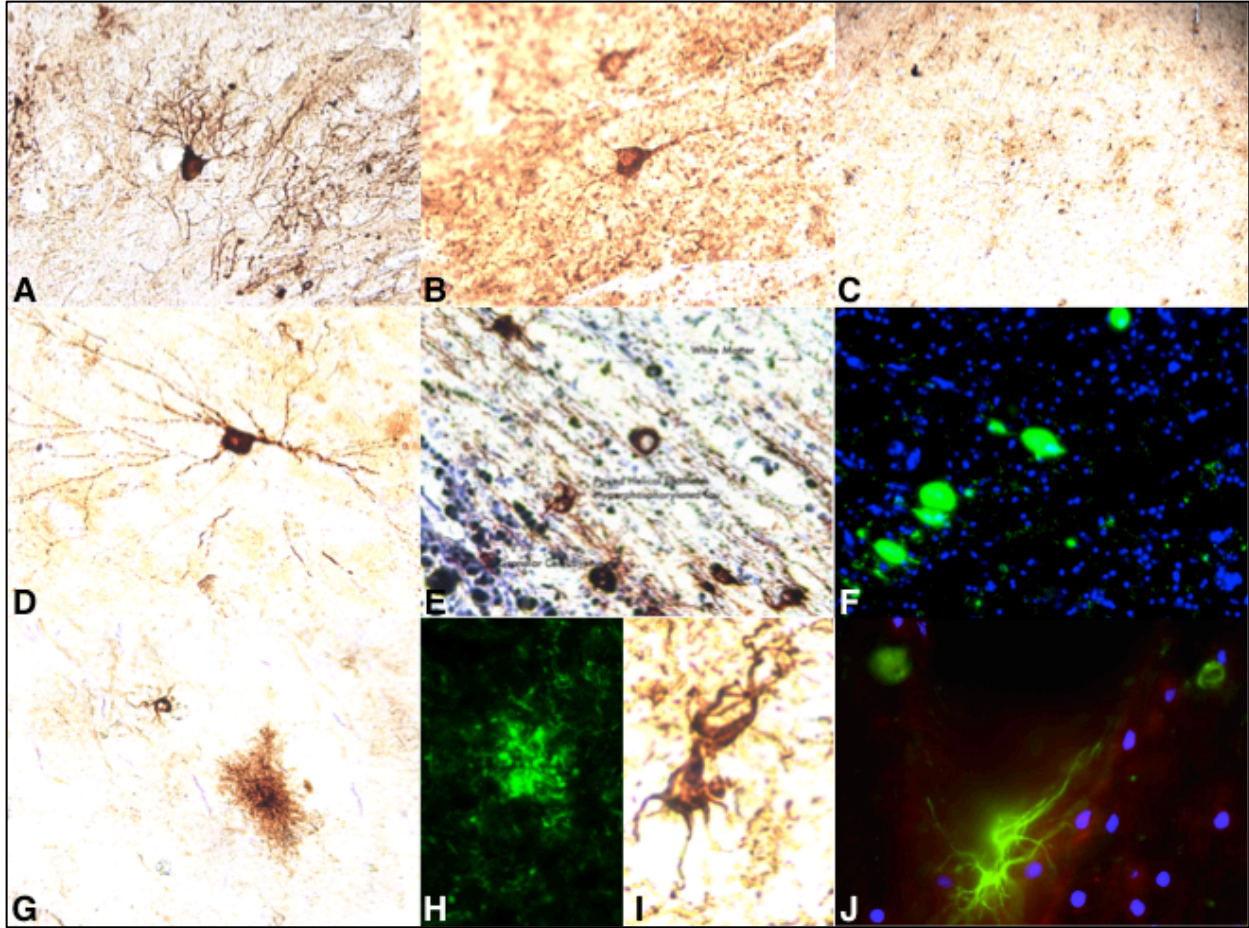


Figure 3.8 Paired Helical Filamentous (PHF) Tau immunofluorescence and immunohistochemistry in the PSP brain.

Paired Helical Filamentous (PHF) Tau stained with the AT8 antibody (Thermofischer) in the PSP brain. Staining the dentate nucleus of the cerebellar white matter highlights a large border neuron invaded by intracellular tau (A). An interneuron in the occipital lobe (B) demonstrates the heavy neuronal tau present in the deeper cortical layers, as well as a bipolar neuron found in the same tissue section. Projection neurons extending to the white matter from the pre-motor cortex display extensive axons and dendrites (C). The granular layer border of the hematoxylin-stained cerebellar cortex and the cerebellar white matter displayed heavy tau staining, revealing the hallmark PSP pathology: astrocytic inclusions, coiled bodies and tau fibrils (E). The medulla oblongata displayed fibrils and globose tangles in the nucleated inferior olivary nucleus (F). The cerebellar white matter revealed tufted astrocytes (TA's) using immunohistochemistry (G) and immunofluorescence (H) recognizing the AT8 primary antibody. The astrocytes were extensively labeled in the white matter through IHC (I) and immunofluorescence (J); demonstrating astrocytic inclusions, globose tangles and coiled bodies.

The amyloid beta plaques are relatively globular in shape, but can also appear amorphous. The senile plaques appeared in a variety of sizes (Figure 3.9 C,E) and primarily appeared as extracellular aggregates, but seemed to also outline what might be a pyramidal neuron in one stain. (Figure 3.9F) The tufts were widespread in high density in the superficial

neuronal layers of the neocortex but were primarily limited to layers I & II. The senile plaques were not uniformly distributed throughout the cortical grey matter, but were consistently stained throughout most of the neocortex in the frontal lobe, occipital lobe and the premotor cortex. (**Figure 3.9 A,B,D**) No amyloid beta was detected in the cerebellum or the medulla oblongata.

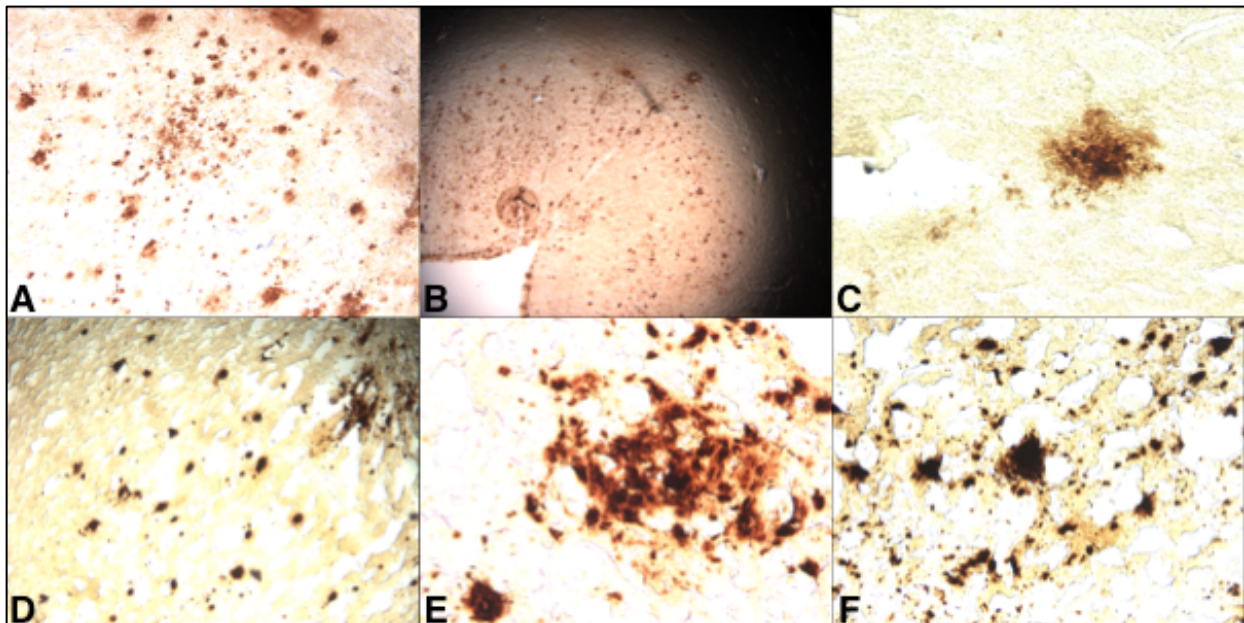


Figure 3.9 Amyloid beta (6F/3D, Dako) immunohistochemistry.

The neocortex displayed the classical senile plaque formation in varying densities (**A/D**). The amyloid beta appeared to be confined to the supragranular layers of the cortical gray matter (**B**). Many of the amyloid deposits are relatively globular(**C**), but many of the deposits are also amorphous. The anti-amyloid beta stained large aggregates of the misfolded protein (**E**) and in one particular stain, appeared to reveal the shape of a pyramidal neuron (**F**) with an abundance of amyloid beta bound to the surface of the neuron.

The medulla oblongata was chosen as a region to evaluate the binding of FDDNP through comparative fluorescence (**Figure 3.12A**) since it demonstrated a heavy amount of tau burden in the neuroanatomy and negatively stained for amyloid beta. The tau presented as globose tangles that were heavily deposited in the interior olivary nucleus (**Figure 3.10G**). A polyclonal anti-rabbit S100B antibody heavily stained the olivocerebellar fiber tract running

laterally connecting the inferior olivary nucleus to the cerebellar peduncle (**Figure 3.10A**). The dorsal portion of the medulla was heavily deposited with tau in the various nuclei; including the cuneate nucleus, hypoglossal nerve and the inferior cerebellar peduncle. (**Figure 3.10 B,C**) The hypoglossal nerve fibers extending inferiorly to the spinal cord contained less tau than the regions immediately adjacent, appearing like a stream amidst the hyperphosphorylated tau with sparse tau deposits. (**Figure 3.10D**) The nucleus ambiguus was covered with hyperphosphorylated tau with fibrils strewn across the lateral fibers intertwined with nuclei containing intracellular tau. (**Figure 3.10H**) The inferior olivary nucleus was covered with tau filaments strewn throughout the olive with globose tangles formed from the neurofibrillary tangles (**Figure 3.10 F,G**). The Raphe nuclei of the medulla also contained heavily stained neurons as seen in the image (**Figure 3.10E**).

Macroscopic images of the IHC stains were used to compare the presence of amyloid beta and p-tau to the *in vitro* [¹⁸F]FDDNP autoradiography. The images reveal a consistent presence of hyperphosphorylated tau throughout the cortices as well as amyloid beta in the same neocortical regions (**Figure 3.9**). In the white matter of the frontal and occipital lobes, the tau was present in lower density than what had been detected in the caudate-putamen or the cerebellum. The medulla and the cerebellum were both found to have high levels of tau but no presence of amyloid beta. The [¹⁸F]FDDNP DVR images paralleled the amyloid beta and tau immunohistochemistry, while also noting the thickness of the tissue sections were 40 μm and the [¹⁸F]FDDNP DVR images have a plane-to-plane thickness of 2.42 mm and a Full Width Half Maximum (FWHM) spatial resolution of 9 mm (Protas et al. 2010). It is easily discernible in regions such as the striatum or the cerebellar white matter that the intense signal reflects the high levels of p-tau in the region (**Figure 3.11**). The levels of [¹⁸F]FDDNP binding in the frontal cortex and the occipital lobe show the highest level of signal in the neocortex, which is consistent with the staining of amyloid and tau (**Figure 3.11 I/II**).

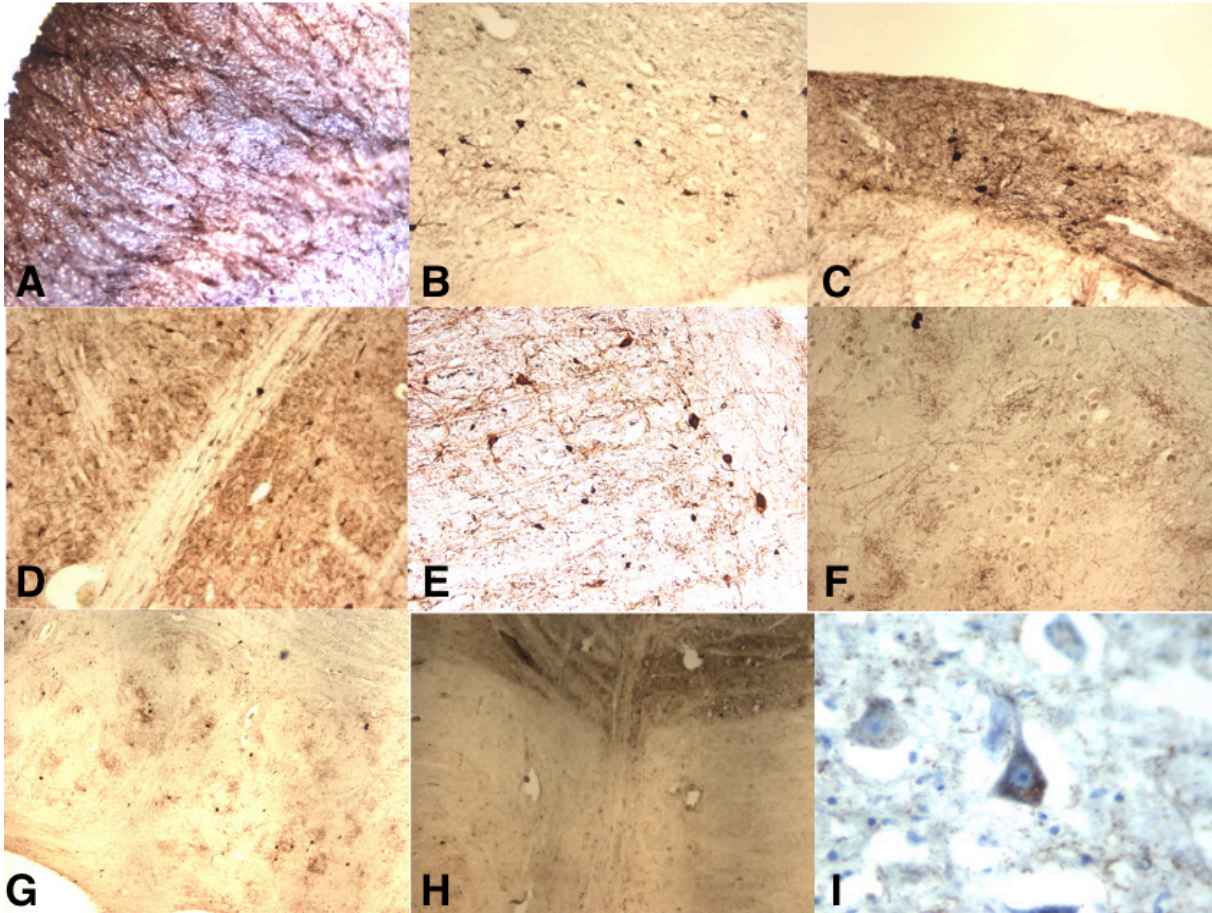


Figure 3.10 Medulla oblongata PHF-tau immunohistochemistry.

The medulla presented with an abundance of Paired Helical Filamentous (PHF) tau in the rostral ventromedial medulla. All immunohistochemistry was stained for hyperphosphorylated tau (**B-I**) with the exception of **Figure 3.8 (A)**, which was stained for the protein S100B. The olivocerebellar fibers were heavily stained for S100B extending from the medial to the lateral portions of the medulla. The regions stained with tau above were: cuneate nucleus (**B**), inferior cerebellar peduncle (**C**), hypoglossal nerve fibers (**D**), raphe nuclei MAG 100x (**E**), inferior olivary nucleus MAG 40x (**F**), inferior olivary nucleus MAG 40x (**G**), nucleus ambiguus MAG 40x (**H**), motor neuron MAG 400x (**I**). The hyperphosphorylated tau was deposited throughout the medulla oblongata, but was most heavily stained in the ventral portion of the medulla.

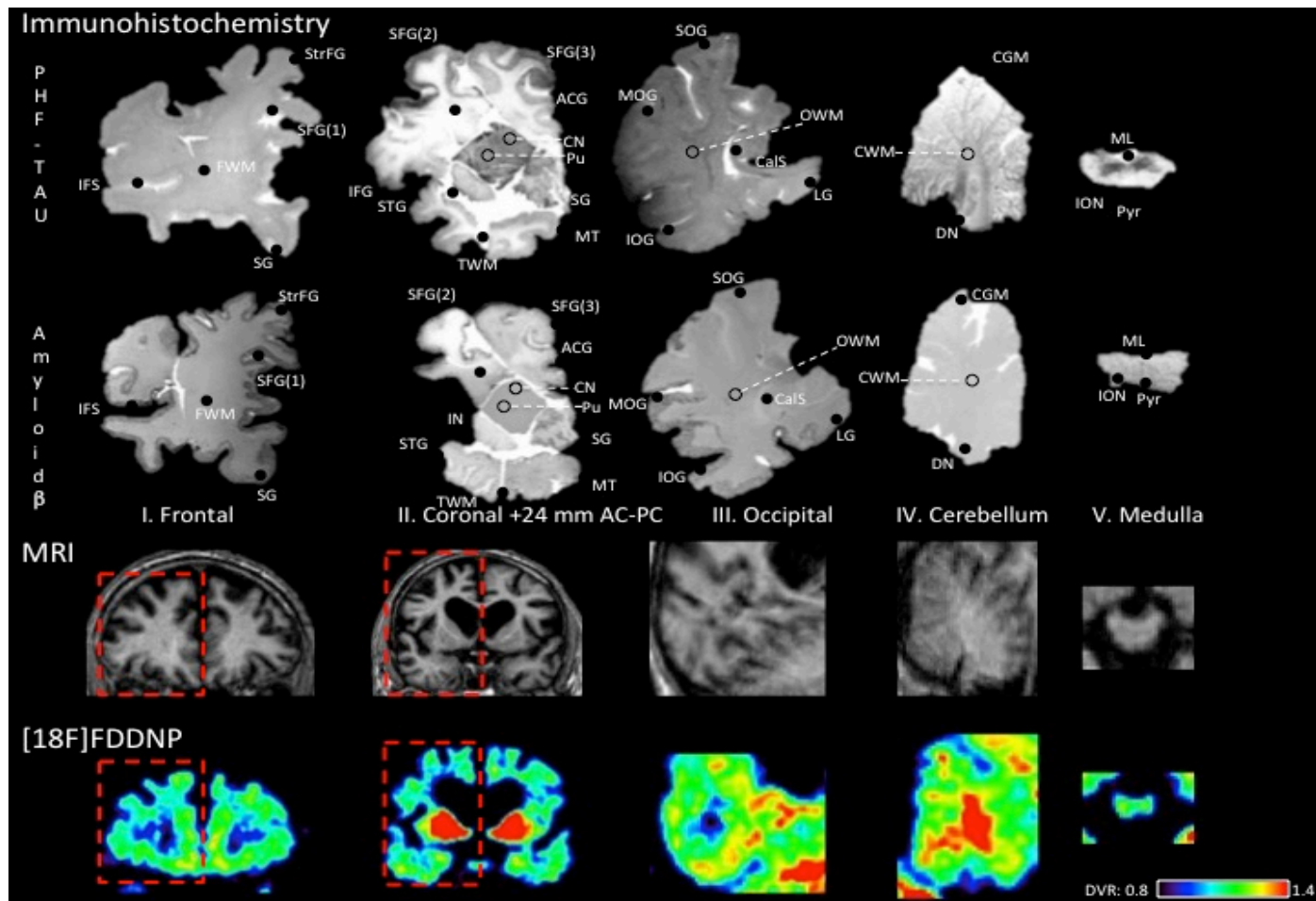


Figure 3.11 The *post mortem* pathology stained for tau and amyloid beta and co-registered to the $[^{18}\text{F}]\text{FDDNP}$ signal.

The *post mortem* pathology co-registered to $[^{18}\text{F}]\text{FDDNP}$ sectioned at a 40 μm thickness were 3-Dimensional Distribution Volume Ratio (DVR) image using the structural MRI as a guide. The frontal lobe, coronal section and the occipital lobe all displayed levels of amyloid beta and hyperphosphorylated tau burden in the cortical gray matter. As the DVR scale indicates the level of binding above background, it correlates with the disease displayed in the Progressive Supranuclear palsy brain. The frontal lobe (I) amyloid and tau staining was confined primarily to the neocortex and was much lower than other regions of the brain. The coronal section (II) was heavily stained for p-tau and the strong signal seen in the basal ganglia is correlated well with the $[^{18}\text{F}]\text{FDDNP}$ binding in the same region. The staining of the occipital lobe (III) was similar to the frontal lobe, where the presence of tau and amyloid was primarily confined to the grey matter; which appears similar to the $[^{18}\text{F}]\text{FDDNP}$ DVR image. The intense staining in the white matter of the cerebellum (IV) also well represented by the corresponding $[^{18}\text{F}]\text{FDDNP}$ image at the bottom. The medulla (V) staining for p-tau was relatively intense and did not appear as intense in the DVR image, but it is noted that in every comparison, the tissue was sectioned at 40 μm while the DVR image is has a PET resolution of 9mm at Full Width Half maximum (FWHM).

The *in vitro* [¹⁸F]FDDNP autoradiography was well correlated with the IHC staining from both the amyloid beta and tau immunohistochemistry. The cerebellar white matter and the medulla oblongata had elevated binding of [¹⁸F]FDDNP and did not display any amyloid beta. The medulla oblongata was chosen as the ideal candidate brain region to perform immunofluorescence and compare it against the fluorescent binding of FDDNP. The inferior olivary nucleus (ION) was picked particularly because it is a highly nucleated region and was initially found to have p-tau throughout the anatomy. Thioflavin S binds amyloid and tau, but since there was not amyloid present in the ION, it was clearly visible that the bound fluorescence is purely to p-tau. The PHF-tau antibody, FDDNP and Thioflavin S all highlighted small fibrils in the ION, but more importantly demonstrated an ability to bind to globose tangles (**Figure 3.12A**). In this work it is shown for the first time that FDDNP binds to globose tangles *in vitro*.

The sulci and the gyri were chosen as regions in the brain neocortex to microscopically compare the binding of [¹⁸F]FDDNP to the IHC stains of Amyloid and p-tau. The [¹⁸F]FDDNP autoradiography signal appears as a composite of both the tau and amyloid signal in the neocortex. (**Figure 3.12B**). The [¹⁸F]FDDNP autoradiograph co-registers well to the immunohistochemical staining with the tau signal appearing more intense than the amyloid beta signal. The macroautoradiography (**Figure 3.12D**) in the tissue sections shows a strong signal in the neocortex of all tissue signals. In the rostral ventromedial medulla the most intense signal comes from the dorsal portion of the medulla. The cerebellum signal showed a strong binding to the dentate nucleus and an intense signal in the white matter and granular layer interface. The dentate nucleus (**DN**) revealed staining for PHF-tau all throughout the sawtooth structure and was reflected in the both the macro- and microautoradiography. (**Figure 3.12C**) The [¹⁸F]FDDNP microautoradiography revealed the binding of the radiotracer to a dentate nucleus neuron. This was confirmed using the microscope under high magnification that [¹⁸F]FDDNP is binding to the intraneuronal Neurofibrillary Tangles (NFT's). The macroautoradiography shows high binding in the cortex of the frontal lobe, the occipital

lobe, and the temporal lobe; regions consistent with the levels of tau and amyloid found and also with the “Alzheimerization of the brain.”

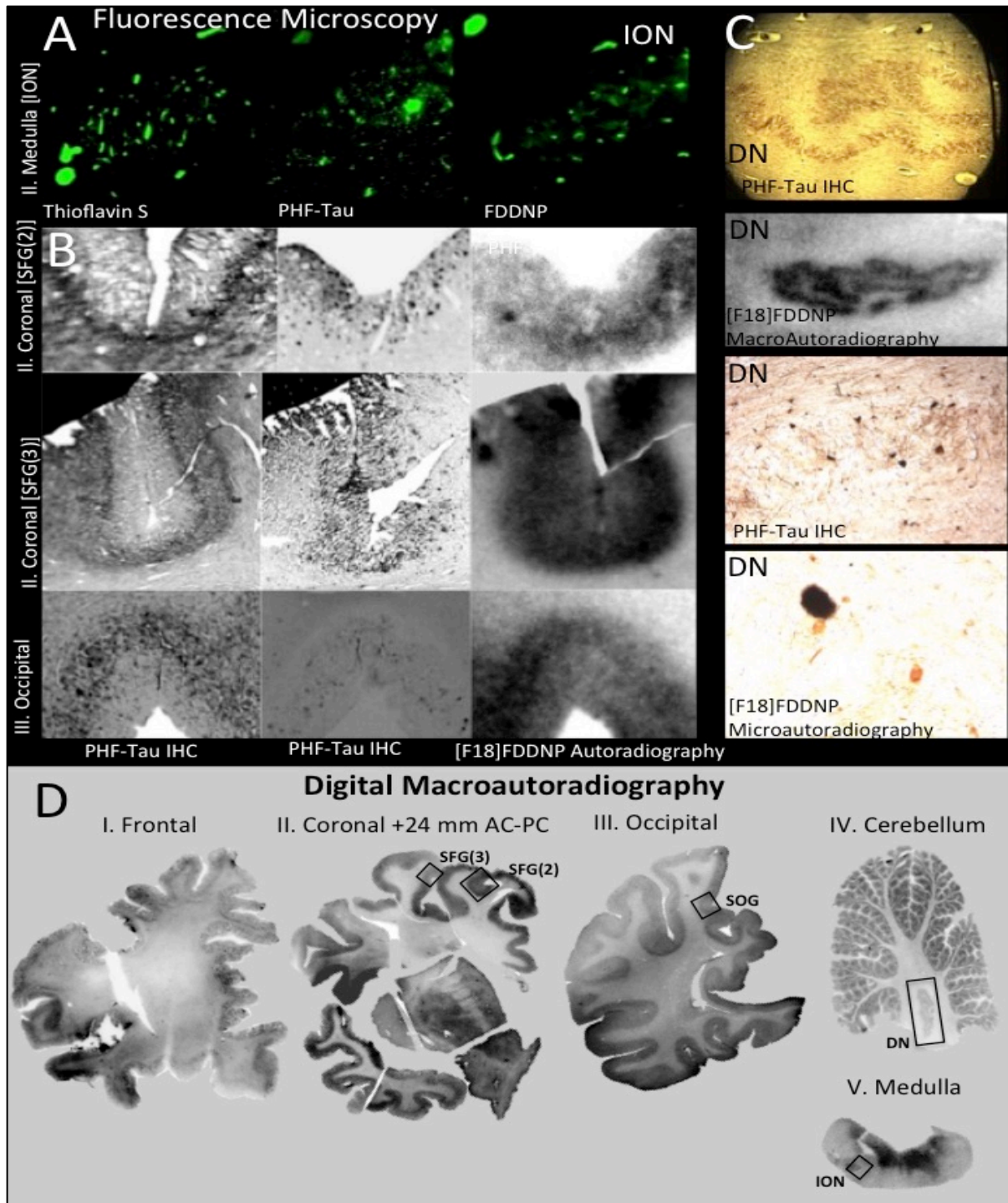


Figure 3.12 The autoradiography and fluorescent histology.

The 40 μm transverse section of the medulla oblongata demonstrated the similar binding profiles of Thioflavin S, PHF-tau and FDDNP (A) in the Inferior Olivary Nucleus (ION) using Fluorescent imaging. The medulla was chosen as a region of interest to investigate fluorescent binding since it was shown to be negative for the presence of amyloid beta through a DAB stain. The sulci and gyri display binding to amyloid beta and PHF-tau protein deposits in the cortical grey matter, consistent with the in vitro [F18]FDDNP autoradiography (B). The dentate nucleus (DN) was used to display the binding similarities between the PHF-tau IHC and both the micro and macro-autoradiography (C). The cerebellum displayed only tau pathology with no presence of amyloid beta, which aids in better displaying of the radiotracer binding to tau only. The digital macroautoradiography (D) demonstrates the contrast in [F18]FDDNP binding in the grey matter to the relatively lower signal in the white matter. The autoradiography correlated well with the tau pathology revealed through antibody staining

Neuroanatomy	Subclassification	[¹⁸ F] FDDNP DVR	Tau IHC	A-beta IHC	
IFS		1.07	3	3	
SG		1.16	3	3	
SFG(1)		1.10	3	3	
StrFG		1.09	3	3	
IFG		1.16	3	2	
STG		1.07	2	2	
SFG(2)		1.04	2	4	
SFG(3)	Grey Matter	1.08	3	3	
ACG		1.12	3	3	
MT		1.12	4	3	
IOG		1.20	3	3	
MOG		1.09	2	1	
SOG		1.23	3	1	
LG		1.21	4	3	
CalS		1.07	3	2	
CGM		1.08	1	0	
FWM		White Matter	1.03	3	1
WM			0.98	3	1
TWM			1.08	2	0
OWM			1.09	3	0
IN		Subcortical Nuclei	1.18	4	1
CN			1.26	3	0
Pu			1.57	4	0
CWM	Cerebellar White Matter	1.28	3	0	
DN		1.34	4	0	
ML	Brainstem	1.28	4	0	
ION		1.24	3	0	
Pyr		1.14	2	0	

Table 3.1. PHF-tau and Amyloid Beta Immunohistochemistry (IHC) grading values alongside their respective [¹⁸F]FDDNP DVR values.

Sampled from 23 anatomical locations, each ROI was evaluated using an [¹⁸F]FDDNP DVR value, a tau score and an amyloid-β score :

IFS(Inferior Frontal Sulcus), FWM(Frontal White Matter), StrFG(Straight Frontal Gyrus), SFG(1)(Superior Frontal Gyrus-1), SG(Straight Gyrus), IFG(Inferior Frontal Gyrus), IN(Insula), WM(White Matter), STG(Superior Temporal Gyrus), TWM(Temporal White Matter), MT(Medial Temporal), CN(Caudate Nucleus), Pu(Putamen), ACG(Anterior Cingulate Gyrus), SFG(2)(Superior Frontal Gyrus-2), SFG(3)(Superior Frontal Gyrus-3), IOG(Inferior Occipital Gyrus), MOG(Medial Occipital Gyrus), SOG(Superior Occipital Gyrus), OWM(Occipital White Matter), CalS(Calcarine Sulcus), LG(Lingual Sulcus), CGM(Cerebral Grey Matter), CWM(Cerebrall White Matter), DN(Dentate Nucleus), ML(Medial Leminiscus), ION(Inferior Olivary Nucleus), Pyr(Medullary Pyramids)

3.4 Statistics

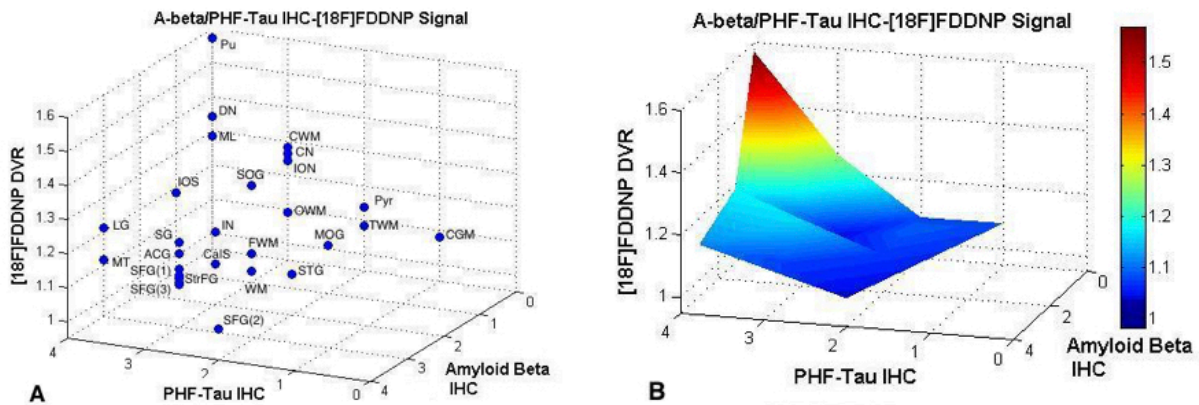


Figure 3.13 The scatterplots of the correlated $[^{18}\text{F}]$ FDDNP and immunohistochemical data. The data was plotted in a 3-dimensional scatter plot (A) with PHF-tau IHC vs. Amyloid Beta IHC with $[^{18}\text{F}]$ FDDNP along the z-axis. The scatter plot did not reveal any particular clusters of neuroanatomy that was indicative of high or low signal in relation to the pathology. A triangular mesh was added to the scatter plot to view the macro relationship of the data (B). The graph indicates that the tau seems to drive the $[^{18}\text{F}]$ FDDNP signal and in this particular case, the amyloid beta IHC is almost independent of the $[^{18}\text{F}]$ FDDNP DVR signal.

Each neuroanatomical point was described by a grade of PHF-tau IHC score, an amyloid beta IHC score and the $[^{18}\text{F}]$ FDDNP DVR value. The scatter plot did not reveal any particular pattern of cluster analysis that would distinguish the points of low IHC staining and high IHC staining in relation to the $[^{18}\text{F}]$ FDDNP DVR signal (**Figure 3.13A**). The triangular mesh overlay (Matlab R2011A, Wolfram) displayed a larger macro relationship with all the points revealing a larger relationship between amyloid, tau and $[^{18}\text{F}]$ FDDNP DVR signal. As the tau signal increases in any particular region, there is a more intense $[^{18}\text{F}]$ FDDNP DVR signal. The amyloid beta IHC signal seems to have an almost inverse correlation where we see the lower depositions of amyloid in the regions of higher $[^{18}\text{F}]$ FDDNP signal. It must be noted that the regions that have lower levels of amyloid also have higher levels of p-tau IHC staining.

The 28 neuroanatomical data points were reclassified into 5 subclassifications based on morphological similarities so the means might be more representative of the relationships between the IHC staining and the [¹⁸F]FDDNP signal. (Table 3.2)

Table 3.2 Means and standard deviations of the binding of [¹⁸F]FDDNP in 5 subclassifications of the neuroanatomy.

The neuroanatomy was categorized into 5 subclassifications based on morphological characteristics and regional similarities. The corresponding [¹⁸F]FDDNP DVR signals were coregistered with the immunohistochemical scores for both amyloid beta (6F/3D) and hyperphosphorylated tau (AT8).

Brain Region	[¹⁸ F]FDDNP DVR	PHF-tau IHC	A-beta IHC
Cortical	1.09±.03	2.7±.82	2.42±1.15
White Matter	1.16±.07	3±.71	2±1.0
Brainstem	1.22±.07	3±1.0	0
Subcortical Nuclei	1.29±.19	3.5±.58	1±1.41
Cerebellum White Matter	1.31±.04	3.5±.71	0

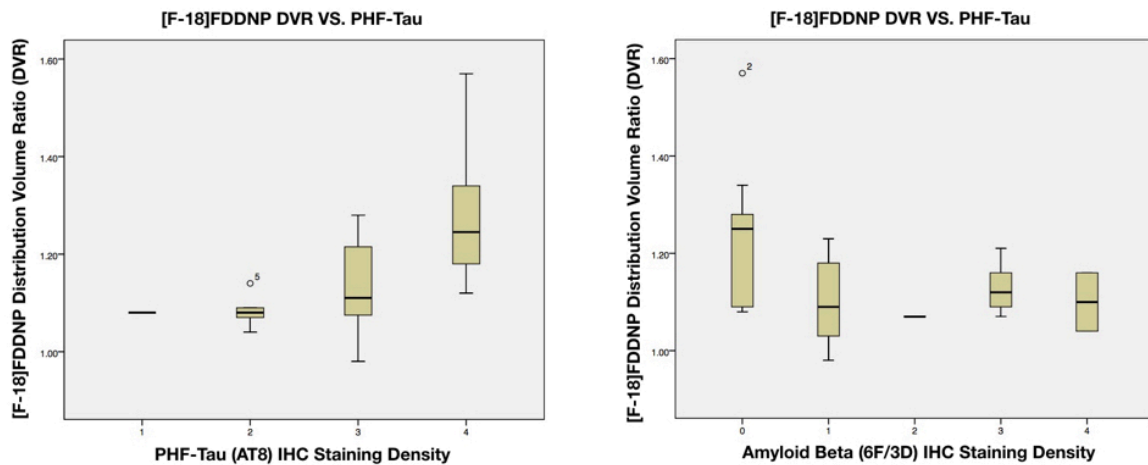


Figure 3.14 [¹⁸F]FDDNP DVR vs. IHC 2-D Box plots in the 28 neuroanatomical regions.

The plots of the [¹⁸F]FDDNP vs. the immunohistochemical staining of both PHF-tau and Amyloid beta in a 2-dimensional box plot were made in SPSS (v24, 2017). It is clear as the staining intensity of PHF-tau positively correlates with [¹⁸F]FDDNP DVR signal and they both increase together. The amyloid beta IHC relationship is inversely correlated between the [¹⁸F]FDDNP DVR signal and the amyloid beta IHC staining, but is less correlated. The box plot was used to visualize the data because the IHC staining was scored on an ordinal scale to reduce the variability in a continuous scale .

The mean values seem to display a stronger correlation between the deposition of hyperphosphorylated tau and amyloid beta in relation to the [¹⁸F]FDDNP DVR signal (Table 3.2). The PHF-tau IHC staining significantly correlated with the [¹⁸F]FDDNP DVR signal as the

Pearson Correlation of 0.962 (p=.004). The Spearman Rho correlation was slightly less at 0.949 (p=.007) between the PHF-tau IHC and [¹⁸F]FDDNP DVR signal. There existed a weaker inverse correlation between the deposition of amyloid beta and the [¹⁸F]FDDNP DVR signal measured by a Pearson correlation of -0.815 (p=.041) and a Spearman's Rho correlation of -0.821 (p=0.044). The correlation between the immunohistochemistry and the [¹⁸F]FDDNP DVR signal demonstrates the contribution of tau in any particular brain region in the particular PSP brain and to a lesser degree the amyloid beta burden. No statistically significant correlation was found between tau and amyloid beta.

Table 3.3 The correlation coefficients between the PHF-tau and Amyloid Beta IHC compares to the [¹⁸F]FDDNP DVR values.

Both indicate a strong correlation between the [¹⁸F]FDDNP DVR signal to the PHF-tau IHC and a strong negative correlation to the Amyloid Beta IHC. The Pearson Correlation Coefficient and Spearman Rho Correlation Coefficient were both calculated for the mean values between the subclassifications. The tau IHC correlations were statistically significant (p<.01) with the amyloid IHC also statistically significant (p<.05) to a lesser degree.

Variable	Pearson Correlation	Significance	Spearman Rho Correlation	Significance	N
DVR	1.0	--	1.0	--	5
PHF-tau IHC	0.962**	.004	.949**	.007	5
Amyloid Beta IHC	-0.815*	.041	-.821*	.044	5

*p<.05 **p<.01

3.5 Discussion

In a previous work with Progressive Supranuclear Palsy patients it was demonstrated that the radiotracer [¹⁸F]FDDNP was retained in regions of the brain that are consistent with the hyperphosphorylated tau protein deposition (Kepe et al. 2013). In this case study, it was shown that [¹⁸F]FDDNP does in fact bind to the hyperphosphorylated tau and amyloid beta proteins in the brain of a patient with PSP. The disease itself is a tauopathy, thus it was not anticipated to find such widespread amyloid beta throughout the neocortex of the patient. At the time of death it was reported by the neuropathologist that the patient had begun to display the pathological effects of Alzheimer's disease referred to as "Alzheimerization of the brain." In the neocortical regions where there was overlapping amyloid and tau signal, it is clear that the binding signal

from both misfolded proteins contribute to the overall signal seen in the autoradiographic image. It was also clear from the autoradiography that the [¹⁸F]FDDNP signal originating from the hyperphosphorylated tau (p-tau) appeared more intense in the autoradiographic images. **(Figure 3.12B)** The frontal cortex, the premotor cortex, the putamen, the temporal cortex and the occipital cortex all contained both p-tau and amyloid beta proteins. The cerebellum and the medulla oblongata were both heavily tau stained regions, which did not express any presence of amyloid beta. Both neuroanatomical regions were chosen to analyze the binding of [¹⁸F]FDDNP to p-tau in the absence of amyloid beta. The binding of FDDNP as viewed under the fluorescent microscope demonstrated the ability of the radiotracer to bind to phosphorylated tau; specifically in the form of globose tangles **(Figure 3.12A)**. As previously reported, FDDNP under fluorescent conditions has been shown to bind to flame-shaped hyperphosphorylated tau tangles in a case of Dementia with Lewy Bodies (DLB). This is the first recorded instance FDDNP has demonstrated an ability to bind to the intracellular tau globose tangles. There was intense *in vitro* [¹⁸F]FDDNP binding to the dorsal portion of the rostral ventromedial medulla.

The inferior olivary nucleus is a small group of nuclei which connect superiorly to the dentate nucleus in the cerebellum. The hypothesis behind the inferior olivary function has suggested that its main function is involved in timing synchronization and learning processes involving nuclei in the olivocerebellar pathways (Voogd et al. 2013). The inferior olive connects to the climbing fibers in the cerebellum and the Purkinje neurons; which may indicate why the PSP patient experiences dysfunctions related to the vertical gaze palsy symptoms that arise during the disease progression (Voogd et al. 2013). The nucleus ambiguus in the dorsal medulla is believed to be responsible for swallowing and speech, as well as its afferent projections extending to the premotor cortex (Ludlow 2015). The impact of tau on the nucleus ambiguus undoubtedly plays a role in this patient's difficulty swallowing during the late stages of PSP.

The cerebellum has been shown through numerous investigations of cerebellar ataxia to be involved in locomotion in the form of limb movement, posture, stability and feed forward control via error feedback signaling (Morton and Bastian 2007). The cerebellum was also implicated in the ability for the mammal to condition a learned response to a stimulus via the mossy fibers in the cerebellum. It was hypothesized that the climbing fibers from the inferior olive are responsible for many of the unconditioned responses converging in the cerebellum (Bracha et al. 2009). The two fiber types converge in the Purkinje neurons where this conditioned response is believed to occur and the error signals can be interpreted into motor function (Bracha et al. 2009). The widespread hyperphosphorylated tau deposition in the cerebellar white matter and dentate nucleus undoubtedly affects the motor coordination of the PSP patient.

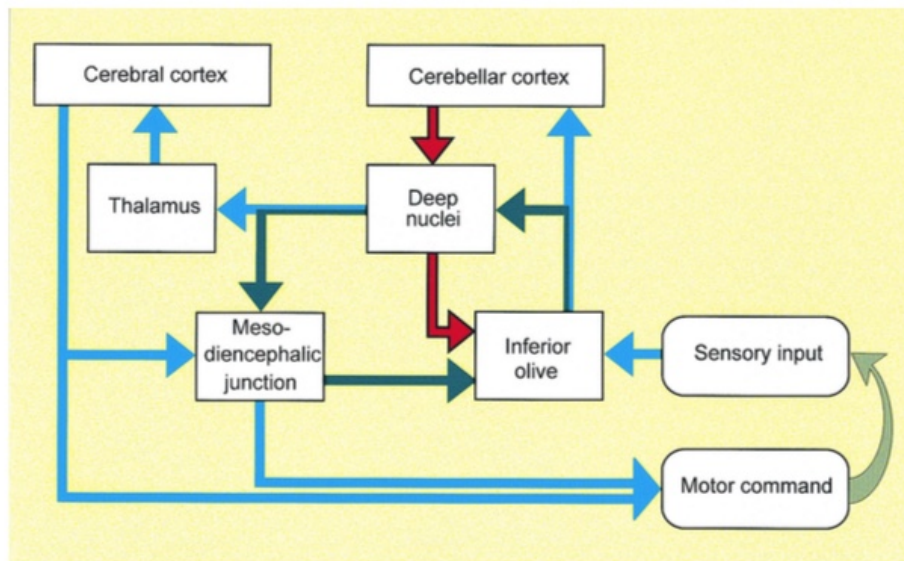


Figure 3.15 The microcircuitry of the inferior olive and the olivocerebellar cortical pathway (De Zeeuw et al. 1998).

The three neuroanatomical loops (dark green arrows) consist of the mesodiencephalic junction, deep nuclei and the inferior olive. The inhibitory neurons are responsible for attenuating signal as part of a feedback loop (red arrow), while the excitatory neurons are sending a positive signal (light blue). The dark green arrows also indicate excitatory neurons and the light green signifies excitation for sensory input. (De Zeeuw et al. 1998)

PSP is a 4R tauopathy and the progression of the disease is driven by the accumulation of hyperphosphorylated tau throughout the brain and most notably within the subcortical nuclei. The progressive neurodegeneration is believed to be driven by the spread of p-tau, so it would be logical that the binding of tau throughout the brain is driving the [¹⁸F]FDDNP signal. The strong Pearson's correlation $r=0.962$ ($p=.004$) between the [¹⁸F]FDDNP DVR signal and the tau immunohistochemistry indicates that the binding of the radiotracer is indeed due to the heavy presence of tau. There was also a significant negative Pearson's correlation $r=-0.821$ ($p=.041$) of amyloid beta IHC to the [¹⁸F]FDDNP DVR signal. The negative correlation may not be representative of the true [¹⁸F]FDDNP signal, since we know the [¹⁸F]FDDNP DVR signal is a composite of both tau and amyloid binding. Since the p-tau is the dominant pathology, it is most likely in larger abundance in the patient brain. Additionally, the amyloid beta pathology does not appear until later in the course of disease progression and every place we find amyloid beta we also find tau. The p-tau is undoubtedly driving the [¹⁸F]FDDNP signal, so it may be considered that the relationship between amyloid beta and [¹⁸F]FDDNP signal may in fact be several orders of magnitude different than the relationship between the binding of [¹⁸F]FDDNP to hyperphosphorylated tau. This examination of a confirmed PSP patient brain is the first to confirm the binding of [¹⁸F]FDDNP to both hyperphosphorylated tau and amyloid beta in a tauopathy.

The *in vivo* [¹⁸F]FDDNP DVR signal is a sum of both the hyperphosphorylated tau and amyloid beta binding in the PSP patient brain. In this particular patient, we are aware that PSP is the primary tauopathy that caused this patient's death and the "Alzheimerization of the brain" appears to occur at the later stages of the disease and is a secondary disease that contributed to co-morbidity. Examining the macroautoradiographic [¹⁸F]FDDNP signal in the sulci of the brain (**Figure 3.12B**) revealed that the majority of the signal in the panels (**Figure 3.4 I – III**) originate from the sites of heavy p-tau staining. It is quite possible that the *in vivo* [¹⁸F]FDDNP signal seen in this patient primarily originates from the binding to hyperphosphorylated tau and

the lower levels of amyloid binding can be considered to be negligible to the sum total [18F]FDDNP signal. The relationship between overall [18F]FDDNP signal to the amyloid and tau pathology can be simplified by the following equation:

$$\begin{aligned} \mathbf{DVR_{Tau} + DVR_{Amyloid} = DVR_{Total}} \\ \mathbf{If, DVR_{Tau} \gg DVR_{Amyloid} \textit{ then, } DVR_{Amyloid} \approx 0} \\ \mathbf{therefore, DVR_{Tau} \approx DVR_{Total}} \end{aligned}$$

Equation 3.1 [18F]FDDNP Total DVR signal in a select case of PSP.

The [18F]FDDNP signal is a composite of the binding of amyloid beta and hyperphosphorylated tau in the diseased brain. In the case where a tauopathy is the primary disease driving the motor and cognitive dysfunction, the amyloid signal may become almost negligible. In this instance the total signal measured *in vivo* can be considered to be equal to the bound [18F]FDDNP signal originating at the site of tau.

The binding of [18F]FDDNP exhibited in this case also raises the idea that while we know the published value of an apparent higher binding site ($K_D=0.12nM$) and a lower affinity binding site ($K_D=1.86nM$) for amyloid beta; the binding affinity of [18F]FDDNP to p-tau may be higher than the binding to amyloid beta. It must also be considered that the tau fibril pathology in similar optical density as the amyloid plaques may contain more binding sites for [18F]FDDNP which would produce a more intense signal. One consideration that must always be made in comparing *in vivo* binding of any PET radiotracer to the *in vitro* binding to *post mortem* brain tissue is the difference in tissue thickness as compared to the slice thickness of any particular plane of the PET image. The *post mortem* brain tissue used for this research was sliced at a thickness of 40 μm to optimize the visibility of both fluorescent and immunohistochemical stains under the microscope. The [18F]FDDNP PET image has a plane separation of 2.42 mm, so the resultant PET image is 60x thicker than the tissue slide (Smid et al. 2013). The [18F]FDDNP parametric DVR image is the result of several layers of signal contributing to a resultant signal seen in the 3-D image.

Spending considerable time analyzing a 4R tauopathy in the PSP patient brain not only helped to enlighten me to the destructive powers of some very small, misfolded proteins, but it has also made it apparent of how widespread these proteins are at the end stages of brain

disease. The appearance of hyperphosphorylated tau in the cerebellar white matter is a fairly rare occurrence in the context of brain disease, but it was noted during microscopic that the most intense presence of p-tau was consistently seen at the interface between the white matter and the granular layer. The myelinated fibers that run parallel to the surface of the granular layer may in some way be responsible for the first appearance of tau in the cerebellum or at least appear to be more vulnerable.

During the course of pathological investigation of the *post mortem* brain tissue in this study, immunofluorescent staining provided confirmation of the binding of FDDNP to globose tangles as confirmed by Thioflavin S and the PHF-tau antibody. One major obstacle that must be overcome in using fluorescent staining in the aging brain is the presence of small lipid vacuoles known as “lipofuscin.” In this study, the lipofuscin autofluorescence was overcome by saturating the lipid pigments with a compound called Sudan Black B (SBB), which is highly lipophilic and binds to the lipid vacuoles. While these small pigments are an annoyance to the researcher using fluorescent investigation, it did make me wonder what exactly these small “fat” globules are doing in the brain of the aging human. After considerable literature search I was unable to find much research on lipofuscin itself and if it plays any role in neurodegenerative disease. It is a wonder if there is anything in these vacuoles that might provide us more information about the brain diseases that ravage patient brains. The investigation of this particular PSP brain highlights the need for a better understanding of the disease origins at the earliest pathological beginnings of neurodegenerative disease with the hope of drastically improving patient outcomes.

CHAPTER FOUR: COMPARISON OF THE *IN VIVO* [¹⁸F]FDDNP PET IMAGING AMONG COHORTS OF PROGRESSIVE SUPRANUCLEAR PALSY (PSP), PARKINSON'S DISEASE (PD), HUNTINGTON'S DISEASE (HD), CHRONIC TRAUMATIC ENCEPHALOPATHY (CTE) AND HEALTHY CONTROL PATIENTS

4.1 Introduction

The ability for an *in vivo* non-invasive imaging method to detect hallmark pathology in a patient living with neurodegenerative disease has offered up an opportunity to identify and treat patients prior to their deaths. Since the disease progression can be variable amongst patients and diseases, it is often difficult to associate patient symptomology with underlying pathology. [¹⁸F]FDDNP has previously demonstrated an ability to bind to the pathology in patient's brains suffering from Alzheimer's disease (Kepe et al. 2006), Germaun-Straussler disease (Kepe et al. 2010), Dementia with Lewy Bodies (DLB) (Smid et al. 2013), PSP (Kepe et al. 2013) and CTE (Barrio et al. 2015). There are many diseases that can present with a spectrum of overlapping symptoms that can be difficult to diagnose and effectively treat. In this study, six cohorts were chosen to compare the binding of [¹⁸F]FDDNP to one another: a younger healthy control group (<60 years), an older healthy control group (>60 years), a group of PSP patients, a group of CTE patients, a group of Huntington's Disease (HD) and a Parkinson's Disease (PD) cohort. In this examination of 98 total patients, the dynamic [¹⁸F]FDDNP scans were performed over a time period of approximately 10 years and were all acquired on either the ECAT HR Scanner (Siemens, CTI) or the Biograph PET/CT scanner (Siemens, CTI). The [¹⁸F]FDDNP had been prepared in the same manner throughout the study as previously described and each patient received a bolus injection of 10 mCi of radioactivity in each study session (Liu et al. 2007). The

cohorts were chosen as part of this study since they are all progressive motor diseases and while PSP and CTE share underlying pathology, PSP and PD can share overlapping symptoms, the HD cohort serves as a negative disease control and our healthy patients serve as a baseline for the healthy brain. The use of [¹⁸F]FDDNP PET can help to provide insight into a patient's neurodegenerative disease and this study examines the binding amongst multiple groups to better inform the binding profiles between different cohorts.

The ability to co-register a structural T1 Magnetic Resonance Image scan to a patient's [¹⁸F]FDDNP PET scan can help guide the selection of ROI's in the neuroanatomy and reduce the error in manual ROI drawing. Many of the MRI's were not available for patients involved in this study, so each patient PET image was examined without the use of an accompanying structural MRI. The first 7 frames, or 6 minutes of each dynamic scan, are summed to produce a perfusion PET image that can be used to highlight the regions where the radiotracer has healthy perfusion in the brain tissue.

Progressive Supranuclear Palsy-Richardson's Syndrome (PSP-RS) is a disease that is often mistaken for PD, especially early in the clinical presentation when there is a therapeutic response to synthetic Dopamine (Liscic et al. 2013). It is critically important that the clinicians are able to differentiate between these two diagnoses and track the pathology *in vivo* as patient's undergo therapeutics focused on reducing the disease burden (Williams et al. 2005). The MRI can often be indicative of PSP when atrophy in the midbrain is clearly visible, but patients may not display the traditional PSP hallmarks especially early in the disease course (**Figure 3.8**). The binding of [¹⁸F]FDDNP to hyperphosphorylated tau should be able to distinguish PSP from PD since there is no tau or amyloid in the pure PD brain.

Most neurodegenerative diseases are essentially death sentences for the patients; whether acute or chronic, research has not provided any substantial solutions to halting the spread of these diseases or any compounds that can reverse the damage they incur. While it may sound rather disparaging, once the brain disease has destroyed healthy neurons or

astrocytes, a particular affected brain region may no longer be capable of functioning normally.

Most recently, it has been made evident that a large number of athletes participating in competitive sports risking traumatic brain injury (TBI) are developing neurodegenerative disease, dubbed Chronic Traumatic Encephalopathy (Small et al. 2013; McKee et al. 2009). A previous study involving CTE patients showed that those athletes who have received more concussive brain trauma had suffered a worse clinical outcome and retained more tau pathology (Barrio et al. 2015). Huntington's disease is a devastating genetic mutation that is detectable long before the pathological burden begins to affect the patient motor function. The huntingtin (htt) fragments incur neuronal degeneration as heavily in the striatum as tau and amyloid based disease, but show no presence of either misfolded protein. The HD patients serve as an appropriate negative disease control; showing disease affects but no pathology with an affinity for [¹⁸F]FDDNP. The Parkinson's disease patients can often be misdiagnosed since the Parkinsonism symptoms are shared across a wide range of neurodegenerative diseases. The pure PD patient will not exhibit abnormal tau or amyloid, but can share symptoms with PSP-P patients. The majority of PSP patients can be classified as two clinical subtypes based on the response to the synthetic dopamine, Levodopa: PSP-Richardson's Disease (PSP-RS) and PSP-Parkinsonism (PSP-P) (Williams et al. 2007). The PSP-P patient may share clinical symptoms with PD patients and show a positive response to Levodopa as a result of the loss of dopaminergic neurons in the substantia nigra. The PSP and CTE patients both share the characteristic hyperphosphorylated tau (p-tau) pathology in the affected regions of the brain. The p-tau pathology in the CTE brain is the 3R isoform and the PSP brain is of the 4R isoform, but the binding of [¹⁸F]FDDNP is incapable of distinguishing between the two different isoforms (Liscic et al. 2013; McKee et al. 2015).

Molecular imaging is one of the few *in vivo* techniques that offer the possibility of being able to track disease during treatment to determine if the pathological burden is being reduced or removed from the patient brain. In this study we address the ability of distinguishing

between patients based on the binding of [¹⁸F]FDDNP to particular neuroanatomy and brain regions. Neurodegenerative diseases are progressive diseases and as we measure the means across each cohort it is noted that each patient cannot possibly be at the same state of progression with their respective diseases. This research is focused on identifying key regions in each cohort that might be impacted by p-tau or amyloid beta. Identifying the key regions will ultimately aid in identifying afflictions when used in collaboration with other clinical diagnostic procedures.

4.2 Materials & Methods

4.2.1 [¹⁸F]FDDNP patient imaging protocol

The radiotracer [¹⁸F]FDDNP was synthesized at the Biomedical Cyclotron located on the UCLA campus as previously described in **Section 3.2.1** (Liu et al. 2007). The compound was synthesized for patient study and a portion of the volume was used to quantify the chemical purity of radioactive [¹⁸F]FDDNP using High Performance Liquid Chromatography (HPLC) and Thin Layer Chromatography (TLC). [¹⁸F]FDDNP has a radioactive half-life ($\tau_{1/2}=109.8$ minutes), which demands sufficient activity to allow 10 mCi of activity to be available at a later time for patient injection. The hydrophobic nature of [¹⁸F]FDDNP requires that it is dissolved in a concentration of 10% Ethanol and diluted to 1% in saline with human serum albumin necessary for human injection, acting to reduce the nonspecific binding *in vivo*.

Patients were scanned on either the Positron Emission Tomography (PET) ECAT HR scanner (Siemens, CTI) or the Biograph PET/CT (Siemens, CTI) Scanner at the UCLA Ahmanson Medical Center; with the two scanners having comparable performance (Trebossen et al. 2009). Prior to the bolus injection of [¹⁸F]FDDNP, a 10-minute attenuation scan was acquired for accurate image reconstruction. As the patient lay supine in the PET scanner, a 5 mCi to 10 mCi bolus of [¹⁸F]FDDNP was injected intravenously and a dynamic scan immediately followed, recording either 18 or 20 frames. The frames consisted of: 6 x 30 second frames, 4 x

180 second frames and either 8 or 10 x 300 second frames for a total scan time between 55 and 65 minutes.

4.2.2 PET Image Reconstruction and Motion Correction

All PET scans used in this study were corrected for decay, scatter, attenuation in the scanner and reconstructed using filtered back projection (Hann filter, 5.5 mm FWHM). The ECAT HR PET scanner reconstructs each frame with 63 contiguous planes and a 2.42 mm plane separation. The Biograph PET/CT scanner produces dynamic frames with 109 contiguous slices and a plane separation of 2.0mm. Motion correction is performed by either using a retrospective adjustment made to the transmission and emission scans performed on the ECAT PET scanner or the CT is used to correct for attenuation and align the PET image to the CT image (Wardak et al. 2010; Ye et al. 2014). In many instances when the patient involved in the study is suffering from a neurodegenerative disease and has a brain PET scan performed, there can be considerable movement during the data collection time period. The movement correction procedure is necessary not only to improve resolution, but also to be able to properly quantitate the PET images.

4.2.3 [¹⁸F]FDDNP parametric DVR Image Co-registration and format conversion

The ECAT and the Biograph PET scanner produces raw image formats that are assembled using motion correction software producing dynamic [¹⁸F]FDDNP PET scans in a “.v” file type (Wardak et al. 2010). In order to produce the parametric DVR image, the file is then converted to an Analyze format with an “.img” file type extension (Robb et al. 1989). Using the “.img” file type, the Logan Analysis is performed to create the parametric DVR image created with the dynamic [¹⁸F]FDDNP scan. The DVR image is converted from the Analyze “.img” file format back to the ECAT7 format using the conversion software MedconX (Nolf 2003). The dynamic PET scan is summed using the first seven frames to provide a perfusion image to delineate the neuroanatomy. The summed image can also be used to re-position the PET image so the brainstem is perpendicular to the axial imaging plane. In the instance where the PET

image was translated and rotated, the [¹⁸F]FDDNP DVR image was co-registered to the summed [¹⁸F]FDDNP image in SPM(Matlab, SPM12) (Friston 2007). The co-registration in SPM12 requires the NIfTI file format, which be converted from the ECAT file format (Nolf 2003). All conversions involving any PET image must be performed with great care to ensure the original voxel intensities are preserved during the conversion process.

4.2.4 Progressive Supranuclear Palsy (PSP) cohort Imaging

The cohort of PSP patients (N=12) had a mean age of 63.8 years of age and all had been clinically diagnosed as probable PSP. The mean MMSE score for the cohort was a mean score of 22.4. Most patients in this study were imaged in a single scan; for those patients with multiple scans, the last [¹⁸F]FDDNP scan was used for the statistical calculations. The neurodegeneration of motor functions within the PSP patient brain has made the acquisition of a Positron Emission Tomography (PET) dynamic scan over a period of 60 minutes extremely difficult for some patients. In this study, there were some PET scans where the data was unusable due to the poor resolution or interrupted PET scans during the data collection. Some of the PSP patients did have a PSP Rating Scale score, but there were not enough scores collected to test the correlation of the scores to the [¹⁸F]FDDNP binding with a statistical significance (Golbe and Ohman-Strickland 2007).

4.2.5 Parkinson's Disease (PD) cohort Imaging

The cohort of PD patients (N=16) with a mean age of 63.2 years of age all who had been clinically diagnosed as probable PD and those that converted during the study were removed from the cohort. The mean MMSE score for the PD cohort was 28.4 across the 16 patients. At the time of being scanned all the patients were diagnosed as likely PD, but it is possible that a misdiagnosis early on in the disease progression is quite possible. Some of the patients did have the UPDRS clinical rating scale score but it was not used in this study since the focus of the study was to compare [¹⁸F]FDDNP binding between the PD and PSP patients (Goetz et al. 2008). The Parkinson patient can often struggle with the motor dysfunctions during the disease

progression, which can make spastic movements difficult to image the PD patient in the PET scanner. The PSP patient may present with Parkinsonism symptoms due to the affected substantia nigra in both diseases, but the p-tau pathology is substantially different from the α -synuclein found in the PD patient. Theoretically the PSP patient should have specific [^{18}F]FDDNP binding in the affected regions and the PD patient should have no binding.

4.2.6 Huntington's Disease (HD) cohort Imaging

The mean age of the cohort of Huntington's disease patients (N=15) was 36.8 years and no MMSE scores were recorded for these patients. The HD patients were all confirmed to possess the expanded CAG repeat in the HTT gene which is indicative of the genetic trait of Huntington's disease (Ross and Tabrizi 2011). HD progression will inevitably lead to chorea, which can make it difficult to image patients in the PET scanner for extended periods of time. The scans used in this study were 60 minutes in duration, making it challenging to scan patients with advanced disease pathology. The HD patient will eventually suffer from motor dysfunction, but does not retain any of the amyloid or p-tau pathology and serves as a negative disease control.

4.2.7 Chronic Traumatic Encephalopathy (CTE) cohort Imaging

The cohort of Chronic Traumatic Encephalopathy patients (N=14) imaged in this study had a mean age of 58.1 years and a mean MMSE score of 27.1. Studying the CTE patients from the perspective of a PET study has the advantage of the disease itself not heavily affecting motor functions in the early stages of the disease. The patients are typically able to endure the PET scanning easier than some of the other cohorts; but the disease can sometimes present with anxiety, which can add difficulty for a prolonged imaging session in a confined scanner. CTE is a disease that has been present in our society for some time, but has only recently been connected to Traumatic Brain Injury as the driving cause (Omalu 2014).

4.2.8 Younger Control (<60 yrs) cohort Imaging

The cohort of patients involved in the study (N=17) had a mean age of 40.4 years and no MMSE scores were recorded or accessible for these patients. It can be safely assumed that all patients classified in the control groups were cognitively healthy and any potential conversions were removed from the study. The younger control serves as an age-matched comparison for HD patients and some CTE patients as well, since the age of onset can be considerably younger for both diseases.

4.2.9 Older Control (>60 yrs) cohort Imaging

The older control patients used in this study (N=24) had a mean age of 71.3 years and no MMSE scores were recorded or available for these patients. The older control cohort served as a baseline for the PSP patients, the PD patients and the cohort of CTE patients. The older control group is important because it helps us to establish a baseline in the normal aging brain which can accumulate amyloid beta while being cognitively normal (Dickson et al. 1992). The healthy control groups serve as a negative control to compare the non-specific binding to the diseased patient brain containing amyloid or tau.

4.2.10 Distribution Volume Ratio (DVR) Logan Analysis

The binding of [¹⁸F]FDDNP to amyloid beta and hyperphosphorylated tau in the human brain is estimated using image analysis techniques developed by Jean Logan as an alternative to arterial blood sampling (Logan et al. 1996). The Logan analysis was adapted to a Single Reference Tissue Model (SRTM) for [¹⁸F]FDDNP using the cerebellar cortex as a reference tissue with little nonspecific binding and adequate tracer perfusion. The bound and unbound tracer is distinguished using the steady state of the [¹⁸F]FDDNP Time Activity Curve (TAC). As long as the efflux time period of the radiotracer is relatively linear, the ratio of concentrations can be estimated using the Logan Analysis (Wong et al. 2007).

The [¹⁸F]FDDNP DVR images are produced using a Sun Microsystem, Unix-based Workstation. The cerebellar grey matter is used as the reference region to build the Distribution

Volume Ratio image, since it is typically free of disease. [¹⁸F]FDDNP is a reversible PET radiotracer, which allows the estimation of the radiotracer concentration during this transient time period of “washing in” and “washing out.” The resultant DVR image is a ratio of bound [¹⁸F]FDDNP to amyloid beta or hyperphosphorylated tau in relation to the unbound tracer in the cerebellar grey matter.

4.2.11 [¹⁸F]FDDNP Parametric DVR Image Analysis

The regions of neuroanatomy chosen to compare in this study are similar to the brain regions selected in previous studies with [¹⁸F]FDDNP.(Kepe et al. 2006; Smid et al. 2013; Kepe et al. 2013) The following neuroanatomy was selected for comparison among the cohorts: cerebellar white matter (CWM), medulla oblongata (MED), pons (PON), ventral midbrain (MBV), dorsal midbrain (MBD), amygdala (AMG), medial temporal lobe (TEM MED), lateral temporal lobe (TEM LAT), occipital lobe (OCC), caudate nucleus (CAU), putamen (PUT), striatum (STR), thalamus (THL), posterior cingulate gyrus (PCG), parietal lobe (PAR), anterior cingulate gyrus (ACG), frontal lobe (FRN), motor cortex (MOT). The DVR values extracted from the Regions of Interest (ROI) are a well-balanced representation of both neuroanatomy and neurological function.

The first seven frames (6 minutes) of each dynamic [¹⁸F]FDDNP scan were summed together to be used as a perfusion image where the healthy, perfused neuroanatomy may be highlighted. The regions of interest are drawn atop the summed image and imported to be overlaid on the parametric image so the underlying DVR values may be extracted for each ROI. The four diseases studied in this research are each unique in the pathology associated with each disease, but also in the regions where they affect the human brain.

4.2.12 Statistical Analysis

The data extracted from each of the 19 Regions of Interest (ROI's) for all members of the 6 cohorts (N=98) resulted in 1,862 [¹⁸F]FDDNP DVR values that were analyzed to evaluate statistical differences between the means (IBM, SPSS v24). All cohorts were analyzed using a

one-way Analysis of Variance (ANOVA) to determine if there was a statistical difference in the group means across the six cohorts. A Levenne's test was administered to determine if the variance was homogenous to be able to statistically compare means. The means that showed heterogeneous variance distributions were administered the Brown-Forsythe test to determine if a significant difference existed amongst the group means. If the Brown-Forsythe test was found to be significant, a *post hoc* Dunnet's T3 test was performed to determine which cohorts had statistically significant means. In the groups where variance was determined to be homogenous, a *post hoc* Bonferroni test was conducted to determine if any significance between the means existed. The results from these studies were also examined in two different manners: by first comparing each cohort to an appropriate age-matched control and then combining all the control patients into a single larger cohort. The larger cohort of control patients represent a spectrum of healthy patients, which might provide a more accurate baseline of [¹⁸F]FDDNP binding to compare against diseased patients. In each neurodegenerative disease there exists a continuous progression of disease that cannot be determined without a pathological analysis of the brain tissue. Using the mean [¹⁸F]FDDNP DVR values to compare both the healthy and diseased brains to one another, incorporate a range of disease progression and thus will also include a range of values. This study aids in a better understanding of the pathologically impacted brain regions by hyperphosphorylated tau and amyloid beta in an effort to distinguish certain neurodegenerative diseases while the patient is still alive.

4.3 Results

Table 4.1 The [¹⁸F]FDDNP DVR binding values (mean ± SD) for the select neuroanatomy across the various cohorts.

The mean DVR values and their respective standard deviations were calculated for all patients in each cohort. The mean values for the young and older control groups were computed and then recalculated as a single, larger cohort for comparison. **Caudate/Putamen were sampled for those patients with MRI's.

	Younger Control (<60 yrs)	Older Control (>60 yrs)	ALL Control Cohort	Progressive Supranuclear Palsy (PSP)	Chronic Traumatic Encephalopathy (CTE)	Huntington's Disease (HD)	Parkinson's Disease (PD)
N	17	24	41	12	14	15	16
Age	40.4 ± 10.4	71.3 ± 10	58.5 ± 10.2	63.8±11.1	58.1 ± 11.5	36.8 ± 7.3	63.2±12.4
MMSE Score	--	--	--	22.4 ± 5.8	27.1 ± 2.7	--	28.4 ± 1.7
Neuroanatomy							
Cerebral Gray Matter	1.0	1.0	1.0	1.0	1.0	1.0	1.0
Cerebral White Matter	1.123 ± 0.08	1.093 ± 0.09	1.105 ± .09	1.194 ± 0.06	1.165 ± 0.08	1.093 ± 0.07	1.167 ± 0.05
Medulla Oblongata	1.117 ± 0.15	1.054 ± 0.27	1.080 ± .23	1.263 ± 0.16	1.164 ± 0.16	1.157 ± 0.21	1.110 ± 0.21
Pons	1.130 ± 0.14	1.186 ± 0.19	1.163 ± .17	1.351 ± 0.10	1.285 ± 0.14	1.205 ± 0.21	1.184 ± 0.19
Midbrain Ventral	1.137 ± 0.18	1.351± 0.20	1.166 ± .19	1.350 ± 0.15	1.341 ± 0.15	1.225 ± 0.18	1.237 ± 0.22
Midbrain Dorsal	1.197 ± 0.14	1.207 ± 0.20	1.203 ± .18	1.332 ± 0.10	1.364 ± 0.13	1.195 ± 0.15	1.231 ± 0.17
Amygdala	1.121 ± 0.13	1.121 ± 0.14	1.121 ± .14	1.043 ± 0.13	1.266 ± 0.14	1.108 ± 0.10	1.143 ± 0.18
Temporal Medial	1.075 ± 0.10	1.051 ± 0.11	1.061 ± .11	1.111 ± 0.12	1.164 ± 0.12	1.115 ± 0.11	1.101 ± 0.07
Temporal Lateral	1.105 ± 0.06	1.104 ± 0.12	1.105 ± .10	1.063 ± 0.09	1.121 ± 0.08	1.117 ± 0.13	1.153 ± 0.11
Occipital	1.066 ± 0.07	1.056 ± 0.11	1.060 ± .09	1.264 ± 0.11	1.056 ± 0.07	1.065 ± 0.09	1.106 ± 0.09
**Caudate	1.316 ± 0.10	1.232 ± 0.12	1.272 ± .12	1.309 ± 0.06	1.405 ± 0.16	1.189 ± 0.13	1.194 ± 0.17
**Putamen	1.309 ± 0.10	1.292 ± 0.13	1.30 ± .11	1.415 ± 0.10	1.396 ± 0.12	1.271 ± 0.10	1.302 ± 0.11
Striatum	*0.603 ± 0.83	1.490 ± 0.13	1.213 ± .61	1.387 ± 0.13	1.538 ± 0.12	1.497 ± 0.13	1.535 ± 0.16
Thalamus Posterior	1.282 ± 0.14	1.343 ± 0.20	1.318 ± .18	1.147 ± 0.14	1.423 ± 0.13	1.290 ± 0.20	1.283 ± 0.20
Cingulate Gyrus Parietal	1.125 ± 0.07	1.123 ± 0.12	1.124 ± .10	1.046 ± 0.09	1.137 ± 0.06	1.116 ± 0.11	1.173 ± 0.10
Anterior Cingulate Gyrus	1.023 ± 0.06	1.016 ± 0.13	1.019 ±	1.117 ± 0.06	1.007 ± 0.08	1.047 ± 0.08	1.072 ± 0.12
Frontal Motor Cortex	1.115 ± 0.09	1.117 ± 0.12	1.116 ± .11	1.039 ± 0.11	1.207 ± 0.09	1.177 ± 0.11	1.150 ± 0.09
	1.060 ± 0.08	1.077 ± 0.12	1.07 ± .11	0.996 ± 0.10	1.116 ± 0.10	1.088 ± 0.11	1.096 ± 0.13
	0.997 ± 0.07	0.987 ± 0.11	.991 ± .1	1.115 ± 0.07	1.027 ± 0.07	1.004 ± 0.07	1.049 ± 0.07

Neuroanatomy	N	Cereb. White Matter	Medial Temporal	Amygdala	Midbrain (Dorsal)	Midbrain (Ventral)	Caudate Nucleus
Younger Control	17	1.123 (0.08)	1.075 (0.10)	1.121 (0.13)	**1.197 (0.14)	*1.137 (0.18)	1.316 (0.10)
Older Control	24	**1.093 (0.09)	*1.051 (0.11)	*1.121 (0.14)	**1.207 (0.20)	1.351 (0.20)	1.232 (0.12)
HD	15	1.093 (0.07)	1.115 (0.11)	*1.108 (0.10)	1.195 (0.15)	1.225 (0.18)	*1.189 (0.13)
PD	16	**1.167 (0.05)	1.101 (0.07)	1.143 (0.18)	1.231 (0.17)	1.237 (0.22)	*1.194 (0.17)
PSP	12	**1.194 (0.06)	1.043 (0.12)	1.126 (0.13)	**1.332 (0.10)	*1.350 (0.15)	1.309 (0.06)
CTE	14	1.165 (0.08)	*1.164 (0.12)	*1.266 (0.14)	**1.364 (0.13)	*1.341 (0.15)	*1.405 (0.16)
ANOVA F-value	--	3.072	2.763	2.593	3.238	3.165	3.461

Table 4.2 The significant [¹⁸F]FDDNP mean values across all cohorts.

Regions that showed a statistically significant difference in the binding of [¹⁸F]FDDNP to the patient brain and the standard deviation is show in parentheses below the mean. The particular cohorts that showed a statistical difference between the binding are in bold and were determined to be significant through a *post hoc* Bonferroni test or a Dunnett's T3 test. All values found to be significant were tested at a confidence level of p<.05. *Bonferroni Test **Dunnett's T3 test

A one way Analysis of Variance (ANOVA) showed a significant difference in the means of the cerebellar white matter ($F_{6,98}=3.072$, $p<.05$), the medial temporal lobe ($F_{6,98}=2.763$, $p<.05$), the amygdala ($F_{6,98}=2,593$, $p<.05$), the dorsal midbrain ($F_{6,98}=3.238$, $p<.05$), the ventral midbrain ($F_{6,98}=3.072$, $p<.05$) and the caudate nucleus ($F_{6,98}=3.461$, $p<.05$) across the six cohorts of patient. Each cohort was further evaluated using Bonferroni's or Dunnett's T3 *post hoc* test to determine a difference in means between each cohort.

A summary of the statistically significant results is detailed in (Table 4.2) with those cohorts who displayed a significant difference in the means amongst cohorts, shown in bold. The cerebellar white matter showed a statistically significant difference between the means of the older control cohort (>60 years) and the PSP cohort ($p=.041$). There was also a statistical difference between the PD cohort and older control cohort found in the white matter of the cerebellum ($p=.036$). The medial temporal lobe showed an increase in the mean [¹⁸F]FDDNP binding above the older control cohort for the CTE cohort within a statistical significance ($p=.031$). The amygdala displayed a significant elevated [¹⁸F]FDDNP binding in the CTE cohort

over the older control cohort ($p=.041$) and also a statistical difference in signal between the CTE cohort and the HD patients ($p=.041$). The [^{18}F]FDDNP binding in the dorsal midbrain was significantly higher in the PSP patients as compared to both the younger control group and the older control group ($p=.039, p=0.031$). The ventral midbrain had a statistical significant difference in the means for both the PSP ($p=.42$) and CTE($p=.43$) cohorts in relation to the younger control group. The caudate nucleus demonstrated an elevated binding of [^{18}F]FDDNP binding in the brain of CTE patients as compared to the HD cohort ($p=.023$) and the PD cohort ($p=.023$).

Many of the calculated [^{18}F]FDDNP DVR mean values were different between cohorts, but the variance and spread were not significant enough to reliably cite at a confidence level of $p<.05$. The results appear consistent with the presence of pathology in the PSP and CTE patients where the mean difference was statistically significant. In both cohorts it can be assumed that there is at least a presence of p-tau present in the patient brains.

In the statistical evaluation, it was considered that the evaluation of the control patients as one large cohort is beneficial when comparing healthy and disease patients who may both have a range of pathology. This was considered in light of the realization that all four of the diseases evaluated in this study may have a range of onset age, disease duration and disease progression. Shown in Table 4.3 are the means recalculated for all control patients and the statistical significances between the cohorts are in bold type. The recalculation of the control patients showed a greater difference in the means between the control and CTE cohorts in the ventral midbrain. A statistical significance also appeared in the Anterior Cingulate Gyrus (ACG) between the control and the CTE cohorts ($p=.052$). The Anterior Cingulate Cortex (ACC) has been associated with decision-making, socially-driven interactions and empathy-related responses, which seems to correlate with the dysfunction CTE patients exhibit during the later stages of CTE (Lavin et al. 2013).

		Cereb. White Matter	Medial Temporal	Amygdala	Midbrain (Dorsal)	Midbrain (Ventral)	Caudate Nucleus	ACG
ALL Controls	N	1.105 (0.09)	1.061 (0.11)	1.121 (0.14)	**1.203 (0.18)	*1.166 (0.19)	1.272 (0.12)	*1.116 0.11
HD	17	1.093 (0.07)	1.115 (0.11)	*1.108 (0.10)	1.195 (0.15)	1.225 (0.18)	*1.189 (0.13)	1.177 (0.11)
PD	24	**1.167 (0.05)	1.101 (0.07)	1.143 (0.18)	1.231 (0.17)	1.237 (0.22)	*1.194 (0.17)	1.150 (.09)
PSP	15	**1.194 (0.06)	1.043 (0.12)	1.126 (0.13)	**1.333 (0.10)	*1.350 (0.15)	1.309 (0.06)	1.117 (.11)
CTE	16	1.165 (0.08)	*1.164 (0.12)	*1.266 (0.14)	**1.364 (0.13)	*1.341 (0.15)	*1.405 (0.16)	*1.207 (.09)
ANOVA F-value	12	3.433	3.351	3.277	4.08	3.789	3.596	2.686

Table 4.3 The significant [¹⁸F]FDDNP mean binding values across all cohorts with the control group reclassified.

Regions that showed a statistically significant difference in the binding of [¹⁸F]FDDNP to the patient brain and the standard deviation is show in parentheses below the mean. The particular cohorts that showed a statistical difference between the binding are in bold and were determined to be significant through a *post hoc* Bonferroni test or a Dunnett's T3 test. All values found to be significant were tested at a confidence level of p<.05. *Bonferroni Test **Dunnett's T3 test

Table 4.4 The [¹⁸F]FDDNP DVR patient binding values in the younger control group. (19 ROIs)

ID	CGM	CW M	MED	PON	MBV	MB D	AM G	TEM MED	TEM LAT	OCC	CAU	PUT	STR	THL	PCG	PAR	ACG	FRN	MOT
YC1	1.00	1.09	1.07	1.00	0.97	1.15	0.99	1.01	1.06	1.07	1.36	1.31	--	1.24	1.05	1.01	1.02	0.97	0.93
YC2	1.00	1.09	1.06	1.14	1.07	1.09	1.14	1.05	1.06	1.07	1.31	1.29	--	1.23	1.11	0.90	1.04	1.01	0.91
YC3	1.00	1.06	0.98	1.03	0.96	1.03	0.98	0.93	1.10	1.04	1.18	1.25	--	1.07	1.06	1.03	1.06	1.08	0.97
YC4	1.00	1.18	1.25	1.09	1.11	1.20	1.16	1.14	1.03	1.00	1.41	1.39	--	1.32	1.11	1.07	1.18	1.06	1.10
YC5	1.00	1.17	1.10	1.20	1.14	1.22	1.21	1.17	1.15	1.11	1.27	1.30	--	1.28	1.19	1.10	1.21	1.09	1.05
YC6	1.00	1.15	1.09	1.16	1.10	1.20	1.16	1.14	1.16	1.08	1.42	1.52	--	1.44	1.22	1.11	1.23	1.09	1.08
YC7	1.00	1.05	0.99	0.99	1.11	1.17	1.09	1.05	1.11	1.05	1.23	1.30	--	1.17	1.15	0.97	1.11	1.03	0.98
YC8	1.00	1.11	1.07	1.09	1.21	1.22	1.10	1.11	1.11	0.99	1.51	1.42	--	1.25	1.06	0.92	1.09	1.11	0.92
YC9	1.00	1.08	1.08	1.09	1.09	1.16	1.09	1.02	1.00	1.04	1.36	1.31	--	1.22	1.10	1.03	1.07	0.99	0.96
YC10	1.00	1.08	0.88	1.07	1.09	1.19	1.13	1.10	1.11	1.09	1.24	1.23	--	1.19	1.10	1.06	1.15	1.00	0.98
YC11	1.00	1.04	1.01	1.02	0.99	0.99	1.01	1.03	1.06	0.99	--	--	0.00	1.17	1.09	0.95	0.96	0.90	0.92
YC12	1.13	1.12	1.07	1.08	0.94	1.12	0.99	0.96	1.06	0.98	--	--	0.00	1.28	1.08	1.02	1.07	1.04	0.94
YC13	1.12	1.24	1.32	1.50	1.63	1.54	1.54	1.25	1.20	1.17	--	--	1.52	1.61	1.23	1.01	1.23	1.25	1.10
YC14	1.00	1.30	1.54	1.32	1.48	1.47	1.11	1.28	1.20	1.16	--	--	1.50	1.48	1.17	1.08	1.30	1.18	1.12
YC15	1.00	0.97	1.09	0.97	0.99	1.04	1.04	0.91	1.05	0.98	1.25	1.18	--	1.11	1.00	0.97	0.99	0.98	0.92
YC16	1.00	1.14	1.24	1.26	1.23	1.25	1.18	1.02	1.16	1.11	1.24	1.18	--	1.38	1.12	1.06	1.08	1.10	1.02
YC17	1.15	1.23	1.15	1.22	1.22	1.32	1.15	1.09	1.17	1.19	--	--	0.00	1.38	1.28	1.09	1.16	1.11	1.05

Table 4.5 The [¹⁸F]FDDNP DVR patient binding values in the Older Control group (>60 yrs).

ID	CGM	CWM	MED	PON	MBV	MBD	AMG	TEMP MED	TEMP LAT	OCC	CAU	PUT	STR	THL	PCG	PAR	ACG	FRN	MOT
OC1	1.00	1.27	1.38	1.56	1.27	1.45	1.26	1.23	1.23	1.24	0.99	1.63		1.52	1.02	1.20	1.30	0.94	1.26
OC2	1.00	1.18	0.00	1.47	1.61	1.54	1.23	1.20	1.29	1.23	--	--	1.66	1.60	1.38	1.23	1.23	1.29	1.11
OC3	1.00	1.27	1.25	1.33	1.46	1.58	1.40	1.22	1.29	1.01	--	--	1.54	1.72	1.32	1.31	1.25	1.22	1.13
OC4	1.00	1.04	1.01	1.02	0.99	0.99	1.01	1.03	1.06	0.99	1.14	1.18	--	1.17	1.09	0.95	0.96	0.90	0.92
OC5	1.00	0.99	0.94	0.95	0.83	0.99	0.87	0.85	0.94	0.86	1.16	1.24	--	1.13	0.95	0.90	0.94	0.91	0.83
OC6	1.00	1.20	1.29	1.36	1.38	1.52	1.31	1.21	1.29	1.24	--	--	1.64	1.68	1.33	1.16	1.31	1.29	1.14
OC7	1.00	1.21	1.20	1.32	1.09	1.08	1.19	1.12	1.13	1.00	1.42	1.40	--	1.32	1.11	0.88	1.20	1.11	0.97
OC8	1.00	1.11	1.18	1.35	1.46	1.38	1.38	1.12	1.07	1.04	--	--	1.36	1.44	1.10	0.90	1.10	1.12	0.98
OC9	1.00	1.06	1.13	1.08	1.15	1.27	0.99	1.05	0.97	1.00	1.34	1.36		1.39	0.99	0.97	1.07	1.02	0.97
OC10	1.00	1.22	1.29	1.46	1.49	1.47	1.29	1.21	1.29	1.21	--	--	1.64	1.69	1.24	1.12	1.34	1.27	1.10
OC11	1.00	1.14	1.13	1.18	1.28	1.35	1.20	1.12	1.25	1.21	--	--	1.48	1.52	1.30	1.12	1.25	1.23	1.08
OC12	1.00	1.07	1.00	1.06	1.06	1.15	1.00	0.95	1.02	1.04	1.30	1.29	--	1.20	1.11	0.95	1.01	0.97	0.92
OC13	1.00	1.06	0.86	1.02	1.02	1.00	1.04	0.98	0.98	0.97	1.30	1.30	--	1.17	1.10	0.97	1.06	1.03	0.96
OC14	1.00	1.00	0.89	1.06	1.09	1.12	1.06	1.10	1.10	1.03	1.34	1.28	--	1.18	1.00	0.89	1.09	1.09	0.88
OC15	1.00	0.91	0.92	0.92	1.01	0.87	1.02	0.99	1.01	0.99	1.08	1.11	--	0.94	1.01	0.96	0.97	0.98	0.87

OC16	1.00	1.07	1.00	1.00	1.25	1.03	1.03	0.99	1.12	0.98	1.33	1.34	--	1.25	1.05	0.85	1.07	1.00	0.88
OC17	1.00	1.05	0.99	1.15	1.01	1.08	0.98	0.84	0.98	0.90	1.18	1.20	--	1.31	1.09	0.89	1.05	1.01	0.82
OC18	1.00	1.02	1.05	0.97	0.98	1.08	0.98	1.00	0.99	1.00	1.19	1.22	--	1.13	1.07	0.93	1.01	1.02	0.91
OC19	1.00	0.99	1.03	1.17	1.14	1.04	0.98	0.94	1.04	1.01	--	--	1.33	1.29	1.02	0.97	0.97	1.00	0.98
OC20	1.00	1.00	1.00	0.98	0.99	1.11	1.10	1.04	0.99	0.99	1.24	1.25	--	1.16	1.01	0.89	1.03	0.98	0.91
OC24	1.00	1.04	1.03	1.10	1.12	1.11	1.04	0.96	1.09	1.03	--	--	1.31	1.20	1.09	1.04	1.06	1.04	0.94

Table 4.6 The [¹⁸F]FDDNP DVR patient binding values in the PSP group.

ID	CGM	CWM	MED	PON	MBV	MBD	AMG	TEMP MED	TEMP LAT	OCC	CAU	PUT	STR	THL	PCG	PAR	ACG	FRN	MOT
PSP1	1.00	1.11	1.15	1.28	1.35	1.14	1.00	1.03	1.08	1.04	--	--	1.32	1.25	1.13	1.00	1.02	1.05	1.00
PSP2	1.00	0.97	1.38	1.22	1.42	1.32	1.02	1.07	1.11	1.13	--	--	1.37	1.38	1.11	1.06	1.09	1.12	1.10
PSP3	1.00	1.17	0.86	1.16	1.12	1.32	1.04	0.94	1.02	0.91	1.23	1.36	--	1.29	1.21	1.07	1.08	0.87	0.93
PSP4	1.00	1.10	1.00	1.20	1.16	1.23	1.11	0.98	1.11	1.07	1.33	1.48	--	1.39	1.13	1.00	1.04	0.94	0.93
PSP5	1.00	1.17	0.86	1.16	1.12	1.32	1.04	0.94	1.02	0.91	1.23	1.36	--	1.29	1.21	1.07	1.08	0.87	0.93
PSP6	1.00	1.10	1.21	1.27	1.37	1.29	1.05	0.83	1.01	0.88	--	--	1.28	1.29	0.99	0.96	0.98	1.01	0.93
PSP7	1.00	1.12	1.32	1.41	1.40	1.45	1.28	1.12	1.17	1.13	--	--	1.65	1.72	1.21	1.02	1.21	1.13	1.01
PSP8	1.00	1.14	1.22	1.36	1.55	1.45	1.24	1.12	1.14	1.06	--	--	1.41	1.46	1.20	1.08	1.22	1.06	1.05
PSP9	1.00	1.05	1.14	1.13	1.28	1.23	1.00	0.99	1.05	1.03	--	--	1.26	1.22	1.00	0.98	1.05	1.00	0.90
PSP10	1.00	1.18	1.20	1.33	1.51	1.43	1.34	1.23	1.23	1.24	--	--	1.59	1.51	1.21	1.16	1.20	1.16	1.07
PSP11	1.00	1.17	1.19	1.40	1.47	1.40	1.34	1.23	1.32	1.20	--	--	1.44	1.48	1.28	1.06	1.35	1.16	1.10
PSP12	1.00	1.10	1.25	1.23	1.47	1.42	1.04	1.03	1.08	1.14	--	--	1.42	1.36	1.10	1.07	1.08	1.10	0.99

Table 4.7 The [¹⁸F]FDDNP DVR patient binding values in the PD group.

ID	CGM	CWM	MED	PON	MBV	MBD	AMG	TEM MED	TEM LAT	OCC	CAU	PUT	STR	THL	PCG	PAR	ACG	FRN	MOT
PD1	1.00	1.15	0.79	1.03	1.00	1.09	1.00	1.08	1.12	1.19	1.11	1.28	--	1.08	1.17	1.28	1.08	0.89	1.23
PD2	1.00	1.17	1.03	1.01	1.12	1.11	0.92	0.98	1.01	1.02	1.10	1.20	--	1.08	1.04	0.95	1.04	0.91	0.99
PD3	1.00	1.30	1.46	1.65	1.64	1.54	1.41	1.21	1.34	1.31	--	--	1.68	1.62	1.33	1.25	1.29	1.31	1.16
PD4	1.00	1.13	0.97	0.99	1.14	1.11	1.02	0.97	1.01	1.01	1.17	1.25	--	1.23	1.12	1.05	1.09	1.02	1.03
PD5	1.00	1.12	1.12	1.08	1.08	1.17	1.09	1.06	1.10	1.05	1.35	1.37	--	1.21	1.20	1.07	1.14	1.01	1.00
PD6	1.00	1.22	1.26	1.46	1.48	1.45	1.35	1.18	1.22	1.10	--	--	1.51	1.44	1.26	1.03	1.28	1.19	1.04
PD7	1.00	1.19	1.04	1.15	1.19	1.19	1.07	1.14	1.08	1.12	1.15	1.25	--	1.16	1.07	0.99	1.11	1.09	0.98
PD8	1.00	1.18	1.17	1.12	1.13	1.21	1.16	1.17	1.11	1.00	1.46	1.52	--	1.31	1.13	0.97	1.17	1.10	1.02
PD9	1.00	1.20	0.96	1.12	1.12	1.16	1.04	1.06	1.13	1.15	1.15	1.23	--	1.23	1.10	1.07	1.07	1.02	1.02
PD10	1.00	1.17	0.83	1.07	1.14	1.12	1.03	1.06	1.06	1.04	0.93	1.22	--	1.03	1.11	1.04	1.10	1.07	1.01
PD11	1.00	1.10	1.12	1.09	1.14	1.23	1.13	1.11	1.08	1.01	--	--	1.40	1.26	1.08	0.92	1.13	1.03	0.95
PD12	1.00	1.17	1.08	1.08	1.15	1.15	1.19	1.20	1.11	1.03	1.44	1.47	--	1.28	1.14	0.88	1.23	1.06	1.00
PD13	1.00	1.18	0.93	1.08	0.96	1.01	0.98	1.05	1.16	1.10	1.07	1.22	--	1.16	1.10	1.10	1.02	1.07	1.09
PD14	1.00	1.10	1.15	1.21	1.33	1.16	1.02	1.08	1.22	1.18	--	--	1.30	1.20	1.21	1.11	1.09	1.13	1.09
PD15	1.00	1.15	1.51	1.52	1.65	1.54	1.50	1.16	1.32	1.18	--	--	1.67	1.65	1.30	1.16	1.27	1.30	1.14
PD16	1.00	1.14	1.35	1.28	1.52	1.45	1.38	1.12	1.38	1.20	--	--	1.65	1.60	1.40	1.28	1.27	1.32	1.04

Table 4.8 The [¹⁸F]FDDNP DVR patient binding values in the HD group.

ID	CGM	CWM	MED	PON	MBV	MBD	AMG	TEM MED	TEM LAT	OCC	CAU	PUT	STR	THL	PCG	PAR	ACG	FRN	MOT
HD1	1.00	1.05	1.09	1.07	1.06	1.02	0.94	0.98	0.91	0.95	1.01	1.21		1.03	0.99	1.02	1.10	0.92	1.01
HD2	1.00	1.10	1.25	1.30	1.37	1.25	1.21	1.09	1.17	1.11			1.36	1.36	1.11	1.13	1.28	1.17	1.15
HD3	1.00	1.22	1.35	1.41	1.47	1.36	1.13	1.33	1.33	1.23	--	--	1.71	1.72	1.27	1.16	1.43	1.29	1.13
HD4	1.00	1.19	1.36	1.45	1.45	1.37	1.11	1.15	1.24	1.10	--	--	1.49	1.47	1.11	1.13	1.24	1.15	1.07
HD5	1.00	0.99	0.99	0.95	1.01	1.05	1.07	1.07	1.01	0.94	1.19	1.18	--	1.09	0.97	1.00	1.13	0.97	0.95
HD6	1.00	1.07	1.10	1.28	1.21	1.33	1.28	1.22	1.21	1.02	1.45	1.46	--	1.41	1.14	1.11	1.16	1.14	1.01
HD7	1.00	1.10	1.53	1.52	1.45	1.38	1.13	1.01	1.17	1.14	--	--	1.54	1.52	1.18	0.97	1.17	1.13	0.92
HD8	1.00	1.12	1.01	1.15	1.24	1.17	1.04	1.07	1.07	1.08	1.24	1.32	--	1.17	1.12	0.94	1.19	1.13	1.03
HD9	1.00	1.13	1.10	1.22	1.22	1.25	1.07	1.09	1.05	1.00	1.18	1.31	--	1.21	1.09	0.97	1.16	1.07	1.00
HD10	1.00	1.02	0.94	0.94	0.97	1.01	1.01	0.98	0.99	0.96	1.04	1.15	--	1.04	0.94	0.95	1.03	0.99	0.94
HD11	1.00	1.02	1.00	1.07	1.09	1.07	1.06	1.05	1.04	1.02	1.21	1.30	--	1.19	1.06	1.02	1.09	0.97	0.91
HD12	1.00	1.20	1.55	1.54	1.43	1.36	1.32	1.34	1.37	1.26	--	--	1.53	1.42	1.38	1.16	1.29	1.22	1.04
HD13	1.00	1.10	1.07	1.21	1.23	1.05	1.13	1.13	1.10	1.06	--	--	1.34	1.39	1.15	1.07	1.19	1.14	0.96
HD14	1.00	1.01	0.89	0.93	1.01	1.03	1.06	1.07	1.02	1.02	1.09	1.16	--	1.12	1.06	1.00	1.02	0.99	0.92
HD15	1.00	1.08	1.14	1.05	1.18	1.21	1.05	1.14	1.08	1.08	1.29	1.34	--	1.22	1.18	1.09	1.16	1.03	1.00

Table 4.9 The [¹⁸F]FDDNP DVR patient binding values in the CTE group.

ID	CGM	CWM	MED	PON	MBV	MBD	AMG	TEM MED	TEM LAT	OCC	CAU	PUT	STR	THL	PCG	PAR	ACG	FRN	MOT
CTE1	1.00	1.11	1.02	1.21	1.33	1.25	0.98	0.99	0.99	0.95	--	--	1.46	1.36	1.16	0.96	1.09	1.04	0.94
CTE2	1.00	1.22	1.08	1.33	1.37	1.40	1.34	1.29	1.25	1.14	1.48	1.49	--	1.37	1.24	1.08	1.26	1.19	1.03
CTE3	1.00	1.22	1.05	1.35	1.30	1.39	1.33	1.35	1.23	1.15	1.59	1.53	--	1.52	1.17	1.10	1.37	1.22	1.13
CTE4	1.00	1.25	1.19	1.17	1.35	1.37	1.24	1.17	1.12	1.04	1.44	1.41	--	1.37	1.09	0.92	1.21	1.09	1.00
CTE5	1.00	1.10	1.50	1.50	1.69	1.59	1.33	1.12	1.23	1.17	--	--	1.72	1.62	1.19	1.15	1.28	1.30	1.05
CTE6	1.00	1.04	1.21	1.24	1.37	1.33	1.39	1.13	1.09	1.07	--	--	1.55	1.50	1.16	0.94	1.23	1.16	0.96
CTE7	1.00	1.14	1.16	1.44	1.46	1.57	1.40	1.33	1.16	1.12	--	--	1.46	1.48	1.13	1.11	1.26	1.17	1.14
CTE8	1.00	1.16	1.11	1.16	1.27	1.23	1.16	1.12	1.04	1.00	1.14	1.20	--	1.18	1.07	0.94	1.08	1.04	1.00
CTE9	1.00	1.02	0.84	1.01	1.02	1.09	1.00	1.02	1.03	0.99	1.21	1.25	--	1.20	1.07	0.99	1.07	0.99	0.93
CTE10	1.00	1.24	1.18	1.30	1.33	1.43	1.41	1.24	1.16	1.03	1.41	1.44	--	1.37	1.14	1.01	1.19	1.16	1.07
CTE11	1.00	1.14	1.26	1.26	1.29	1.25	1.26	1.07	1.09	1.01	--	--	1.41	1.47	1.09	1.04	1.24	1.09	1.00
CTE12	1.00	1.32	1.23	1.42	1.38	1.46	1.34	1.28	1.12	1.05	1.55	1.47	--	1.51	1.17	0.94	1.18	1.01	1.05
CTE13	1.00	1.19	1.09	1.15	1.14	1.35	1.20	1.06	1.07	0.99	1.42	1.38	--	1.38	1.03	0.90	1.14	0.95	0.93
CTE14	1.00	1.17	1.37	1.44	1.47	1.39	1.33	1.12	1.11	1.07	--	--	1.63	1.60	1.20	1.03	1.30	1.22	1.13

4.4 Discussion

In this study of 98 different patients scanned with [^{18}F]FDDNP, it was challenging to compare cohorts that were scanned across a 10 year period, but the preparation of the radiotracer was produced in a consistent manner and maintained at a radiochemical purity of greater than 99%. Each patient involved in the study received a radioactive bolus injection between 5 to 10 mCi. Unfortunately, many of the patients did not have structural Magnetic Resonance Images that could be used to co-register the PET signal to the neuroanatomy. In dealing with particularly small structures of neuroanatomy, the precision which a ROI is drawn can potentially introduce artifacts to the extracted [^{18}F]FDDNP parametric DVR values. The summed image is an adequate resource for larger neuroanatomy, but may introduce error for smaller structures. All ROI's drawn on each patient brain involved in this study were drawn on each image twice to ensure consistency. The summed images served to act as a perfusion PET image, in place of an MRI, capable of highlighting the brain anatomy the radiotracer passes through as it binds to its target. A structural MRI would improve the accuracy of tracing the neuroanatomy and make it possible to coregister the parametric DVR images to a brain template capable of extracting whole neuroanatomical volume DVR values. In some neurodegenerative diseases there can be severe atrophy or ventricular enlargement, which may stretch or shrink regions of the brain as the software attempts to warp the MRI to the pre-existing template.

The results from this [^{18}F]FDDNP study reinforce the key pathological differences between these neurodegenerative diseases; especially as it relates to CTE and PSP. Both diseases are tauopathies, but the CTE cohort has a higher mean binding in the amygdala, which is a known group of nuclei affected by the deposition of hyperphosphorylated tau in cases of confirmed CTE. The amygdala has been specifically identified as a region in the brain notable for its activation during fear or anxiety inducing events and even in a rare case of almost completely absent bilateral amygdala nuclei, a patient can experience a complete absence of fear (Shin and Liberzon 2010; Adolphs et al. 1994). PSP also shows a higher mean [^{18}F]FDDNP

signal in the cerebellar white matter, the midbrain and the caudate nucleus. All three brain regions are nucleated anatomy; critical components in neurotransmission and are also key brain regions notable for their deposition of hyperphosphorylated tau in both CTE and PSP. It is important to differentiate between Parkinson's disease and Progressive Supranuclear Palsy patients, since both patients can exhibit Parkinsonian symptoms and proper diagnosis can be difficult early in the disease progression (Liscic et al. 2013). The Anterior Cingulate Gyrus (ACG) mean [¹⁸F]FDDNP DVR was elevated in the CTE patients above the control patients. Research has been shown the ACG to be associated with decision-making, socially-driven interactions and empathy-related response (Lavin et al. 2013). The executive features of the ACG are consistent with some of the symptoms in Chronic Traumatic Encephalopathy, such as behavioral, mood impairments and impulse control (Stern et al. 2013). The Huntington's Disease and Parkinson's Disease cohorts have reduced binding as compared to the control patients in the caudate nucleus, which could possibly be attributed to neurodegeneration and a loss of functionally active neurons, but it still remains unclear. What is needed in this field is software that is capable of detecting boundaries in neuroanatomy that would be capable of segmenting a patient's MRI without the use of warping to a template.

This work set about to investigate the binding properties of [¹⁸F]FDDNP alongside its predictive and diagnostic capabilities between a variety of neurodegenerative disease patients. It was demonstrated that [¹⁸F]FDDNP binding to tau was strongly correlated both *in vivo* and *in vitro* in the diseased PSP brain. The relationship between [¹⁸F]FDDNP and hyperphosphorylated tau appears to consist of a higher binding affinity or at least be capable of revealing a heavy burden of tau in the midst of amyloid beta. As has previously been suggested, hyperphosphorylated tau may be a better indicator of disease progression in patients with neurodegenerative diseases that contain both amyloid beta and hyperphosphorylated tau (Braak et al. 2006). This thought drives the importance of imaging p-tau in patients with advancing neurodegenerative disease.

In the course of this work, it became clear how important and necessary proper structural brain MRI's are required to properly map the human brain to extract the associated [¹⁸F]FDDNP DVR binding values. Without the structural MRI's the poor PET resolution can be challenging for the researcher to highlight small and difficult to delineate neuroanatomy. Software was used to co-register the PET images to those patients that had structural MRI's (SPM12) and other software was investigated as to whether existing templates could be applied to the patient PET images to extract DVR values from previously existing Volumes of Interest (VOI's). Unfortunately, while some software packages such as Brainsuite have the ability to segment the brain of a patient, it is necessary to warp the PET image to the predefined template. While this may not be a cause for concern in some instances, if the brain of a neurodegenerative patient has suffered from atrophy or neuronal loss, this may cause distortions in the amount of activity in any of these VOI's. Additionally, the software may attempt to stretch the neuroanatomy of the patient PET image to fit the template; stretching the bound [¹⁸F]FDDNP activity in any given VOI over an artificially larger area and thereby reducing the bound activity in any particular brain region.

Using the summed images methods to define neuroanatomical regions, it has been shown that there is a statistical significance of [¹⁸F]FDDNP binding in both PSP and CTE patients. This offers the potential application of being able to track neurodegenerative disease before cell loss begins to affect neurocognitive or motor functions of a patient. Especially as it relates to CTE, since we are only recently discovering the underlying pathology affecting this group of patients. Imagine that we could track athletes as they begin their football careers and scan them after they have received a concussion to determine if we are able to see any increase in binding of [¹⁸F]FDDNP to any particular brain regions to determine if the player is already accumulating hyperphosphorylated tau. Brain diseases do not all appear the same and do not appear to be created equal within every patient. One of the questions that still looms over every researcher studying any particular brain disease is "how quickly does this disease progress?"

Unfortunately for most debilitating brain diseases, the symptoms do not appear until there is severe cell loss in any particular brain region and the dysfunction becomes readily apparent. In order for researchers to find a potential effective therapeutic to prevent some of these debilitating diseases from progressing, the origins of the diseases need to be better understood. Tracking the appearance of pathology in the earliest stages and formations of these diseases might offer hope to patients everywhere.

Bibliography

- Adachi, M., T. Kawanami, H. Ohshima, Y. Sugai, and T. Hosoya. 2004. 'Morning glory sign: a particular MR finding in progressive supranuclear palsy', *Magn Reson Med Sci*, 3: 125-32.
- Adolphs, R., D. Tranel, H. Damasio, and A. Damasio. 1994. 'Impaired recognition of emotion in facial expressions following bilateral damage to the human amygdala', *Nature*, 372: 669-72.
- Agdeppa, E. D., V. Kepe, J. Liu, S. Flores-Torres, N. Satyamurthy, A. Petric, G. M. Cole, G. W. Small, S. C. Huang, and J. R. Barrio. 2001. 'Binding characteristics of radiofluorinated 6-dialkylamino-2-naphthylethylidene derivatives as positron emission tomography imaging probes for beta-amyloid plaques in Alzheimer's disease', *J Neurosci*, 21: Rc189.
- Ahmed, M., J. Davis, D. Aucoin, T. Sato, S. Ahuja, S. Aimoto, J. I. Elliott, W. E. Van Nostrand, and S. O. Smith. 2010. 'Structural conversion of neurotoxic amyloid-beta(1-42) oligomers to fibrils', *Nat Struct Mol Biol*, 17: 561-7.
- Alzheimer, A., R. A. Stelzmann, H. N. Schnitzlein, and F. R. Murtagh. 1995. 'An English translation of Alzheimer's 1907 paper, "Über eine eigenartige Erkrankung der Hirnrinde"', *Clin Anat*, 8: 429-31.
- Alzheimer, Alois. 1906. 'Über einen eigenartigen schweren Erkrankungsprozeß der Hirnrinde.', *Neurology Central*, 25.
- Armstrong, R. A., P. L. Lantos, and N. J. Cairns. 2007. 'Progressive supranuclear palsy (PSP): a quantitative study of the pathological changes in cortical and subcortical regions of eight cases', *J Neural Transm (Vienna)*, 114: 1569-77.
- Barrio, Jorge R., Gary W. Small, Koon-Pong Wong, Sung-Cheng Huang, Jie Liu, David A. Merrill, Christopher C. Giza, Robert P. Fitzsimmons, Bennet Omalu, Julian Bailes, and Vladimir Kepe. 2015. 'In vivo characterization of chronic traumatic encephalopathy using [F-18]FDDNP PET brain imaging', *Proceedings of the National Academy of Sciences*, 112: E2039-E47.
- Beach, T. G., J. A. Schneider, L. I. Sue, G. Serrano, B. N. Dugger, S. E. Monsell, and W. Kukull. 2014. 'Theoretical impact of Florbetapir (18F) amyloid imaging on diagnosis of Alzheimer dementia and detection of preclinical cortical amyloid', *J Neuropathol Exp Neurol*, 73: 948-53.
- Biancalana, M., and S. Koide. 2010. 'Molecular mechanism of Thioflavin-T binding to amyloid fibrils', *Biochim Biophys Acta*, 1804: 1405-12.
- Blau, M., W. Nagler, and M. A. Bender. 1962. 'Fluorine-18: a new isotope for bone scanning', *J Nucl Med*, 3: 332-4.
- Blennow, Kaj, Henrik Zetterberg, Jenny Wei, Enchi Liu, Ronald Black, and Michael Grundman. 2010. *Immunotherapy with bapineuzumab lowers CSF tau protein levels in patients with Alzheimer's disease.*

- Braak, H., I. Alafuzoff, T. Arzberger, H. Kretschmar, and K. Tredici. 2006. 'Staging of Alzheimer disease-associated neurofibrillary pathology using paraffin sections and immunocytochemistry', *Acta Neuropathol*, 112.
- Braak, H., and E. Braak. 1995. 'Staging of Alzheimer's disease-related neurofibrillary changes', *Neurobiol Aging*, 16: 271-8; discussion 78-84.
- Bracha, Vlastislav, Svitlana Zbarska, Krystal Parker, Andrew Carrel, Gary Zenitsky, and James R. Bloedel. 2009. 'The cerebellum and eyeblink conditioning: learning vs. network performance hypotheses', *Neuroscience*, 162: 787.
- Brier, Matthew R., Brian Gordon, Karl Friedrichsen, John McCarthy, Ari Stern, Jon Christensen, Christopher Owen, Patricia Aldea, Yi Su, Jason Hassenstab, Nigel J. Cairns, David M. Holtzman, Anne M. Fagan, John C. Morris, Tammie L. S. Benzinger, and Beau M. Ances. 2016. 'Tau and A β imaging, CSF measures, and cognition in Alzheimer's disease', *Science Translational Medicine*, 8: 338ra66.
- Brion, J. P., C. Smith, A. M. Couck, J. M. Gallo, and B. H. Anderton. 1993. 'Developmental changes in tau phosphorylation: fetal tau is transiently phosphorylated in a manner similar to paired helical filament-tau characteristic of Alzheimer's disease', *J Neurochem*, 61: 2071-80.
- Buee, L., T. Bussiere, V. Buee-Scherrer, A. Delacourte, and P. R. Hof. 2000. 'Tau protein isoforms, phosphorylation and role in neurodegenerative disorders', *Brain Res Brain Res Rev*, 33: 95-130.
- Cohen, A. D., G. D. Rabinovici, C. A. Mathis, W. J. Jagust, W. E. Klunk, and M. D. Ikonomovic. 2012. 'Using Pittsburgh Compound B for in vivo PET imaging of fibrillar amyloid-beta', *Adv Pharmacol*, 64: 27-81.
- Cole, G. B., G. Keum, J. Liu, G. W. Small, N. Satyamurthy, V. Kepe, and J. R. Barrio. 2010. 'Specific estrogen sulfotransferase (SULT1E1) substrates and molecular imaging probe candidates', *Proc Natl Acad Sci U S A*, 107: 6222-7.
- De Zeeuw, C. I., J. I. Simpson, C. C. Hoogenraad, N. Galjart, S. K. Koekkoek, and T. J. Ruigrok. 1998. 'Microcircuitry and function of the inferior olive', *Trends Neurosci*, 21: 391-400.
- Dickson, D. W. 2017. 'Neuropathology of Parkinson disease', *Parkinsonism Relat Disord*.
- Dickson, Dennis W., Howard A. Crystal, Linda A. Mattiace, David M. Masur, Alan D. Blau, Peter Davies, Shu-Hui Yen, and Miriam K. Aronson. 1992. 'Identification of normal and pathological aging in prospectively studied nondemented elderly humans', *Neurobiology of Aging*, 13: 179-89.
- Dirac, P. A. M. 1928. 'The Quantum Theory of the Electron', *Proceedings of the Royal Society of London. Series A*, 117: 610.
- Ehrlich, Michelle E. 2012. 'Huntington's Disease and the Striatal Medium Spiny Neuron: Cell-Autonomous and Non-Cell-Autonomous Mechanisms of Disease', *Neurotherapeutics*, 9: 270-84.

- Friston, K. 2007. 'CHAPTER 1 - A short history of SPM.' in, *Statistical Parametric Mapping* (Academic Press: London).
- Friston, K. J., A. P. Holmes, K. J. Worsley, J. P. Poline, C. D. Frith, and R. S. J. Frackowiak. 1994. 'Statistical parametric maps in functional imaging: A general linear approach', *Human Brain Mapping*, 2: 189-210.
- Gallamini, Andrea, Colette Zwarthoed, and Anna Borra. 2014. 'Positron Emission Tomography (PET) in Oncology', *Cancers*, 6: 1821-89.
- Gaugler, Joseph Ph.D., James, Bryan Ph.D., Tricia Johnson, Ph.D. Scholz, Ph.D., Weuve, Jennifer, M.P.H., Sc.D. 2016. '2016 Alzheimer's disease facts and figures', *Alzheimer's & Dementia: The Journal of the Alzheimer's Association*, 12: 459-509.
- Gendreau, Kerry L., and Garth F. Hall. 2013. 'Tangles, Toxicity, and Tau Secretion in AD – New Approaches to a Vexing Problem', *Frontiers in Neurology*, 4: 160.
- Gennarelli, T. A., J. H. Adams, and D. I. Graham. 1981. 'Acceleration Induced Head Injury in the Monkey. I. The Model, Its Mechanical and Physiological Correlates.' in Kurt Jellinger, Filippo Gullotta and Miroslav Mossakowski (eds.), *Experimental and Clinical Neuropathology: Proceedings of the First European Neuropathology Meeting, Vienna, May 6–8, 1980* (Springer Berlin Heidelberg: Berlin, Heidelberg).
- Goedert, M., R. Jakes, and E. Vanmechelen. 1995. 'Monoclonal antibody AT8 recognises tau protein phosphorylated at both serine 202 and threonine 205', *Neuroscience Letters*, 189: 167-70.
- Goetz, Christopher G., Barbara C. Tilley, Stephanie R. Shaftman, Glenn T. Stebbins, Stanley Fahn, Pablo Martinez - Martin, Werner Poewe, Cristina Sampaio, Matthew B. Stern, Richard Dodel, Bruno Dubois, Robert Holloway, Joseph Jankovic, Jaime Kulisevsky, Anthony E. Lang, Andrew Lees, Sue Leurgans, Peter A. LeWitt, David Nyenhuis, C. Warren Olanow, Olivier Rascol, Anette Schrag, Jeanne A. Teresi, Jacobus J. van Hilten, and Nancy LaPelle. 2008. 'Movement Disorder Society - sponsored revision of the Unified Parkinson's Disease Rating Scale (MDS - UPDRS): Scale presentation and clinimetric testing results', *Movement Disorders*, 23: 2129-70.
- Golbe, L. I., and P. A. Ohman-Strickland. 2007. 'A clinical rating scale for progressive supranuclear palsy', *Brain*, 130: 1552-65.
- Graeber, M. B., S. Kosel, R. Egensperger, R. B. Banati, U. Muller, K. Bise, P. Hoff, H. J. Moller, K. Fujisawa, and P. Mehraein. 1997. 'Rediscovery of the case described by Alois Alzheimer in 1911: historical, histological and molecular genetic analysis', *Neurogenetics*, 1: 73-80.
- Hardy, J. 2017. 'The discovery of Alzheimer-causing mutations in the APP gene and the formulation of the "amyloid cascade hypothesis"', *FEBS J*, 284: 1040-44.
- Hebert, L. E., J. Weuve, P. A. Scherr, and D. A. Evans. 2013. 'Alzheimer disease in the United States (2010-2050) estimated using the 2010 census', *Neurology*, 80: 1778-83.

- Itolikar, S. M., S. B. Salagre, and C. R. Kalal. 2012. 'Hummingbird sign', 'penguin sign' and 'Mickey mouse sign' in progressive supranuclear palsy', *J Assoc Physicians India*, 60: 52.
- Jacobson, A., A. Petric, D. Hogenkamp, A. Sinur, and J. R. Barrio. 1996. '1,1-Dicyano-2-[6-(dimethylamino)naphthalen-2-yl]propene (DDNP): A Solvent Polarity and Viscosity Sensitive Fluorophore for Fluorescence Microscopy', *Journal of the American Chemical Society*, 118: 5572-79.
- Jenkins, Edmund C. 1972. 'Wire-Loop Application of Liquid Emulsion to Slides for Autoradiography in Light Microscopy', *Stain Technology*, 47: 23-26.
- Kang, J., H. G. Lemaire, A. Unterbeck, J. M. Salbaum, C. L. Masters, K. H. Grzeschik, G. Multhaup, K. Beyreuther, and B. Muller-Hill. 1987. 'The precursor of Alzheimer's disease amyloid A4 protein resembles a cell-surface receptor', *Nature*, 325: 733-6.
- Karran, E., M. Mercken, and B. De Strooper. 2011. 'The amyloid cascade hypothesis for Alzheimer's disease: an appraisal for the development of therapeutics', *Nat Rev Drug Discov*, 10: 698-712.
- Kelenyi, G. 1967. 'Thioflavin S fluorescent and Congo red anisotropic stainings in the histologic demonstration of amyloid', *Acta Neuropathol*, 7: 336-48.
- Kepe, V., Y. Bordelon, A. Boxer, S. C. Huang, J. Liu, F. C. Thiede, J. C. Mazziotta, M. F. Mendez, N. Donoghue, G. W. Small, and J. R. Barrio. 2013. 'PET imaging of neuropathology in tauopathies: progressive supranuclear palsy', *J Alzheimers Dis*, 36: 145-53.
- Kepe, V., B. Ghetti, M. R. Farlow, M. Bresjanac, K. Miller, S. C. Huang, K. P. Wong, J. R. Murrell, P. Piccardo, F. Epperson, G. Repovs, L. M. Smid, A. Petric, P. Siddarth, J. Liu, N. Satyamurthy, G. W. Small, and J. R. Barrio. 2010. 'PET of brain prion protein amyloid in Gerstmann-Straussler-Scheinker disease', *Brain Pathol*, 20: 419-30.
- Kepe, Vladimir, Sung - Cheng Huang, Gary W. Small, Nagichettiar Satyamurthy, and Jorge R. Barrio. 2006. 'Visualizing Pathology Deposits in the Living Brain of Patients with Alzheimer's Disease.' in, *Methods in Enzymology* (Academic Press).
- Kim, M. 2013. 'Beta conformation of polyglutamine track revealed by a crystal structure of Huntingtin N-terminal region with insertion of three histidine residues', *Prion*, 7: 221-8.
- Kipps, C. M., A. J. Duggins, N. Mahant, L. Gomes, J. Ashburner, and E. A. McCusker. 2005. 'Progression of structural neuropathology in preclinical Huntington's disease: a tensor based morphometry study', *J Neurol Neurosurg Psychiatry*, 76: 650-5.
- Klunk, W. E., H. Engler, A. Nordberg, Y. Wang, G. Blomqvist, D. P. Holt, M. Bergstrom, I. Savitcheva, G. F. Huang, S. Estrada, B. Ausen, M. L. Debnath, J. Barletta, J. C. Price, J. Sandell, B. J. Lopresti, A. Wall, P. Koivisto, G. Antoni, C. A. Mathis, and B. Langstrom. 2004. 'Imaging brain amyloid in Alzheimer's disease with Pittsburgh Compound-B', *Ann Neurol*, 55: 306-19.
- Klunk, W. E., B. J. Lopresti, M. D. Ikonovic, I. M. Lefterov, R. P. Koldamova, E. E. Abrahamson, M. L. Debnath, D. P. Holt, G. F. Huang, L. Shao, S. T. DeKosky, J. C. Price, and C. A. Mathis. 2005. 'Binding of the positron emission tomography tracer Pittsburgh

- compound-B reflects the amount of amyloid-beta in Alzheimer's disease brain but not in transgenic mouse brain', *J Neurosci*, 25: 10598-606.
- Koo, Edward H., Peter T. Lansbury, and Jeffery W. Kelly. 1999. 'Amyloid diseases: Abnormal protein aggregation in neurodegeneration', *Proceedings of the National Academy of Sciences*, 96: 9989-90.
- Kubota, R., S. Yamada, K. Kubota, K. Ishiwata, N. Tamahashi, and T. Ido. 1992. 'Intratumoral distribution of fluorine-18-fluorodeoxyglucose in vivo: high accumulation in macrophages and granulation tissues studied by microautoradiography', *J Nucl Med*, 33: 1972-80.
- Lacy, M., T. Kaemmerer, and S. Czipri. 2015. 'Standardized mini-mental state examination scores and verbal memory performance at a memory center: implications for cognitive screening', *Am J Alzheimers Dis Other Demen*, 30: 145-52.
- Landau, S. M., C. Breault, A. D. Joshi, M. Pontecorvo, C. A. Mathis, W. J. Jagust, M. A. Mintun, and Initiative Alzheimer's Disease Neuroimaging. 2013. 'Amyloid-beta imaging with Pittsburgh compound B and florbetapir: comparing radiotracers and quantification methods', *J Nucl Med*, 54: 70-7.
- Lavin, Claudio, Camilo Melis, Ezequiel Mikulan, Carlos Gelormini, David Huepe, and Agustin Ibanez. 2013. 'The anterior cingulate cortex: an integrative hub for human socially-driven interactions', *Frontiers in Neuroscience*, 7: 64.
- Leyns, Cheryl E. G., and David M. Holtzman. 2017. 'Glial contributions to neurodegeneration in tauopathies', *Molecular Neurodegeneration*, 12: 50.
- Liscic, R. M., K. Srulijes, A. Groger, W. Maetzler, and D. Berg. 2013. 'Differentiation of progressive supranuclear palsy: clinical, imaging and laboratory tools', *Acta Neurol Scand*, 127: 362-70.
- Liu, Jie, Vladimir Kepe, Alenka Žabjek, Andrej Petrič, Henry C. Padgett, Nagichettiar Satyamurthy, and Jorge R. Barrio. 2007. 'High-Yield, Automated Radiosynthesis of 2-(1-{6-[(2-[¹⁸F]Fluoroethyl)(methyl)amino]-2-naphthyl}ethylidene)malononitrile ([¹⁸F]FDDNP) Ready for Animal or Human Administration', *Molecular Imaging and Biology*, 9: 6-16.
- Lockhart, A., J. R. Lamb, T. Osredkar, L. I. Sue, J. N. Joyce, L. Ye, V. Libri, D. Leppert, and T. G. Beach. 2007. 'PIB is a non-specific imaging marker of amyloid-beta (Aβ) peptide-related cerebral amyloidosis', *Brain*, 130: 2607-15.
- Loening, A. M., and S. S. Gambhir. 2003. 'AMIDE: a free software tool for multimodality medical image analysis', *Mol Imaging*, 2: 131-7.
- Logan, J., J. S. Fowler, N. D. Volkow, G. J. Wang, Y. S. Ding, and D. L. Alexoff. 1996. 'Distribution volume ratios without blood sampling from graphical analysis of PET data', *J Cereb Blood Flow Metab*, 16: 834-40.
- Ludlow, Christy L. 2015. 'Central Nervous System Control of Voice and Swallowing', *Journal of clinical neurophysiology : official publication of the American Electroencephalographic Society*, 32: 294-303.

- Maarouf, C. L., I. D. Daus, T. A. Kokjohn, D. G. Walker, J. M. Hunter, J. C. Kruchowsky, R. Woltjer, J. Kaye, E. M. Castano, M. N. Sabbagh, T. G. Beach, and A. E. Roher. 2011. 'Alzheimer's disease and non-demented high pathology control nonagenarians: comparing and contrasting the biochemistry of cognitively successful aging', *PLoS One*, 6: e27291.
- Martland, H. S. 1928. 'Punch drunk', *Journal of the American Medical Association*, 91: 1103-07.
- McKee, A. C., T. D. Stein, P. T. Kiernan, and V. E. Alvarez. 2015. 'The neuropathology of chronic traumatic encephalopathy', *Brain Pathol*, 25: 350-64.
- McKee, A. C., R. A. Stern, C. J. Nowinski, T. D. Stein, V. E. Alvarez, D. H. Daneshvar, H. S. Lee, S. M. Wojtowicz, G. Hall, C. M. Baugh, D. O. Riley, C. A. Kubilus, K. A. Cormier, M. A. Jacobs, B. R. Martin, C. R. Abraham, T. Ikezu, R. R. Reichard, B. L. Wolozin, A. E. Budson, L. E. Goldstein, N. W. Kowall, and R. C. Cantu. 2013. 'The spectrum of disease in chronic traumatic encephalopathy', *Brain*, 136: 43-64.
- McKee, Ann C., Robert C. Cantu, Christopher J. Nowinski, E. Tessa Hedley-Whyte, Brandon E. Gavett, Andrew E. Budson, Veronica E. Santini, Hyo-Soon Lee, Caroline A. Kubilus, and Robert A. Stern. 2009. 'Chronic Traumatic Encephalopathy in Athletes: Progressive Tauopathy After Repetitive Head Injury', *Journal of Neuropathology & Experimental Neurology*, 68: 709-35.
- McKeith, I. G., D. W. Dickson, J. Lowe, M. Emre, J. T. O'Brien, H. Feldman, J. Cummings, J. E. Duda, C. Lippa, E. K. Perry, D. Aarsland, H. Arai, C. G. Ballard, B. Boeve, D. J. Burn, D. Costa, T. Del Ser, B. Dubois, D. Galasko, S. Gauthier, C. G. Goetz, E. Gomez-Tortosa, G. Halliday, L. A. Hansen, J. Hardy, T. Iwatsubo, R. N. Kalaria, D. Kaufer, R. A. Kenny, A. Korczyn, K. Kosaka, V. M. Lee, A. Lees, I. Litvan, E. Londos, O. L. Lopez, S. Minoshima, Y. Mizuno, J. A. Molina, E. B. Mukaetova-Ladinska, F. Pasquier, R. H. Perry, J. B. Schulz, J. Q. Trojanowski, and M. Yamada. 2005. 'Diagnosis and management of dementia with Lewy bodies: third report of the DLB Consortium', *Neurology*, 65: 1863-72.
- Mez, J., D. H. Daneshvar, P. T. Kiernan, and et al. 2017. 'Clinicopathological evaluation of chronic traumatic encephalopathy in players of american football', *JAMA*, 318: 360-70.
- Miller, Yifat, Buyong Ma, and Ruth Nussinov. 2011. 'Synergistic Interactions between Repeats in Tau Protein and A β Amyloids May Be Responsible for Accelerated Aggregation via Polymorphic States', *Biochemistry*, 50: 5172-81.
- Mirra, S. S., A. Heyman, D. McKeel, S. M. Sumi, B. J. Crain, L. M. Brownlee, F. S. Vogel, J. P. Hughes, G. van Belle, and L. Berg. 1991. 'The Consortium to Establish a Registry for Alzheimer's Disease (CERAD). Part II. Standardization of the neuropathologic assessment of Alzheimer's disease', *Neurology*, 41: 479-86.
- Morishima-Kawashima, M., M. Hasegawa, K. Takio, M. Suzuki, H. Yoshida, A. Watanabe, K. Titani, and Y. Ihara. 1995. 'Hyperphosphorylation of tau in PHF', *Neurobiol Aging*, 16: 365-71; discussion 71-80.
- Morton, Susanne M., and Amy J. Bastian. 2007. 'Mechanisms of cerebellar gait ataxia', *The Cerebellum*, 6: 79.

- Murray, M. E., V. J. Lowe, N. R. Graff-Radford, A. M. Liesinger, A. Cannon, S. A. Przybelski, B. Rawal, J. E. Parisi, R. C. Petersen, K. Kantarci, O. A. Ross, R. Duara, D. S. Knopman, C. R. Jack, Jr., and D. W. Dickson. 2015. 'Clinicopathologic and ¹¹C-Pittsburgh compound B implications of Thal amyloid phase across the Alzheimer's disease spectrum', *Brain*, 138: 1370-81.
- Nag, S., B. Sarkar, A. Bandyopadhyay, B. Sahoo, V. K. Sreenivasan, M. Kombrabail, C. Muralidharan, and S. Maiti. 2011. 'Nature of the amyloid-beta monomer and the monomer-oligomer equilibrium', *J Biol Chem*, 286: 13827-33.
- Nolf, E., Voet, T. 2003. "XMedCon- An Open-Source Medical Image Conversion ToolKit." In, Conversion software. Annual Congress of the European Association of Nuclear Medicine: EANM.
- Nutt, Ronald. 2002. 'The History of Positron Emission Tomography', *Molecular Imaging & Biology*, 4: 11-26.
- Okamura, N., and K. Yanai. 2010. 'Florbetapir (18F), a PET imaging agent that binds to amyloid plaques for the potential detection of Alzheimer's disease', *IDrugs*, 13: 890-9.
- Olsson, F., S. Schmidt, V. Althoff, L. M. Munter, S. Jin, S. Rosqvist, U. Lendahl, G. Multhaup, and J. Lundkvist. 2014. 'Characterization of intermediate steps in amyloid beta (A β) production under near-native conditions', *J Biol Chem*, 289: 1540-50.
- Omalu, B. 2014. 'Chronic traumatic encephalopathy', *Prog Neurol Surg*, 28: 38-49.
- Parikh, N. D., and D. K. Klimov. 2015. 'Molecular Mechanisms of Alzheimer's Biomarker FDDNP Binding to A β Amyloid Fibril', *J Phys Chem B*, 119: 11568-80.
- Pashby, Thomas. 2012. 'Dirac's Prediction of the Positron: A Case Study for the Current Realism Debate', *Perspectives on Science*, 20: 440-75.
- Phelps, M. E., E. J. Hoffman, N. A. Mullani, and M. M. Ter-Pogossian. 1975. 'Application of annihilation coincidence detection to transaxial reconstruction tomography', *J Nucl Med*, 16: 210-24.
- Piao, Y. S., S. Hayashi, K. Wakabayashi, A. Kakita, I. Aida, M. Yamada, and H. Takahashi. 2002. 'Cerebellar cortical tau pathology in progressive supranuclear palsy and corticobasal degeneration', *Acta Neuropathol*, 103: 469-74.
- Priller, C., T. Bauer, G. Mitteregger, B. Krebs, H. A. Kretzschmar, and J. Herms. 2006. 'Synapse formation and function is modulated by the amyloid precursor protein', *J Neurosci*, 26: 7212-21.
- Prince, Martin and Comas-Herrera, Adelina and Knapp, Martin and Guerchet, Maelenn and Karagiannidou, Maria. 2016. 'World Alzheimer report 2016: improving healthcare for people living with dementia: coverage, quality and costs now and in the future'.
- Protas, H. D., S. C. Huang, V. Kepe, K. Hayashi, A. Klunder, M. N. Braskie, L. Ercoli, S. Bookheimer, P. M. Thompson, G. W. Small, and J. R. Barrio. 2010. 'FDDNP binding using MR derived cortical surface maps', *Neuroimage*, 49: 240-8.

- Raber, Jacob, Derek Wong, Gui-Qiu Yu, Manuel Buttini, Robert W. Mahley, Robert E. Pitas, and Lennart Mucke. 2000. 'Alzheimer's disease: Apolipoprotein E and cognitive performance', *Nature*, 404: 352-54.
- Rich, D. A. 1997. 'A brief history of positron emission tomography', *J Nucl Med Technol*, 25: 4-11.
- Robb, R. A., D. P. Hanson, R. A. Karwoski, A. G. Larson, E. L. Workman, and M. C. Stacy. 1989. 'Analyze: A Comprehensive, operator-interactive software package for multidimensional medical image display and analysis', *Computerized Medical Imaging and Graphics*, 13: 433-54.
- Rodriguez, E. A., Y. Wang, J. L. Crisp, D. R. Vera, R. Y. Tsien, and R. Ting. 2016. 'New Dioxaborolane Chemistry Enables [(18)F]-Positron-Emitting, Fluorescent [(18)F]-Multimodality Biomolecule Generation from the Solid Phase', *Bioconjug Chem*, 27: 1390-99.
- Ross, Christopher A., and Sarah J. Tabrizi. 2011. 'Huntington's disease: from molecular pathogenesis to clinical treatment', *The Lancet Neurology*, 10: 83-98.
- Sabri, Osama, John Seibyl, Christopher Rowe, and Henryk Barthel. 2015. 'Beta-amyloid imaging with florbetaben', *Clinical and Translational Imaging*, 3: 13-26.
- Salles, Antonio A. F. De, and Alessandra A. Gorgulho. 2010. '7.0 Tesla MRI Brain Atlas: In vivo atlas with cryomacrotome correlation', *Surgical Neurology International*, 1: 4.
- Schrödinger, E. 1935. 'Die gegenwärtige Situation in der Quantenmechanik', *Naturwissenschaften*, 23: 807-12.
- Sevigny, Jeff, Ping Chiao, Thierry Bussière, Paul H. Weinreb, Leslie Williams, Marcel Maier, Robert Dunstan, Stephen Salloway, Tianle Chen, Yan Ling, John O'Gorman, Fang Qian, Mahin Arastu, Mingwei Li, Sowmya Chollate, Melanie S. Brennan, Omar Quintero-Monzon, Robert H. Scannevin, H. Moore Arnold, Thomas Engber, Kenneth Rhodes, James Ferrero, Yaming Hang, Alvydas Mikulskis, Jan Grimm, Christoph Hock, Roger M. Nitsch, and Alfred Sandrock. 2016. 'The antibody aducanumab reduces A β plaques in Alzheimer's disease', *Nature*, 537: 50-56.
- Shin, J., V. Kepe, J. R. Barrio, and G. W. Small. 2011. 'The merits of FDDNP-PET imaging in Alzheimer's disease', *J Alzheimers Dis*, 26 Suppl 3: 135-45.
- Shin, Lisa M., and Israel Liberzon. 2010. 'The Neurocircuitry of Fear, Stress, and Anxiety Disorders', *Neuropsychopharmacology*, 35: 169-91.
- Shoghi-Jadid, K., G. W. Small, E. D. Agdeppa, V. Kepe, L. M. Ercoli, P. Siddarth, S. Read, N. Satyamurthy, A. Petric, S. C. Huang, and J. R. Barrio. 2002. 'Localization of neurofibrillary tangles and beta-amyloid plaques in the brains of living patients with Alzheimer disease', *Am J Geriatr Psychiatry*, 10: 24-35.
- Shukla, A. K., and U. Kumar. 2006. 'Positron emission tomography: An overview', *J Med Phys*, 31: 13-21.

- Small, G. W., V. Kepe, P. Siddarth, L. M. Ercoli, D. A. Merrill, N. Donoghue, S. Y. Bookheimer, J. Martinez, B. Omalu, J. Bailes, and J. R. Barrio. 2013. 'PET scanning of brain tau in retired national football league players: preliminary findings', *Am J Geriatr Psychiatry*, 21: 138-44.
- Small, Gary W., Vladimir Kepe, Linda M. Ercoli, Prabha Siddarth, Susan Y. Bookheimer, Karen J. Miller, Helen Lavretsky, Alison C. Burggren, Greg M. Cole, Harry V. Vinters, Paul M. Thompson, S. C. Huang, N. Satyamurthy, Michael E. Phelps, and Jorge R. Barrio. 2006. 'PET of Brain Amyloid and Tau in Mild Cognitive Impairment', *New England Journal of Medicine*, 355: 2652-63.
- Smid, L. M., V. Kepe, H. V. Vinters, M. Bresjanac, T. Toyokuni, N. Satyamurthy, K. P. Wong, S. C. Huang, D. H. Silverman, K. Miller, G. W. Small, and J. R. Barrio. 2013. 'Postmortem 3-D brain hemisphere cortical tau and amyloid-beta pathology mapping and quantification as a validation method of neuropathology imaging', *J Alzheimers Dis*, 36: 261-74.
- Smid, L. M., T. D. Vovko, M. Popovic, A. Petric, V. Kepe, J. R. Barrio, G. Vidmar, and M. Bresjanac. 2006. 'The 2,6-disubstituted naphthalene derivative FDDNP labeling reliably predicts Congo red birefringence of protein deposits in brain sections of selected human neurodegenerative diseases', *Brain Pathol*, 16: 124-30.
- Snellman, Anniina, Johanna Rokka, Francisco R. López-Picón, Olli Eskola, Mario Salmona, Gianluigi Forloni, Mika Scheinin, Olof Solin, Juha O. Rinne, and Merja Haaparanta-Solin. 2014. 'In vivo PET imaging of beta-amyloid deposition in mouse models of Alzheimer's disease with a high specific activity PET imaging agent [(18)F]flutemetamol', *EJNMMI Research*, 4: 37-37.
- Steele, J. C., J. Richardson, and J. Olszewski. 1964. 'Progressive supranuclear palsy: A heterogeneous degeneration involving the brain stem, basal ganglia and cerebellum with vertical gaze and pseudobulbar palsy, nuchal dystonia and dementia', *Archives of Neurology*, 10: 333-59.
- Steele, Richardson, Olszewski. 1964. 'Progressive Supranuclear Palsy', *Archives of Neurology*, 10: 16.
- Stern, Robert A., Daniel H. Daneshvar, Christine M. Baugh, Daniel R. Seichepine, Philip H. Montenegro, David O. Riley, Nathan G. Fritts, Julie M. Stamm, Clifford A. Robbins, Lisa McHale, Irene Simkin, Thor D. Stein, Victor E. Alvarez, Lee E. Goldstein, Andrew E. Budson, Neil W. Kowall, Christopher J. Nowinski, Robert C. Cantu, and Ann C. McKee. 2013. 'Clinical presentation of chronic traumatic encephalopathy', *Neurology*, 81: 1122-29.
- Sun, Anyang, Xuan V. Nguyen, and Guoying Bing. 2002. 'Comparative Analysis of an Improved Thioflavin-S Stain, Gallyas Silver Stain, and Immunohistochemistry for Neurofibrillary Tangle Demonstration on the Same Sections', *Journal of Histochemistry & Cytochemistry*, 50: 463-72.
- Tabaton, M., and E. Tamagno. 2007. 'The molecular link between beta- and gamma-secretase activity on the amyloid beta precursor protein', *Cell Mol Life Sci*, 64: 2211-8.

- Tauber, C., E. Beaufils, C. Hommet, M. J. Ribeiro, J. Vercouillie, E. Vierron, K. Mondon, J. P. Cottier, V. Gissot, D. Guilloteau, and V. Camus. 2013. 'Brain [18F]FDDNP binding and glucose metabolism in advanced elderly healthy subjects and Alzheimer's disease patients', *J Alzheimers Dis*, 36: 311-20.
- Tawana, K., and D. B. Ramsden. 2001. 'Progressive supranuclear palsy', *Mol Pathol*, 54: 427-34.
- Teng, E., V. Kepe, S. A. Frautschy, J. Liu, N. Satyamurthy, F. Yang, P. P. Chen, G. B. Cole, M. R. Jones, S. C. Huang, D. G. Flood, S. P. Trusko, G. W. Small, G. M. Cole, and J. R. Barrio. 2011. '[F-18]FDDNP microPET imaging correlates with brain Abeta burden in a transgenic rat model of Alzheimer disease: effects of aging, in vivo blockade, and anti-Abeta antibody treatment', *Neurobiol Dis*, 43: 565-75.
- Teplow, D. B. 1998. 'Structural and kinetic features of amyloid beta-protein fibrillogenesis', *Amyloid*, 5: 121-42.
- Ter-Pogossian, Michel M. 1992. 'The origins of positron emission tomography', *Seminars in Nuclear Medicine*, 22: 140-49.
- Tolboom, N., M. Yaqub, W. M. van der Flier, R. Boellaard, G. Luurtsema, A. D. Windhorst, F. Barkhof, P. Scheltens, A. A. Lammertsma, and B. N. van Berckel. 2009. 'Detection of Alzheimer pathology in vivo using both 11C-PIB and 18F-FDDNP PET', *J Nucl Med*, 50: 191-7.
- Tombaugh, T. N., and N. J. McIntyre. 1992. 'The mini-mental state examination: a comprehensive review', *J Am Geriatr Soc*, 40: 922-35.
- Trebossen, R., C. Comtat, V. Brulon, P. Bailly, and M. E. Meyer. 2009. 'Comparison of two commercial whole body PET systems based on LSO and BGO crystals respectively for brain imaging', *Med Phys*, 36: 1399-409.
- Tsuboi, Yoshio, Hirotake Uchikado, and Dennis W. Dickson. 2007. 'Neuropathology of Parkinson's disease dementia and dementia with Lewy bodies with reference to striatal pathology', *Parkinsonism Relat Disord*, 13: S221-S24.
- Turner, P. R., K. O'Connor, W. P. Tate, and W. C. Abraham. 2003. 'Roles of amyloid precursor protein and its fragments in regulating neural activity, plasticity and memory', *Prog Neurobiol*, 70: 1-32.
- Vilar, M., H. T. Chou, T. Luhrs, S. K. Maji, D. Riek-Loher, R. Verel, G. Manning, H. Stahlberg, and R. Riek. 2008. 'The fold of alpha-synuclein fibrils', *Proc Natl Acad Sci U S A*, 105: 8637-42.
- Voogd, Jan, Yoshikazu Shinoda, Tom J. H. Ruigrok, and Izumi Sugihara. 2013. 'Cerebellar Nuclei and the Inferior Olivary Nuclei: Organization and Connections.' in Mario Manto, Jeremy D. Schmahmann, Ferdinando Rossi, Donna L. Gruol and Noriyuki Koibuchi (eds.), *Handbook of the Cerebellum and Cerebellar Disorders* (Springer Netherlands: Dordrecht).
- Vuono, R., S. Winder-Rhodes, R. de Silva, G. Cisbani, J. Drouin-Ouellet, M. G. Spillantini, F. Cicchetti, and R. A. Barker. 2015. 'The role of tau in the pathological process and clinical expression of Huntington's disease', *Brain*, 138: 1907-18.

- Wakabayashi, Koichi, and Hitoshi Takahashi. 2004. 'Pathological heterogeneity in progressive supranuclear palsy and corticobasal degeneration', *Neuropathology*, 24: 79-86.
- Walsh, D. M., I. Klyubin, J. V. Fadeeva, W. K. Cullen, R. Anwyl, M. S. Wolfe, M. J. Rowan, and D. J. Selkoe. 2002. 'Naturally secreted oligomers of amyloid beta protein potently inhibit hippocampal long-term potentiation in vivo', *Nature*, 416: 535-9.
- Wang, H. W., J. F. Pasternak, H. Kuo, H. Ristic, M. P. Lambert, B. Chromy, K. L. Viola, W. L. Klein, W. B. Stine, G. A. Krafft, and B. L. Trommer. 2002. 'Soluble oligomers of beta amyloid (1-42) inhibit long-term potentiation but not long-term depression in rat dentate gyrus', *Brain Res*, 924: 133-40.
- Wang, Yipeng, and Eckhard Mandelkow. 2016. 'Tau in physiology and pathology', *Nat Rev Neurosci*, 17: 22-35.
- Wardak, M., K. P. Wong, W. Shao, M. Dahlbom, V. Kepe, N. Satyamurthy, G. W. Small, J. R. Barrio, and S. C. Huang. 2010. 'Movement correction method for human brain PET images: application to quantitative analysis of dynamic 18F-FDDNP scans', *J Nucl Med*, 51: 210-8.
- Weingarten, M. D., A. H. Lockwood, S. Y. Hwo, and M. W. Kirschner. 1975. 'A protein factor essential for microtubule assembly', *Proc Natl Acad Sci U S A*, 72: 1858-62.
- Wiederschain, G. Ya. 2011. 'The Molecular Probes handbook. A guide to fluorescent probes and labeling technologies', *Biochemistry (Moscow)*, 76: 1276-76.
- Williams, D. R., J. L. Holton, C. Strand, A. Pittman, R. de Silva, A. J. Lees, and T. Revesz. 2007. 'Pathological tau burden and distribution distinguishes progressive supranuclear palsy-parkinsonism from Richardson's syndrome', *Brain*, 130: 1566-76.
- Williams, David R., Rohan de Silva, Dominic C. Paviour, Alan Pittman, Hilary C. Watt, Linda Kilford, Janice L. Holton, Tamas Revesz, and Andrew J. Lees. 2005. 'Characteristics of two distinct clinical phenotypes in pathologically proven progressive supranuclear palsy: Richardson's syndrome and PSP-parkinsonism', *Brain*, 128: 1247-58.
- Wimo, Anders, Maëleann Guerchet, Gemma-Claire Ali, Yu-Tzu Wu, A. Matthew Prina, Bengt Winblad, Linus Jönsson, Zhaorui Liu, and Martin Prince. 2017. 'The worldwide costs of dementia 2015 and comparisons with 2010', *Alzheimer's & Dementia*, 13: 1-7.
- Wong, Koon-Pong, Kepe Vladimir, G. W. Small, N. Satyamurthy, J. R. Barrio, and S. C. Huang. 2007. "Comparison of simplified methods for quantitative analysis of [F-18]FDDNP PET data." In *2007 IEEE Nuclear Science Symposium Conference Record*, 3146-50.
- Xu, Shaohua, Kurt R. Brunden, John Q. Trojanowski, and Virginia M. Y. Lee. 2010. 'Characterization of tau fibrillization in vitro', *Alzheimer's & dementia : the journal of the Alzheimer's Association*, 6: 110-17.
- Ye, H., K. P. Wong, M. Wardak, M. Dahlbom, V. Kepe, J. R. Barrio, L. D. Nelson, G. W. Small, and S. C. Huang. 2014. 'Automated movement correction for dynamic PET/CT images: evaluation with phantom and patient data', *PLoS One*, 9: e103745.